2015

Developing a decadal-scale stalagmite record of hydroclimate and atmospheric variability for western Iberia (Portugal) during the Late Holocene

Diana Lynn Thatcher
Iowa State University

Developing a decadal-scale stalagmite record of hydroclimate and atmospheric variability for western Iberia (Portugal) during the Late Holocene

by

Diana Lynn Thatcher

A thesis submitted to the graduate faculty

in partial fulfillment of the requirements for the degree of

MASTER OF SCIENCE

Co-majors: Geology, Environmental Science

Program of Study Committee:
Alan D. Wanamaker, Jr., Major Professor
William Simpkins
William Gutowski

Iowa State University

Ames, Iowa

2015

DEDICATION

This work is dedicated to my family – my husband, Matt, and my children, Andrew, Hannah, Mary, and Sarah. I hope that by watching me do this and learn such great new things you will be inspired to do what you love!

TABLE OF CONTENTS

ACKNOWLEDGEMENTS

Thank you to my Program of Study committee – Dr. Alan Wanamaker, Dr. William Gutowski, and Dr. William Simpkins. A special thanks to Dr. Rhawn Denniston for bringing me to the cave in Portugal and for trying to teach me everything he knows about speleothems.

Thank you to Suzanne Ankerstjerne for running hundreds and hundreds of carbonate samples, to Mark Mathison for helping fix whatever is broken, to Maddie Mette for always being willing to answer my questions – no matter how silly – and for being such a great office-mate, and to DeAnn Frisk for doing all that you do for me and everyone in the department. Thank you to Dr. Alan Wanamaker for his support and guidance and for giving me a chance.

Thank you to various groups for funding me and my research - Environmental Science Fellowship, Bowen Fellowship, Smith Fellowship, travel funding from the ISU Environmental Science and ISU Geology departments, and Teaching Assistantship funding from the Department of Geological and Atmospheric Sciences.

CHAPTER 1: GENERAL INTRODUCTION

Introduction

Paleoclimatology

This study is done within the realm of paleoclimatology, the study of Earth's climate which considers the entire history of the Earth and focuses on the patterns and causes of climate change (Cronin, 2010) and assesses past climates prior to instrumental records (IPCC, 2013). The broad reasoning behind all studies within paleoclimatology is to better understand the climate of the past in order to better understand current and future climates and climate change. Without the perspective of past climates, we cannot begin to understand the present processes and those that will be at work in the future. That is the motivation driving this work and most paleoclimate research.

Evidence of what the climate was like at times in the past has been preserved in natural archives and the record contained within these archives can be used to reconstruct past temporal or spatial environmental changes (Jones et al., 2009). It is the job of the paleoclimatologist to piece the evidence together to understand the mechanisms that created the visible evidence. Paleoclimatologists scour the planet looking for clues about past climate (www.earthobservatory.nasa.gov). Things such as erratic boulders, Large boulders that were transported by glacial ice (Darvill et al., 2015), ocean and lake sediment cores (Yuretich et al., 1999), tree rings (Cook et al., 1998), appearance and disappearance of diatom and other marine species (Bracht-Flyr and Fritz, 2012), speleothems (Bar-Matthews et al., 1999), ice cores (Petit et al., 1999), pollen records (Desprat et al., 2003), lake and ocean levels (McGee et al., 2012), corals

(Asami et al., 2009), and mollusks (Wanamaker et al., 2011) are some of the archives that scientists use to study climates of the past.

Paleoclimatology uses natural archives to reconstruct Earth's climate across many time scales. Ancient carbonates and cherts indicate that the Earth's average temperature during the Archean (4 to 2.5 billion years ago) was, at least at times, 55 ^{o} C (Knauth, 2005), much higher than today's average of 15^{o} C. Deep time studies of glacial sediments have shown that during the time period 750 to 580 million years ago, the Earth was completely or mostly enveloped in ice, the Snowball (or Slushball) Earth hypothesis (Kirschvink, 1992). Perhaps one of the most studied paleoclimate time periods is the Cenozoic and the large climatic changes that took place during the global cooling that began 65 Ma (Fischer, 1981). Foraminiferal $\delta^{18}O$ values (Shackleton, 1967) indicate the presence of continental ice which accompanied Cenozoic cooling. Contained within this cooling was a brief period of global warmth about 55.5 Ma, the Paleocene-Eocene Thermal Maximum, which was associated with elevated levels of greenhouse gases (Zachos et al., 2003; Zachos et al., 2005).

When considering possible causes of some of the Earth's past major climate changes, insolation related to Earth/Sun orbital dynamics and the related changes in the Earth's solar energy input appear to be an important factor. Three aspects of the Earth's orbit vary because of gravitational forces in the solar system (Berger and Loutre, 1991). These three aspects are obliquity (the tilt of the Earth's axis), precession (accounts for wobble and the precession of the equinoxes), and eccentricity (accounts for the changing shape of the Earth's orbit around the sun) (Berger et al., 2005). These

three orbital parameters vary on different time frames (41 ka obliquity, 22 ka precession, 100 and 405 ka eccentricity) and they determine the solar insolation received at the top of the atmosphere. These parameters can be calculated to derive solar insolation values going back in time (Berger, 1978; Berger and Loutre, 1991).

Past glacial cycles occurred on 41 kyr cycles and during the mid-Pleistocene Transition, ca. 1Ma to 700ka, the period of glacial activity shifted to approximately 100 kyr cycles. This ice age periodicity is not the result of the 100 kyr periodicity of the eccentricity parameter (Imbrie et al., 1993) and leads to discrepancies such as the "100kyr problem" or the "eccentricity myth" (Maslin and Ridgewell, 2005). The mechanics that cause the Earth to go into and out of ice ages are poorly understood, a problem that paleoclimatology aims to understand (Paillard, 2015).

During the time period 115,000 to 22,000 years BP, an interval referred to as the last glacial interval, after the peak interglacial warmth and before the last deglaciation (Cronin, 2010), there are records in natural archives documenting millennial-scale climate events that don't correspond with changes expected due to orbital processes. Sharp spikes were noted in oxygen isotopes from Greenland ice cores by Dansgaard and Oeschger suggesting large warming periods in atmospheric temperatures (up to 15 ^{o}C) during cold glacial intervals (Dansgaard et al., 1984; Oeschger et al., 1984). Heinrich events are millennial-scale phenomena studied by paleoclimatologists and are massive iceberg discharges that left ice-rafted debris on the floor of the Atlantic Ocean (Ruddiman, 1977; Heinrich, 1988; Bond et al, 1992, Bond et al., 1993). Together, Dansgaard-Oeschger events and Heinrich events make up the Bond cycles that

dominated glacial climates (Bond, 1993; Lehman, 1993; Bond, 1999). Evidence of these events comes not only from the indicated archives (ice cores and ice-rafted debris) but are evident in speleothems around the world (Wang et al., 2001), indicating that these events had global-scale (or at least hemispheric-scale) impacts. Further work to ascertain exact timing and mechanisms of these millennial-scale events is another intensely studied area of paleoclimatology.

Rapid Climate Change (RCC) Events

During the Holocene (11.5 ka to present), after the Last Glacial Maximum, the climate of the Earth stabilized relative to the large changes of glacial cycles, yet there has still been variability (Fischer et al., 2004). During the Holocene, there are more natural archives to study these variations and to better understand the mechanisms causing changes. The size of changes is smaller, yet the presence of humans during this time means that these Rapid Climate Change (RCC) events, changes that have occurred on human timescales of hundreds of years or less, could have potentially been major disruptions to the civilizations of these times (Mayewski et al., 2004). Mayewski (2004) identified 6 periods of RCC during the Holocene – 9-8ka, 6-5 ka, 4.2-3.9ka, 3.5-2.5ka, 1200-1000 yr BP, and the last RCC event beginning about 600 years ago. This research will add to the knowledge of the most recent two RCC events – the Medieval Climate Anomaly (1200-1000 yr BP) and the Little Ice Age (beginning about 600 years ago).

Medieval Times/Medieval Climate Anomaly

Chapter 2 of this research will document changes recorded in stalagmites during the Medieval Climate Anomaly (MCA), a period of time which is the most recent

counterpart to modern warmth and allows for comparison of anthropogenic and natural forcings (Trouet et al, 2009). At least in Europe, the MCA was a time of warmth and makes a good comparison for today's warmth. Some significant differences between today's climate and the MCA are that during the MCA the warmth was likely regional not global, like today, and atmospheric CO_2 levels during Medieval times were lower than today's CO_2 levels.

We, as humans, cannot ignore the implications of past, present, and future climates on our lives. Many humans are aware of the possible implications of future climate change, specifically rapid warming likely due to increased levels of greenhouse gases in the atmosphere. Our ancestors were keenly aware of changes in weather and climate as well, as it affected their livelihood and health. Medieval times were a time of cathedral building, cultural flowering, and a time of general prosperity in much of Europe due, at least in part, to the climate of that time (Fagan, 2008). Written records of wine harvests (Ladurie, 1971), crop flourish or failure at a time when margins in farming were very slim, trade routes opening and closing (Buckland et al., 1996) such as between Greenland and Europe, and fewer conflicts at times of climate stability make this link between humans and climate apparent to us as we interpret historical, instrumental, and proxy records (Fagan, 2008). Buntgen et al. (2011) determined from tree ring records in northern Europe that warm and wet summers occurred during periods of Roman and Medieval prosperity, further linking human well-being and climate.

Little Ice Age

While Medieval times were characterized by general prosperity, the time of the climate regime that followed, the Little Ice Age (LIA), was generally characterized by hardships such wars, plague, and famines (Fagan, 2000). Generally defined as ca. 1300 to 1850 (Fagan, 2000; Grove, 1988) but sometimes defined as starting later (1450 AD, Trouet et. al, 2009), the Little Ice Age was a time of cooler conditions - 0.5 to 0.7 ^{o}C cooler than present time, according to borehole measurements from Greenland Ice cores (Dahl-Jensen et al., 1998). Temperatures were only modestly cooler hemispherically, but certain parts of the world experienced more intense cold during the LIA (Lamb, 1977). Definitions of the beginning and ending of the MCA and the beginning of the LIA vary, as conditions changed at different times in different locations. The MCA began as early as 550 AD from records in Finland (Seppa and Birks, 2002) and as late as 1100 AD from records in the Sierra Nevadas (USA, Graumlich, 1993). The ending of the LIA is almost always 1800-1850 AD, but the beginning ranges from 1200 from Alaskan lake records (Hu et al., 2001) to 1600 in the records of several Greenland ice cores (Fischer et al., 1999). Some of the natural archives available from this time show glacier advances (Grove, 1988), lower air temperatures (Lamb, 1977; Mann et al., 1999; Mann et al., 1998; Zhang and Crowley, 1989), lower snowlines (Grove, 1988), and sea ice expansion (Dansgaard, 1975) during the LIA.

Speleothems

Speleothems are a natural calcium carbonate archive and the information contained within speleothems can be a proxy of past climate. They are a reliable record

of past climate because they provide exceptional climate chronologies with precision unprecedented with other proxies (Henderson, 2006). It has been argued that speleothems provide the most definitive archives of the global climate system (Fairchild and Baker, 2012). An increased understanding of climatic controls on $\delta^{18}O$ values from speleothems has propelled speleothems to the forefront of paleoclimatology (Lachniet, 2009) and they have become important proxies for reconstructing past climates. Although speleothems can indicate much about the climate system, there are problems with interpreting these records (Lachniet, 2009) and karst regions are not found everywhere on the planet limiting the spatial coverage of these records.

Speleothem is a general terms for carbonate cave formations, such as stalagmites, stalactites, and flowstone (Henderson, 2006). They have been used on various timescales and to study different regions and climate processes. Speleothems have proved useful as a proxy to record meteorological events and short- and long-term climatic changes such as El Nino-Southern Oscillation variability (Frappier, 2002), Heinrich events and Dansgaard/Oeschger events (Genty et al., 2003; Wang et al., 2001), hurricane and tropical storm tracks/landfall (Frappier, 2007), changes in permafrost (Vaks et al., 2013), changes in the location of the Intertropical Convergence Zone (Fleitmann et al., 2007), and monsoon variability (Denniston et al., 2013; Wang et al., 2001).

As noted above, speleothems make an excellent proxy for recording and reconstructing past climates partly due to the ability to accurately and absolutely date different portions of the sample (McDermott, 2004). The two methods generally used

for dating are layer (or laminae) counting (Baker et al., 2011) and uranium-thorium disequilibrium methods (Fairchild et al., 2006). A third method uses the 20th century ^{14}C bomb spike to accurately pinpoint the time in which nuclear weapons testing was done and led to an increase in atmospheric ^{14}C (Baker and Fairchild, 2012). This method is obviously only useful for speleothems growing during the latter portion of the 20th century. Lamina counting is useful in stalagmites which show annual layers of growth and seasonality is often apparent in the growth of fluorescent bands and/or layers of different chemical composition deposited seasonally. Lamina counting can be paired with uranium-thorium dating or U-Th methods can be used independently. Uranium is incorporated into the crystalline calcite lattice of the speleothems where, over time, 235-uranium radioactively decays to 230-thorium (Fairchild and Baker, 2012). Uranium-thorium dating is possible due to the fact that uranium is highly water soluble and thorium is much less water soluble (Dorale et al, 2004). Ideally, initial thorium in the stalagmite is zero and any thorium present in the stalagmite is a result of this radioactive decay. Initial thorium can be brought into the growing calcite by detrital materials (Dorale et al., 2004). Thorium-230 can be accurately measured, along with uranium amounts, via Inductively Coupled Plasma- Mass Spectrometry (ICP-MS) to determine the number of years since the layer of calcite was formed. Corrections for initial thorium are made and different values for initial thorium are used for different cave systems.

Calcite $\delta^{18}O$ values

Isotopes are variations of elements with different numbers of neutrons but the same number of protons. For example, carbon has three common – carbon-12, carbon-13, carbon-14. Carbon-12 has an abundance of 98.89%, carbon-13 has an abundance of 1.109%, and carbon-14 has an abundance of 1 part per trillion. Carbon-12 is by far the most abundant, carbon-14 is a radioactive element, and, even at small abundances, carbon-13 is an important isotope and is abundant enough to detect using standard isotope ratio mass spectrometry (IRMS). Similarly, oxygen-18 has an abundance of 0.2% while oxygen-16 has an abundance of 99.762%. Fractionation of these isotopes can occur during processes, such as evaporation and condensation, which preferentially incorporate either the lighter or heavier isotopes. Fractionation occurs because the bonds of the lighter isotopes are weaker and, therefore, easier to break (Gat, 1996). An understanding of these fractionation processes and measurements of the deviations of rare isotopes in the sample from the standard used allows for a greater understanding of all conditions where these processes occur.

Some stable isotopes that are measured and are used to assess climatic variability are ^{18}O and ^{16}O (as well as ^{13}C and ^{12}C). The variations of ^{18}O and ^{16}O within the stalagmite are measured with a mass spectrometer and are expressed in delta (δ) notation as given in Equation 1 (Sharp, 2007). The standard generally used for carbonates is Vienna Pee Dee Belemnite (VPDB). The isotopic ratio of the sample is expressed in per mil, parts per thousand or, simply, ‰.

$$\delta^{18}O_{sample}=\left(\frac{\frac{^{18}O}{^{16}O}_{sample}}{\frac{^{18}O}{^{16}O}_{standard}}-1\right)*1000$$

Equation 1

At equilibrium conditions, the $\delta^{18}O$ values contained within the calcite of speleothems is a function of the temperature at calcite formation and the $\delta^{18}O$ of the source water (Epstein et al., 1953).

$$\delta^{18}O_{calcite}=f\ (T,\ \delta^{18}O_{water})$$

Equation 2

The calcite-water fractionation is affected by temperature such that calcite $\delta^{18}O$ changes by -0.23 ‰ per 1^{o}C change in temperature at equilibrium (O'Neil et al., 1969; Friedman and O'Neil, 1977). In Buraca Glorioso, the temperature inside the cave changes very little throughout the year (see Chapter 2). Calcite isotopic variability is on the order of 4 ‰ (see Chapter 2) over the course of the 2300+ year history recorded in the stalagmite from Buraca Glorioso, as documented in this research, which would indicate that the changes in the $\delta^{18}O$ calcite values through time are largely reflecting changes in the $\delta^{18}O$ values of the source water and only slightly reflecting temperature changes. If changes in $\delta^{18}O$ were solely reflecting temperature changes, for example, the signal recorded in the Buraca Glorioso stalagmite would be indicative of a 17-18 ^{o}C change in cave temperature, an unlikely temperature change.

The source water for forming speleothems is the water that makes its way into the cave and is derived from precipitation falling above the cave. These source water isotopic changes could be a result of the source of the moisture to the cave changing

(Atlantic versus Mediterranean). There are distinct differences in $\delta^{18}O$ values from the Mediterranean Sea and the Atlantic Ocean and these differences would be reflected in the $\delta^{18}O$ signal from precipitation derived from these different locations (LeGrande and Schmidt, 2006). At Buraca Glorioso, changing moisture source is not likely causing the changes in isotopic values. Precipitation events sourced from the Mediterranean are rare and light in nature and these events are likely not changing the $\delta^{18}O$ signal contained within in the calcite substantially. Since the $\delta^{18}O$ of the drip water in the cave is very similar to the $\delta^{18}O$ of the local precipitation falling on the rock above the cave (Domínguez-Villar et al., 2008), a greater understanding of the causes of changes in the $\delta^{18}O$ values in the precipitation is needed.

The $\delta^{18}O$ of precipitation is a function of many factors including latitude, altitude, longitude or continentality effect, relative humidity, precipitation source, temperature, and amount of precipitation (Dansgaard, 1964). The $\delta^{18}O$ of precipitation changes as the moisture moves from equatorial regions of the globe to higher latitudes (Dansgaard, 1954), $\delta^{18}O$ changes as moisture is moved inland away from the coast and into a continent (essentially longitude in north-south oriented Portugal), $\delta^{18}O$ changes as moisture is moved up in elevation, $\delta^{18}O$ changes as moisture is precipitating, $\delta^{18}O$ changes as water evaporates from rain droplets, $\delta^{18}O$ changes as precipitation continues, $\delta^{18}O$ changes as a result of convection, and as the relative humidity increases in the precipitation region. $\delta^{18}O$ values of rain falling in dry months are higher than $\delta^{18}O$ values of precipitation falling in wetter months (Friedman et al., 1962). The

possible factors influencing the $\delta^{18}O$ of the calcite in Buraca Glorioso are summarized in Figure 1-1.

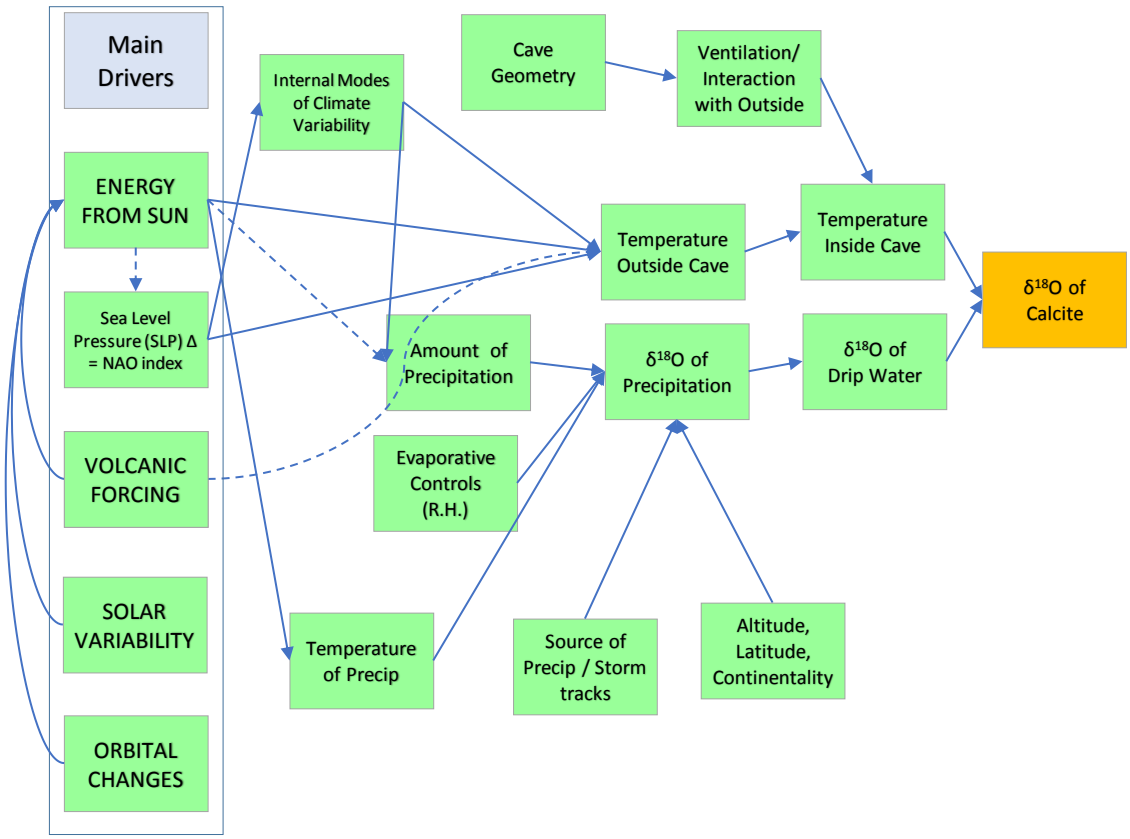

Figure 1-1. Factors that affect the $\delta^{18}O$ of speleothem calcite from Buraca Glorioso.

Calcite $\delta^{13}C$ values

Interpreting the $\delta^{13}C$ signal from the stalagmite is not a straightforward task (Martín-Chivelet et al., 2011) and multiple factors likely affect the record (McDermott, 2004; Fairchild et al., 2006). Some of these factors that control the $\delta^{13}C$ of the speleothem calcite are summarized in Figure 1-2. Analysis of the individual values may not be revealing but looking at the trends within an individual record and trends visible

in multiple records can reveal common mechanisms controlling the $\delta^{13}C$ values (Martín-Chivelet et al., 2011).

Factors important for controlling the $\delta^{13}C$ of the calcite in the cave include CO_2 degassing of the drip water, changes in the vegetation density above the cave, the type of vegetation above the cave (C_3 or C_4 dominated plants), the amount of prior calcite precipitation, mixing between the atmospheric CO_2 and the biological CO_2 in roots and microbes, the CO_2 of the atmosphere, $\delta^{13}C$ of the limestone above the cave, and open or closed system behavior (Fairchild and Baker, 2012; Zhang et al., 2015). The pCO_2 of the groundwater, residence time in the soil and rock, type of flow through the rock, and water interactions with the soil and rock are also likely important controls on the $\delta^{13}C$ value of the drip water entering the cave. CO_2 degassing of the drip water can be determined by measuring the partial pressure of carbon dioxide (CO_2) within the cave (pCO_2) (Mattey et al., 2008). Changes in vegetation about the cave may influence the $\delta^{13}C$ values of the speleothems in the cave (Dorale etal., 1998; Zhang et al., 2015). These changes in vegetation could be changes from C_3 to C_4 plants or changes in vegetation density, and both of these changes are related to changes in climate (Zhang et al., 2015).

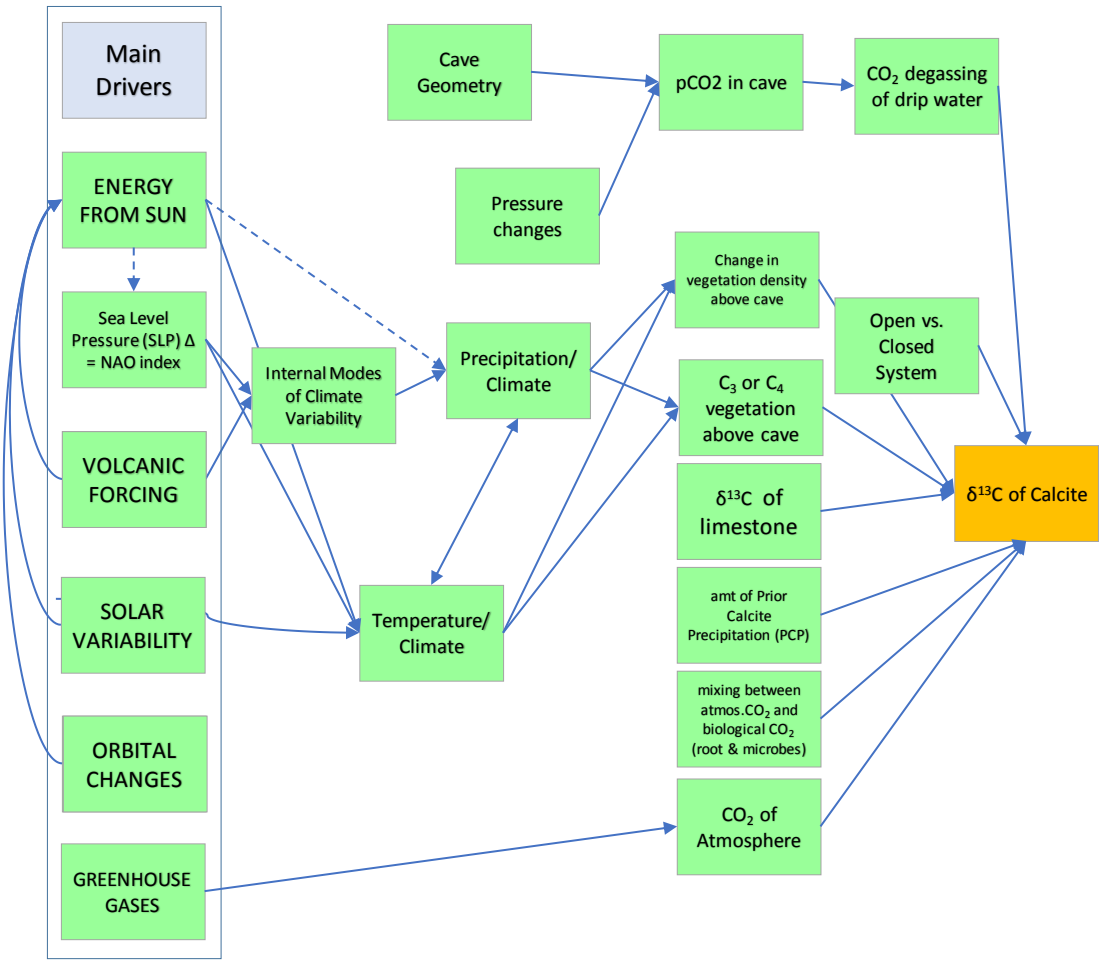

Figure 1-2. Factors that affect the $\delta^{13}C$ values contained within the speleothem calcite in Buraca Glorioso.

North Atlantic Oscillation

The North Atlantic Oscillation (NAO) is the dominant mode of atmospheric variability in the North Atlantic sector (Hurrell, 1995) and the NAO instrumental record in this region dates to 1864 (Hurrell, 1995; www.ucar.edu). The NAO index is a label given to a re-distribution of mass in the atmospheric which creates sea-level pressure differences between the area near Iceland and the area near the Azores (Hurrell et al.,

2003). It is a way to simplify a complex, natural behavior and broad generalizations about the behavior of this system are useful for characterizing climatic variability.

The NAO index is defined as the sea-level pressure (SLP) difference between Iceland and the Azores (Wallace and Gutzler, 1981). A high NAO index (+ mode) is defined by a larger difference in sea-level pressure between the Icelandic Low and the Azores High, as currently measured in Reykjavik and Lisbon. In this situation, there is a higher pressure gradient between the two nodes of the NAO system which increases westerlies and causes the storm track off the Atlantic to bring higher precipitation amounts to northern Europe leaving southern Europe dry (Hurrell, 1995). A lower NAO index (- mode) is defined by a smaller sea-level pressure difference between the Icelandic Low and the Azores high. During NAO negative modes, the gradient is relaxed, westerlies are suppressed, northern Europe has drier conditions, and southern Europe has wetter conditions (www.ucar.edu).

The dipoles of the NAO system are located near Iceland and the Azores and the NAO index can be calculated using Lisbon, Portugal SLP values and SLP values from Reykjavik, Iceland. The Lisbon/Reykjavik index is most commonly used and is the record that dates to 1864. Multiple methods for calculating NAO index exist (See introduction of Lehner et al., 2012 for additional ways to index NAO). The NAO accounts for 31% of the hemispheric interannual variance over the time period 1936-1996 (Hurrell, 1996) and while the NAO does not account for the majority of the variability in the north Atlantic region, it is the dominant factor. Moreover, its mode is linked to extreme weather events, such as the winter of 2009-2010 which brought extreme cold to Europe

in a winter of extremely low NAO indices (Cattiaux et al., 2010). Heavier precipitation, linked with negative NAO indices, is a major cause of landslides in Portugal (Trigo et al., 2005).

NAO reconstructions

Previous NAO reconstructions have used multiple proxies including tree rings and Greenland ice accumulation and have reconstructed the behavior of the NAO as far back as ca. 1400-1600 (Cook et al.,2002; Luterbacher et al., 1999; Appenzeller et al., 1998). The ice core reconstruction of Appenzeller et al. (1998) shows recent variability on time scales of 80-90 years and that the NAO is an intermittent climate oscillation with sometimes active and sometimes passive phases. The Cook et al. (2002) reconstruction using early precipitation data, modeling data, and monthly SLP data dates to 1400 AD and verifies against European instrumental and non-instrumental data back through 1500 AD. Persistent positive-phase NAO appeared to have occurred before 1650 AD as well as during the 20th century. The Luterbacher et al., (1999) reconstruction shows interdecadal fluctuations much like that of Cook et al. (2002).

Additionally, previous research has attempted to extend reconstructed NAO behavior back through Medieval times, including a study by Trouet et al. (2009). This reconstruction uses a proxy from a location likely outside of the main influence of the NAO system, northwest Africa (Morocco), a site often but not consistently under the influence of the NAO system (Lehner et al., 2012). Trouet et al. (2009) used Palmer Drought Severity Index reconstruction based on tree ring widths from Morocco (Esper et al., 2007), capturing the hydroclimate variability in Morocco. The Moroccan record does

seem to capture some hydroclimate variability but the "average" value might be closer to a z-score of 2 instead of 0 (see Figure 1-3). Thus far, the scientific community is lacking records from strategic (highly influenced by the NAO) locations to most accurately study NAO behavior (Lehner et al., 2012). Modeling results (Lehner et al., 2012) have been unable to verify the 400 year positive NAO behavior from the Trouet et al. (2009) reconstruction. Instrumental data show NAO variability on a sub-decadal time scale (www.ucar.edu) which also makes a 400 year persistently positive NAO mode seem unlikely. The Trouet et al. (2009) record during the MCA seems to be dominated by the Scottish stalagmite, which may not be a record sensitive enough to document the variability in the NAO.

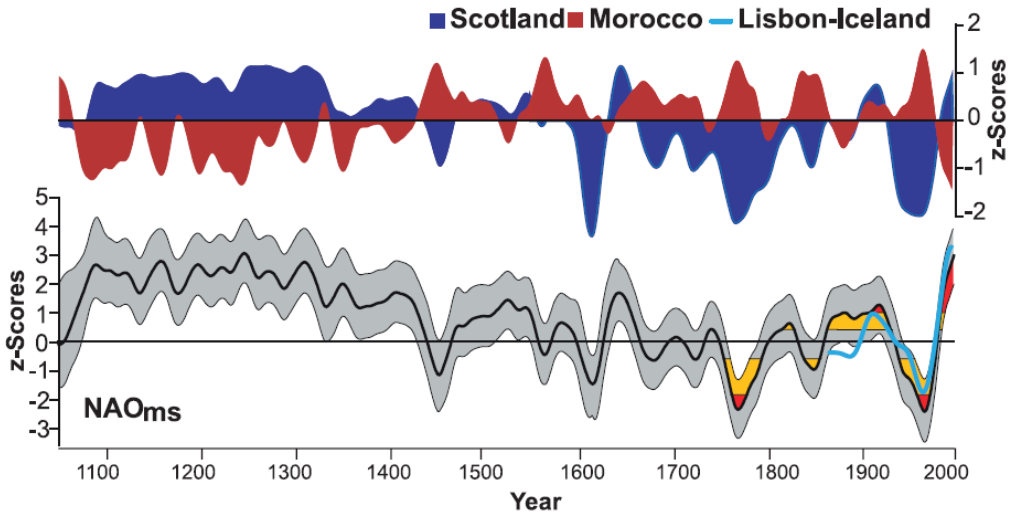

Figure 1-3. Trouet et al. (2009) NAO reconstruction from Morocco (red in top plot) and Scotland (blue in top plot) proxies. Note persistently positive NAO index, indicated by z-score >0, from <1100 to >1400 AD (grey in bottom plot). Light blue line indicates calibration with modern instrumental record.

Portugal

The Iberian Peninsula (specifically Portugal) is ideal for studying the NAO since it is consistently under the influence of the NAO and the climate of the region is highly sensitive to changes in global climate and NAO behavior (see Figure 1-4), yet long, well-dated climate proxies are lacking in this area (Martín-Chivelet et al., 2011). A well-dated proxy (or set of proxies) of considerable length from this area would allow for better understanding of variability of past climates and the processes that control climate to better constrain current and future climate changes.

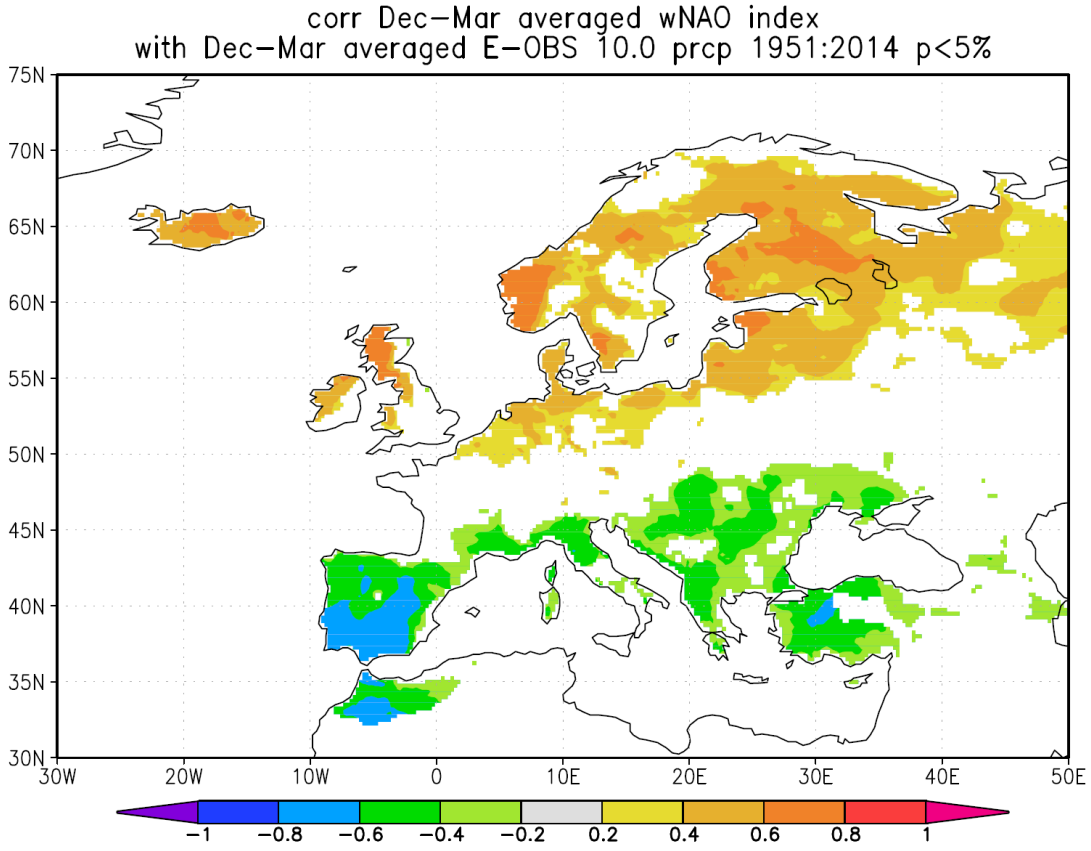

Figure 1-4. Time-averaged December – March precipitation correlated (r-values) with time-averaged wNAO index. Note high anti-correlation values in Portugal. Higher wNAO index = lower precipitation amounts for Portugal. (KMNI Climate Explorer - climexp.knmi.nl)

To most accurately study the NAO and its variability, a study site consistently under the influence of the southern node of the NAO system was chosen. Portugal is consistently under the influence of the NAO system and the variability in the NAO likely can be studied effectively using stalagmites (and other proxy records) from Portugal. Previous studies have used locations that are near Portugal, but not in Portugal. The most well-known of these reconstructions is that of Trouet et al. (2009).

Portugal's winter precipitation is strongly influenced by the wNAO index (Gallego et al., 2005). The amount of winter precipitation in Portugal is highly variable and is negatively correlated with the mode of the wNAO index (positive or negative). Winters with high values of the NAO index have an average precipitation of 47 mm/month while low values of the NAO have an average precipitation of 134 mm/month (Trigo et al., 2005). This has implications for the people of the Mediterranean region, especially Portugal. Among other things, the winters with higher precipitation also have increased numbers of landslides causing property damage (Trigo et al., 2005).

Instrumental data over the past 150 years in North America and Europe allow us to accurately assess past climate in these areas over this time frame. In other parts of the world and over the ocean, the records are sparse even over this time frame. Going back in time farther than 150 years, there are almost no reliable records of temperature, pressure, and precipitation. Extending climatic records back in time and to cover regions not adequately represented by modern records is the role of the climate proxy. Numerous proxies exist (corals, mollusks, tree ring, sediments, speleothems, ice cores) in both terrestrial and marine environments. The subject of this

research is a high-resolution, precipitation-sensitive speleothem proxy from a strategic location in central Portugal and will be used to reconstruct climate in Portugal over the past 2600 years with specific focus on the behavior of the North Atlantic Oscillation and the effects of changing NAO behavior on Portugal's climate. This work will also assess the contribution of other drivers of the climate system in the region – solar insolation, solar irradiance variability, volcanic forcing as well as internal modes that drive temperature and precipitation variability.

Hypotheses

Two central hypotheses are guiding this research: 1) The hydroclimate of the Iberian Peninsula during Medieval times (MCA) was more variable than that presented by Trouet et al. (2009) and was characterized by mostly dry conditions punctuated by several wetter time periods during the MCA; 2) The $\delta^{18}O$ and $\delta^{13}C$ values contained within the calcite from Buraca Glorioso are driven by several factors including insolation changes due to changes in orbital parameters, changes in total solar irradiance (by sun spots, etc.), volcanic forcing, and variability of both temperature and precipitation, which are linked to, among other things, variability of the NAO.

Thesis organization

This thesis is separated into four parts. Chapter 1 includes a broad introduction to paleoclimate and the problems being investigated with paleoclimate methods and proxies. Also included in this introductory chapter are the problems being addressed with this work, specifically the climate of Medieval times and the Little Ice Age in

Portugal/Iberian Peninsula and the longer-term drivers of the climate of the Iberian Peninsula.

Chapter 2 describes the hydroclimate of Portugal and the Iberian Peninsula during Medieval times, including the Medieval Climate Anomaly, and the transition from this period to the subsequent Rapid Climate Change event, commonly known as the Little Ice Age. Much anecdotal evidence exists, such as the diary of Manuel de Almeida (Alcoforado et al., 2000), from these time periods, which reveal large changes in Europe's climate (Lamb, 1965) likely due to, at least in part, changes in the behavior of the North Atlantic Oscillation during this time. In this research, the hydroclimate of southwestern Europe is inferred from carbon and oxygen isotope data micromilled from a stalagmite from a central Portugal cave. The age model for this stalagmite was obtained using uranium-thorium disequilibrium methods. Environmental data, including temperature, relative humidity, and pressure, for this area have been obtained and data collection is ongoing.

Chapter 3 describes the hydroclimate of Portugal and the Iberian Peninsula in earlier times inferred from a Portuguese stalagmite, extending the hydroclimate record of the area back to ~600BC using $\delta^{13}C$ and $\delta^{18}O$ variability. This record is paired with other proxy records to further investigate drivers of climate throughout the Holocene in the Iberian Peninsula and the North Atlantic sector.

The concluding remarks section of this thesis (Chapter 4) outlines the major findings from this study regarding the hydroclimate of Portugal and the major drivers of the $\delta^{18}O$ and $\delta^{13}C$ signal contained in the stalagmite. Chapter 4 also describes future

work to further the understanding of the hydroclimate of the Iberian Peninsula and the way it presents itself in the Buraca Glorioso cave system.

References

Alcoforado, M.–J., Nunes, M., García, J.C., Taborda, J.P., 2000. Temperature and precipitation reconstruction in southern Portugal during the late Maunder Minimum (AD 1675-1715). Holocene 10, 333-340.

Appenzeller, C, 1998. North Atlantic Oscillation Dynamics Recorded in Greenland Ice Cores. Science 282, 446-449.

Asami, R., Felis, T., Deschamps, P., Hanawa, K., Iryu, Y., Bard, E., Durand, N., Murayama, M., 2009. Evidence for tropical South Pacific climate change during the Younger Dryas and the Bolling-Allerod from geochemical records of fossil Tahiti corals. Earth Planet. Sci. Lett. 288, 96-107.

Baker, A., Wilson, R., Fairchild, I., Franke, J., Spotl, C., Trouet, V., 2011. High resolution $\delta^{18}O$ and $\delta^{13}C$ records climate from an annually laminated Scottish stalagmite and relationship with last millennium climate change. Global Planet. Change 79, 303-311.

Bar-Matthews, M., Ayalon, A., Kaufman, A., Wasserburg, G., 1999. The Eastern Mediterranean paleoclimate as a reflection of regional events: Soreq Cave, Israel. Earth Planet. Sci. Lett. 166, 85-95.

Berger, A., Loutre, M., 1991. Insolation values for the climate of the last 10 million years. Quat. Sci. Rev. 10, 297-317.

Berger , A., Melica, J., Loutre, M., 2005. On the origin of the 100-kyr cycles in the astronomical forcing. Paleoceanography 20, PA4019.

Berger, A., 1978. Long-term variation of daily insolation and Quaternary climatic changes. J. Atmos. Sci. 35, 2362-2367.

Bond, G., Heinrich, H., Broecker, W., Labeyrie, L., McManus, J., Andrews, J., Huon, S., Jantschik, R., Clasen, S., Simet, C., Tedesco, K., Klas, M., Bonani, G., Ivy, S., 1992. Evidence for massive discharges of icebergs into the North Atlantic Ocean during the glacial period. Nature 360, 245-249.

Bond, G., Broecker, W., Johnsen, S., McManus, J., Labeyrie, L., Jouzel, J., Bonani, G., 1993. Correlations between climate records from North Atlantic sediments and Greenland ice. Nature 365, 143-147.

Bond, G., Showers, W., Elliot, M., 1999. The North Atlantic's 1-2 kyr climate rhythm: Relation to Heinrich events, Dansgaard/Oeschger cycles and the Little Ice Age. In: Clark, P., Webb, R., Keigwin, L. (Eds.) Mechanisms of Global Climate Change at Millennial Time Scales, American Geophysical Union, Washington, D.C.

Bracht-Flyr, B., Fritz, S., 2012. Synchronous climate change inferred from diatom records in four western Montana lakes in the U.S. Rocky Mountains. Quat. Res. 77, 456-467.

Buckland, P., Amorosi, T., Barlow, L., Dugmore, A., Mayewski, P., McGovern, H., Ogilvie, A., Sadler, J., Skidmore, P., 1996. Bioarchaeological and climatological evidence for the fate of Norse farmers in medieval Greenland. Antiquity 70, 88-96.

Buntgen, U., Tegel,W., Nicolussi, K., McCormick, M., Frank, D., Trouet, V., Kaplan, J., Herzig, F., Heussner, K., Wanner, H., Luterbacher, J., Esper, J., 2011. 2500 Years of European Climate Variability and Human Susceptibility. Science 331, 578-582.

Cattiaux, J., Vautard, R., Cassou, C., Yiou, P., Masson-Delmotte, V., Codron, F., 2010. Winter 2010 in Europe: A cold extreme in a warming climate. Geophys. Res. Lett., 37, 1-6.

Cook, E., D'Arrigo, R., Briffa,K., 1998. A reconstruction of the North Atlantic Oscillation using tree-ring chronologies from North America and Europe. Holocene 8, 9-17.

Cook, E., D'Arrigo, R., Mann, M., 2002. A Well-Verified, Multiproxy Reconstruction of the Winter North Atlantic Oscillation Index since A.D. 1400. J. Clim. 15, 1754-1764.

Cronin, T., 2010. Paleoclimates. Columbia University Press, New York.

Dahl-Jensen, D., Mosegaard, K., Gundestrup, N., Clow, G.D., Johnsen, S.J., Hansen, A.W. and Balling, N. 1998. Past temperatures directly from the Greenland Ice Sheet. Science 282, 268-271.

Dansgaard, W., 1954. The O^{18}-abundance in fresh water. Geochim. Cosmichim. Acta 6,241-260.

Dansgaard, W., 1964. Stable isotopes in precipitation. Tellus 16, 436-468.

Dansgaard, W., Johnsen, S., Reeh, N., Gundestrup, N., Clausen, H., Hammer, C., 1975. Climatic changes, Norsemen and modern man. Nature 255, 24.

Dansgaard, W., Johnsen, S., Clausen, H., Dahl-Jensen, D., Gundestrup, N., Hammer, C., 1984. North Atlantic climate oscillations revealed by deep Greenland ice cores. In: Hansen, J., Takahashi, T. (Eds.) Climate Processes and Climate Sensitivity. American Geophysical Union, Washington, D.C., pp. 288-298.

Darvill, C., Bentley, M., Stokes, C., 2015. Geomorphology and weathering characteristics of erratic boulder trains on Tierra del Fuego, southernmost South America: Implications for dating of glacial deposits. Geomorphology 228, 382-397.

Denniston, R., Wyrwoll, K.-H., Polyak, V., Brown, J., Asmerom, Y., Wanamaker, A., LaPointe, Z., Cleary, D., Cugley, J., Woods, D., 2013. A Stalagmite record of Holocene Indonesian-Australian summer monsoon variability from the Australian tropics. Quat. Sci. Rev. 78, 155-168.

Desprat, S., Goni, M.F.S., Loutre, M.-F., 2003. Revealing climatic variability of the last three millennia in northwestern Iberia using pollen influx data. Earth Planet. Sci. Lett. 213, 63-78.

Domínguez-Villar, D., Wang, X., Cheng, H., Martín-Chivelet, J., Edwards, R.L., 2008. A high-resolution late Holocene speleothem record from Kaite Cave, northern Spain: $\delta^{18}O$ variability and possible causes. Quat. Int. 187, 40-51.

Dorale, J., Edwards, R.L., Ito, E., Gonzalez, L., 1998. Climate and Vegetation History of the Midcontinent from 75 to 25 ka: A Speleothem Record from Crevice Cave, Missouri, USA. Science 282, 1871-1874.

Dorale, J., Edwards, R.L., Alexander, E.C., Shen, C.-C., Richards, D., Cheng, H., 2004., Uranium-series dating of Speleothems: Current Techniques, Limits, & Applications In: Sasowsky, I.D., Mylroie, J. (Eds.), Studies of Cave Sediments: Physical and Chemical Records of Paleoclimate. Kluwer Academic/Plenum Publishers, New York, pp. 177-197.

Epstein, S., Mayeda, T., 1953. Variation of $\delta^{18}O$ content in waters from natural sources. Geochim. Cosmochim. Acta 4, 213-224.

Esper, J., Frank, D., Buntgen, U., Verstege, A., Luterbacher, J., Xoplaki, E., 2007. Long-term drought severity variations in Morocco. Geophys. Res. Lett. 34, 1-5.

Fagan, B., 2000. The Little Ice Age: How Climate Made History. Basic Books, New York.

Fagan, B., 2008. The Great Warming. Bloomsberry Press, New York.

Fairchild, I., Smith, C., Baker, A., Fuller, L., Spotl, C., Mattey, D., McDermott, F., 2006. Modification and preservation of environmental signals in speleothems. Earth Sci. Rev. 75, 105-153.

Fairchild, I., A. Baker, 2012. Speleothem Science: From Process to Past Environments. Wiley-Blackwell, Oxford.

Fischer, A., 1981. Climatic oscillations in the biosphere in: Nitecki, M. (Ed.), Biotic Crises in Ecological and Evolutionary Time. Academic Press, New York, pp. 103-131.

Fischer H., Wahlen, M., Smith, J., Mastroianni, D., Deck, B., 1999. Ice core recordsof atmospheric CO2 around the last three glacial terminations. Science 283, 1712-1714.

Fischer, H., Kumke, T., Lohmann, G., Miller, H., Negendank, J., 2004. The Climate in Historical Times: Towards a Synthesis of Holocene Proxy Data and Climate Models. Springer-Verlag, Berlin.

Fleitmann, D., Burns, S., Mangini, A., Mudelsee, M., Kramers, J., Villa, I., Neff, U., Al-Subbary, A., Buettner, A., Hippler, D., Matter, A., 2007. Holocene ITCZ and Indian monsoon dynamics recorded in stalagmites from Oman and Yemen (Socotra). Quat. Sci. Rev. 26, 170-178.

Frappier, A., Sahagian, D., Gonzalez, L., Carpenter, S., 2002. El Nino Events Recorded by Stalagmite Carbon Isotopes. Science. 298, 565.

Frappier, A., Sahagian, D., Carpenter, S., Gonzalez, S., Frappier, B., 2007. Stalagmite stable isotope record of recent tropical cyclone events. Geology. 35, 111-114.

Friedman, I., Machta, L., Soller, R., 1962. Water vapor exchange between a water droplet and its environment. J. Geophys. Res. 67, 2761-2770.

Friedman, I., O'Neil, J., 1977. Data of Geochemistry, Sixth Edition. U.S. Government Printing Office, Washington, D.C.

Gallego, M., García, J., Vaquero, J., 2005. The NAO signal in daily rainfall seriesover the Iberian Peninsula. Clim. Res. 29, 103-109.

Gat, J., 1996. Oxygen and hydrogen isotopes in the hydrologic cycle. Annu. Rev. Earth Pl. Sc. 24,225-262.

Genty, D., Blamart, D., Ouahdi, R., Gilmour, M., Baker, A., Jouzel, J., Van-Exter, S., 2003. Precise dating of Dansgaard-Oeschger climate oscillations in western Europe from stalagmite data. Nature, 421, 833-837.

Graumlich, L., 1993. A 1000-year record of temperature and precipitation in the Sierra Nevada. Quat. Res. 39, 249-255.

Grove, J., 1988. The Little Ice Age. Methuen, London.

Heinrich, H., 1988. Origin and consequence of cyclic ice rafting in the northeast Atlantic Ocean during the past 130,000 years. Quat. Res. 29, 142-152.

Henderson, G., 2006. Caving into new Chronologies. Science 313, 620-622.

Hu, F., Ito, E., Brown, T., Curry, B., Engstrom, D., 2001. Pronounced climatic variations during the last two millennia in the Alaska Range. P. Natl. Acad. Sci. USA 98, 10552-10556.

Hurrell, J.,1995. Decadal Trends in the North Atlantic Oscillation: Regional Temperatures and Precipitation. Science.269, 676-679.

Hurrell, J., 1996. Influence of variations in extratropical wintertime teleconnections on Northern Hemisphere temperature. Geophy. Res. Lett. 23, 665-668.

Hurrell, K., Kushnir, T., Ottersen, G., Visbeck, M., 2003. An Overview of the North Atlantic Oscillation. Geophys. Monogr. 134, 1-35.

Hurrell, James & National Center for Atmospheric Research Staff (Eds.). Last modified 05 Sept 2014. “The Climate Data Guide: Hurrell North Atlantic Oscillation (NAO) Index (station-based.” Retrieved from https://climatedataguide.ucara.edu/climate-data/hurrell-north-atlantic-oscillation-nao-index-station-based.

Imbrie, J., Berger, A., Boyle, E.,Clemens, S., Duffy, A., Howard, W., Kukla, G., Kutzbach, J., Martinson, D., McIntyre, A., Mix, A., Molfino, B., Morley, J., Peterson, L., Pisias, N., Prell, W., Raymo, M., Shackleton, N., Toggweiler, J., 1993. On the structure and origin of major glaciation cycles. 2. The 100,000-year cycle. Paleoceanography 8, 699-735.

IPCC, 2013. Fifth Assessment Report (AR5), Climate Change 2013: The Physical Science Basis. Contribution of Work Group I to the Fifth Assessment Report of the Intergovernmental Panel on Climate Change, Cambridge Press, Cambridge, United Kingdom and New York, NY, USA. 1552 pp.

Jones, P., Briffa, K., Osborn, T., Lough, J., van Ommen, T., Vinther, B., Luterbacher, J., Wahl, E., Zwiers, F., Mann,M., Schmidt, G., Ammann, C., Buckley, B., Cobb, K., Esper, J., Goosse, H., Graham, N., Jansen, E., Kiefer, T., Kull, C., Kuttel, M., Mosley-Thompson, E., Overpeck, J., Riedwyl, N., Schulz, M., Tudhope, A., Villalba, R., Wanner, H., Wolff, E., Xoplaki, E., 2009. High-resolution palaeoclimatology of the last millennium: a review of current status and future prospects. Holocene 19, 3-49.

Kirschvink, J., 1992. Late Proterozoic low-latitude global glaciation: The Snowball Earth. In: J. W. Schopf and C. C. Klein (Eds.) The Proterozoic biosphere: A multi-disciplinary study. Cambridge University Press, Cambridge.

Knauth, L., 2005. Temperature and salinity history of the pre-Cambrian ocean: Implications for the course of microbial evolution. Palaeogeography, Palaeoclimatology, Palaeoecology 219, 53-69.

Lachniet, M., 2009. Climatic and environmental controls on speleothem oxygen-isotope values. Quat. Sci. Rev. 28, 412-432.

Ladurie, E., 1971. Times of feast, times of famine. Doubleday, New York.

Lamb, H., 1965. The Early Medieval Warm Epoch and its Sequel. Palaeogeography, Palaeoclimatology, Palaeoecology. 1, 13-37.

Lamb, H., 1977. Climate History and the Future. Princeton University Press, Princeton, NJ.

LeGrande, A.N., Schmidt, G.A., 2006. Global gridded data set of the oxygen isotopic composition in seawater. Geophys. Res. Lett. 33, L12604, doi:10.1029/2006GL026011.

Lehner, F., Raible, C., Stocker, T., 2012. Testing the robustness of a precipitation proxy-based North Atlantic Oscillation reconstruction. Quat. Sci. Rev. 45, 85-94.

Lehman, S., 1993. Ice sheets, wayward winds, and sea change. Nature 365, 108-109.

Luterbacher, J., Schmutz, C., Gyalistras, D., Xoplaki, E., Wanner, H., 1999. Reconstruction of monthly NAO and EU indices back to AD 1675. Geophys. Res. Lett. 26, 2745-2748 .

Mann, M., Bradley, R., Hughes, M., 1998. Global scale temperature patterns and climate forcing over the past six centuries. Nature 392, 779-788.

Mann, M., Bradley, R., Hughes, M., 1999. Northern hemisphere temperatures during the past millennium: Inferences, uncertainties, and limitations. Geophys. Res. Lett. 26, 759-762.

Mann, M., Bradley, R., Hughes, M., 1999. Northern Hemisphere temperatures during the past millennium: Inferences, uncertainties, and limitations. Geophys. Res. Lett. 26, 759-762.

Martín-Chivelet, J., Muñoz-García, M., Edwards., L., Turrero, M., Ortega, A., 2011. Land surface temperature changes in Northern Iberia since 4000 yr BP, based on $\delta^{13}C$ of speleothems. Global Planet. Change 77, 1-12.

Maslin, M, Ridgwell, A., 2005. Mid-Pleistocene revolution and the "Eccentricity myth." Geological Society of London, Special Publications. 247, 19-34.

Mattey, D., Lowry, D. Duffet, J., Fisher, R., Hodge, E., Fisia, S., 2008. A 53 year seasonally resolved oxygen and carbon isotope record from a modern Gilbraltar speleothem: reconstructed drip water and relationship to local precipitation. Earth Planet. Sci. Lett. 269, 80-95.

Mayewski, P., Rohling, E., Stager, J., Karlen, W., Maasch, K., Meeker, L., Meyerson, E., Gasse, F., van Kreveld, S., Holmgren, K., Lee-Thorp, J., Rosqvist, G., Rack, F., Staubwasser, M., Schneider, R., Steig, E., 2004. Holocene Climate Variability. Quat. Res. 62, 243-255.

McDermott, F., 2004. Paleoclimate reconstruction from stable isotope variations in speleothems: A review. Quat. Sci. Rev. 23, 901-918.

McGee, D., Quade,J., Ewards, R.L., Broecker, W., Cheng, H., Reiners, P., Evenson, N., 2012. Lacustrine cave carbonates: Novel archives of paleohydrologic change in the Bonneville Basin, Utah, USA). Earth Planet. Sci. Lett. 351-352,182-194.

Oeschger, H., Beer, J., Siegenthaler, U., Stauffer, B., Dansgaard, W., Langway, C., 1984. North Atlantic climate oscillations revealed by deep Greenland ice cores. In: Hansen, J., Takahashi, T. (Eds.) Climate Processes and Climate Sensitivity. American Geophysical Union, Washington, D.C., pp. 299-306.

O'Neil, J., Clayton, R., Mayeda, T., 1969. Oxygen isotope fractionation in divalent metal carbonates. J. Chem. Phys. 51, 5547-5557.

Paillard, D., 2015. Quaternary glaciations: from observations to theories. Quat. Sci. Rev. 107, 11-24.

Petit, J., Jouzel, J., Raynaud, D., Barkov, N., Barnola, J.-M., Basile, I., Bender, M., Chappellaz, J., Davis, M., Delaygue, G., Delmotte, M., Kotlyakov, V., Legrand, M., Lipenkov, V., Lorius, C., Pepin, L., Rita, C., Saltzman, E., Stievenard, M., 1999. Climate and atmospheric history of the past 420,000 years from the Vostok ice core, Antarctica. Nature 399, 429-436.

Ruddiman, W., 1977. Late Quaternary deposition of ice-rafted sand in the subpolar North Atlantic (lat 40^{o} to 65^{o}N). Geological Society of America Bulletin 88, 1813-1827.

Seppa, H., Birks, H., 2002. Holocene climate reconstructions from the Fennoscandian tree-line area based on pollen data from Toskaljavri. Quat. Res. 57, 191-199.

Sharp, Z., 2007. Principles of Stable Isotope Geochemistry. Pearson Prentice Hall, Upper Saddle, NJ.

Shackleton, N., 1967. Oxygen isotope analyses and Pleistocene temperature re-assessed. Nature 215, 15-17.

Trigo, R., Zezere, J., Rodrigues, M., Trigo, I., 2005. The Influence of the North Atlantic Oscillation on Rainfall Triggering of Landslides near Lisbon. Nat. Hazards 36, 331-354.

Trouet , V., Esper, J., Graham, N.E., Baker, A., Scourse, J.D., Frank, D.C., 2009. Persistent positive North Atlantic Oscillation mode dominated the Medieval climate anomaly. Science 324, 78-80.

Vaks, A., Gutareva, O., Breitenbach, S., Avirmed, E., Mason, A., Thomas, A., Osinzev, A., Kononov,A., Henderson, G., 2013. Speleothems Reveal 500,000-Year History of Siberian Permafrost. Science 12, 183-186.

Wallace, J., Gutzler, D., 1981. Teleconnections in the Geopotential Height Field during the Northern Hemisphere Winter. Mon. Weather Rev. 109, 784-812.

Wanamaker, A., Hetzinger, S., Halfar, J., 2011. Reconstructing mid- to high- latitude marine climate and ocean variability using bivalvaes, coralline algae, and marine sediment cores from the Northern Hemisphere. Palaeogeography, Palaeoclimatology, Palaeoecology 302, 1-9.

Wang, Y.J., Cheng, H., Edwards, R.L., An, Z.S., Wu, J.Y., Shen, C.-C., Dorale, J.A., 2001. A High-Resolution Absolute-Dated Late Pleistocene Monsoon Record from Hulu Cave, China. Science. 294, 2345-2348.

Yuretich, R., Melles, M., Sarata, B., Grobe, H., 1999. Clay Minerals in the Sediments of Lake Baikal: A Useful Climate Proxy. J. Sediment. Res. 3, 588-596.

Zachos , J., Wara, M., Bohaty, S., Delaney, M., Petrizzo, M., Brill, A., Bralower, T., Premoli-Silva, I., 2003. A transient rise in tropical sea surface temperature during the Paleocene-Eocene thermal maximum. Science 302, 1551-1554.

Zachos, J., Kump, J., 2005. Carbon cycle feedbacks and the initiation of Antarctic glaciation in the earliest Oligocene. Global Planet. Change 47, 51-66.

Zhang, J., Crowley, T., 1989. Historical climate records in China and reconstruction of past climates. J. Clim. 2, 833-849.

Zhang, H., Cai, Y., Tan,L., Cheng, H., Qin, S., An, Z., Edwards, R.L., Ma, L., 2015. Large variations of $\delta^{13}C$ values in stalagmites from southeastern China during historical times: implications for anthropogenic deforestation. Boreas 44, 1-15.

CHAPTER 2: INFERRED HYDROCLIMATE FROM PORTUGUESE SPELEOTHEM RECORD DURING THE MEDIEVAL CLIMATE ANOMALY AND LITTLE ICE AGE

A paper to be submitted to Earth and Planetary Science Letters

Diana L. Thatcher[1], Alan D. Wanamaker[1], Rhawn F. Denniston[2], Yemane Asmerom[3], Victor J. Polyak[3]

[1]Iowa State University, Ames, Iowa

[2]Cornell College, Mount Vernon, Iowa

[3]University of New Mexico, Albuquerque, New Mexico

Abstract

The hydroclimate of the Iberian Peninsula has been suggested to be persistently dry during Medieval times due to a persistently positive North Atlantic Oscillation (NAO) mode (Trouet et al., 2009). However, modeling results and proxy records from the region indicate that substantial wet intervals likely occurred. We present a sub-decadal stable isotope record from a calcite stalagmite (Buraca Glorioso, 39^{o}N, 8^{o}W) showing an inferred variable hydroclimate during Medieval times (~800 to 1300 AD) during the Medieval Climate Anomaly (MCA). Calcite $\delta^{18}O$ values at this location are dependent on the relative amounts of precipitation received. Drier (wetter) conditions would lead to more (less) evaporation during precipitation events and higher (lower) $\delta^{18}O$ values. Winter precipitation in Portugal is strongly dependent on the behavior of the NAO and this record has important implications for study of the NAO and its behavior in the past. In this study $\delta^{18}O$ and $\delta^{13}C$ records from Portugal are compared with other proxy records from Morocco, Spain, and Scotland. Although this $\delta^{18}O$ and $\delta^{13}C$ record implies positive NAO conditions throughout much of the MCA, precipitation appears to have

been more variable at this location than would be suggested by the NAO reconstruction of Trouet et al. (2009).

1 Introduction

The North Atlantic Oscillation (NAO) is the dominant mode of atmospheric variability in the north Atlantic region (Hurrell, 1995) and influences Northern Hemisphere precipitation and temperature patterns (Hurrell and Van Loon, 1997), especially winter precipitation patterns (Hurrell et al., 2003). The NAO is defined as the normalized difference in atmospheric sea level pressure between the Icelandic low and the Azores high (Rogers, 1984) and is often measured using with sea level pressure measurements from Reykjavik, Iceland and Lisbon, Portugal. A NAO positive mode (high NAO index) is characterized by a deepened Icelandic low and strengthened Azores high which causes increased westerlies allowing storms to cross northern Europe and leaves southern Europe (including Portugal) dry. The NAO negative mode (low NAO index) is characterized by a relaxed pressure gradient and decreased westerlies which allows storms to have a more southern track. Southern Europe (including Portugal) is wetter and northern Europe is drier. Instrumental data have been used to calculate the NAO index since 1864 and proxy reconstructions for the past hundreds and thousands of years allow for a better understanding of the natural variability of the NAO system.

A recent NAO reconstruction (Trouet et al., 2009) presented a 947-year long record using a precipitation-sensitive speleothem record from NW Scotland (Proctor et al., 2000) and a tree ring- based Palmer Drought Severity Index reconstruction from Morocco (Esper et al., 2007). The main finding of this reconstruction was the presence

of a persistently positive NAO index (see Figure 1-3) during the Medieval Climate Anomaly (MCA), roughly the years 800 to 1300 AD (Trouet et al., 2009). The Trouet et al. (2009) reconstruction suggested that the Medieval Climate Anomaly was dominated by persistently positive NAO conditions for almost 400 years yet modeling results (Lehner et al., 2012) have not been able to reproduce such results for this time period. Such persistency of the NAO regime has not been seen in modern instrumental records (Pinto and Raible, 2012) as the NAO has shown variability on a quasi-biennial and quasi-decadal time scale (Hurrell and Van Loon, 1997). The results of Trouet et al. (2009) need further verification from precipitation-sensitive climate proxies – and ideally from proxies that are located in an area consistently under the influence of the NAO, such as the proxies employed in the work presented here.

In the current study, $\delta^{18}O$ and $\delta^{13}C$ isotopes are investigated from a stalagmite from central Portugal. The record of this stalagmite covers the time period 653 BC to 1790 AD although this manuscript will primarily focus on the time since ~800 AD. The cave is sensitive to precipitation and the precipitation in the area is sensitive to the behavior of the NAO (Figure 2-1).

The goals of this study are to (1) develop an oxygen and carbon isotope record from a stalagmite from Portugal along with environmental data from inside and outside of the cave; (2) to compare this proxy record with others from near the southern node of the NAO and to contrast this proxy record with other records from near the northern node of the NAO; and (3) to assess the behavior of the NAO during Medieval times and

the Little Ice Age (LIA) and the possible presence of a persistently positive NAO mode throughout the MCA.

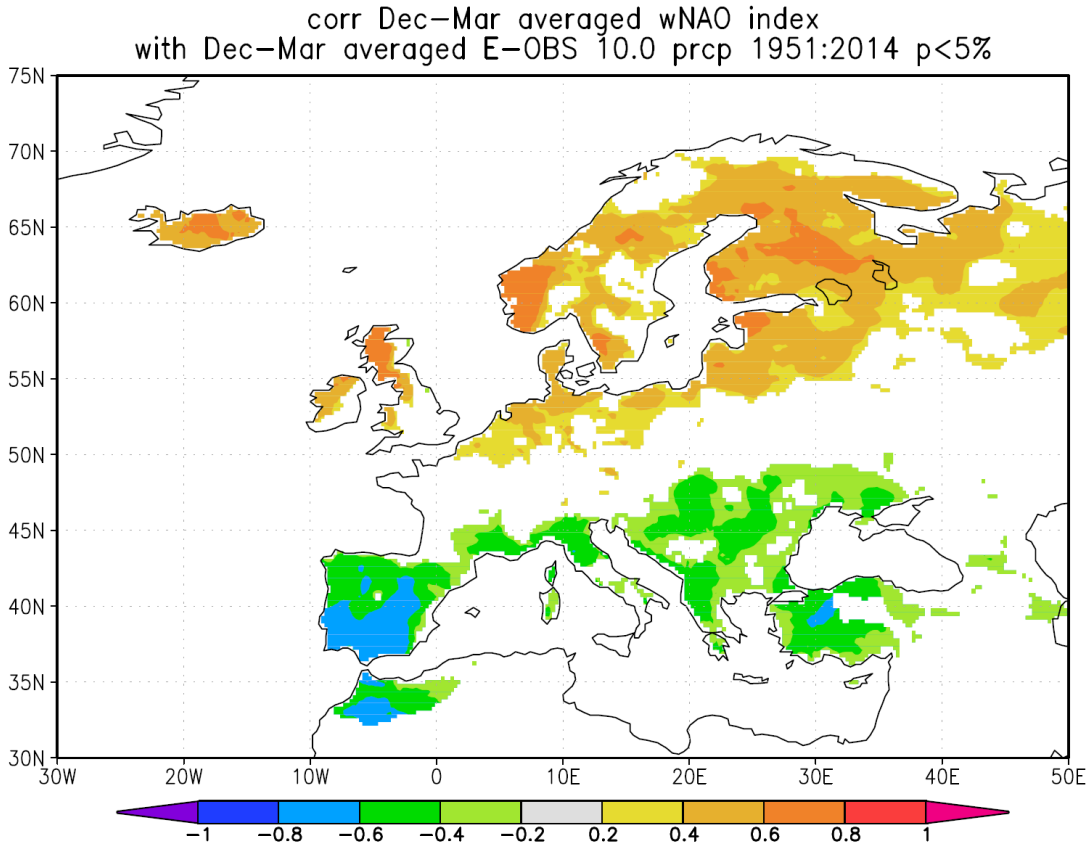

Figure 2-1. Time-averaged December – March precipitation correlated (r-values) with time-averaged wNAO index. Note high anti-correlation values in Portugal. Higher wNAO index = lower precipitation amounts for Portugal. (KMNI Climate Explorer - climexp.knmi.nl)

2 Case setting

2.1 Present day climate of the Iberian Peninsula

The Iberian Peninsula is principally comprised of the countries Spain and Portugal and is bounded by the Atlantic Ocean to the west and the Mediterranean Sea to the east. The Iberian Peninsula is situated in close proximity to other European

countries as well as those of northern Africa, allowing for comparisons between our location and that of other, long-term proxy records.

The Iberian Peninsula (approx. 38-42^{o}N latitude, 2-10^{o}W long) is situated in an ideal location for studying the NAO, the primary mode of variability in the North Atlantic region. Much of the precipitation in the region is derived from Atlantic moisture and storms coming from the Atlantic Ocean. Occasional storms from a general easterly direction cause light amounts of precipitation in the region to have a Mediterranean source. A change in the precipitation source location would change the $\delta^{18}O$ values of the resulting precipitation, as the $\delta^{18}O$ values of the ocean/sea water are different for the Atlantic Ocean and Mediterranean Sea (LeGrande and Schmidt, 2006). Because Mediterranean precipitation events are light in nature and rare, moisture to the cave from these events is negligible and will not be considered with this record.

The climate of the country of Portugal is split between cool summer (Csb) Mediterranean and hot summer (Csa) Mediterranean (Köppen Climate Classification). Buraca Glorioso is located in the hot summer Mediterranean climate which indicates average temperature in the warmest month above 22 ^{o}C and at least four months averaging above 10^{o}C. There is a strong seasonal component to the climate of Portugal, with dry summers and wet winters (October-April). Annual rainfall at nearby stations averages (30-year average) range from 660 mm in Monte Real (56 m asl) and 697mm in Santarem (107 m asl) to 840mm in Alcobaça (38 m asl). Rainfall is seasonal in central Portugal, with > 77% of rainfall occurring from October to March and > 45% of rainfall occurring during the winter timeframe – December to March. This strong seasonality in

precipitation gives rise to winter being the rainiest season while the transitional seasons, spring and fall, are the most irregular (Santos et al., 2015). Summer precipitation is irregular and scarce (Santos et al., 2015) and, for this cave location, may not contribute to cave drip water.

Storm tracks and resulting rainfall amounts and patterns are highly correlated with the strength and position of the Azores high and are intricately linked to the behavior of the NAO (Hurrell, 1996; Thompson, 2000). During negative NAO index conditions, Portugal is in a wetter precipitation mode due to the weakening of the westerlies and the subsequent southerly shift in the storm track in Europe. During positive NAO index conditions, Portugal experiences drier conditions due to the strengthening of the westerlies across Europe which sends storms from the Atlantic across northern Europe and leaves the Iberian Peninsula and Portugal dry.

2.2 Cave Setting

The principal speleothem of interest to this study is GH-13-6 and was collected from Buraca Glorioso in August 2013. Buraca Glorioso is located at an altitude of 425 m asl above sea level. Vegetation near the cave consists of olive trees, Mediterranean aromatic flora, thorny plants, small shrubs and grasses. The vegetation above the cave consists of similar species, thin soil, and abundant vegetation. Drip water comes into the cave from precipitation falling on rocks above the cave. The drip water travels approximately 30-40 meters through the overlying rock before entering the cave. The entrance to the cave is about 1 meter wide and 0.5 m high. The cave is formed in limestone rock and the ground surrounding the cave is littered with marine shells.

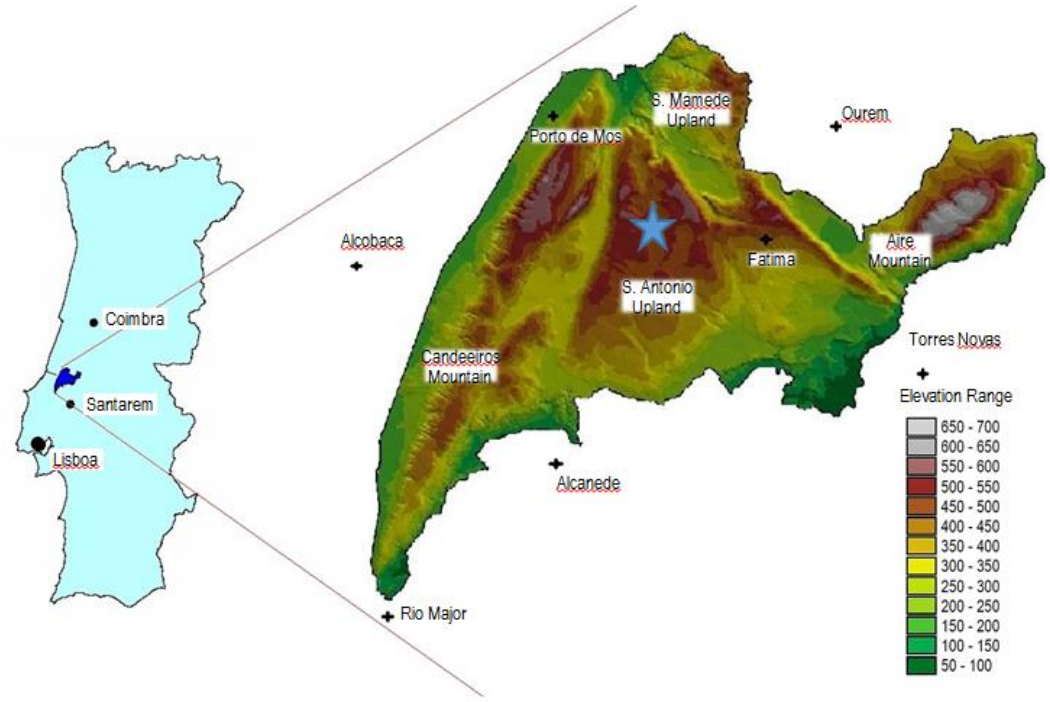

Figure 2-2. Map of Portugal with location of Estremadura Limestone Massif highlighted and cave location indicated by a star. (www.mindat.org)

Buraca Glorioso is a cave formed in Mesozoic limestone, located in west central Portugal (see Figure 2-2) in a topographically distinctive area known as the Estremadura Limestone Massif (ELM) that makes up the center portion of the country (Rodrigues and Fonseca, 2010). Rodrigues and Fonseca (2010) consider it the most important karst relief in Portugal. The ELM is 20 km from the Atlantic Ocean and about 100 km from Lisbon. The most important topographical features of the area are formed by mainly compact limestones, oolitic limestones, and dolomitic limestones (Almeida et al., 1995). These limestones are mid-Jurassic in age and formed by a shallow, epicontinental sea (Almeida et al., 1995). The highly soluble limestone rock is a large aquifer and contains abundant fossils, active conduits and both surface and underground karst formations (Rodrigues and Fonseca, 2010). This entire region underwent an important and long-

lasting uplift (beginning approximately 100Ma) during the late Cretaceous to Paleogene (Pais et al., 2012). The exact mechanism of this uplift is not well understood, however, it is likely related to late Cretaceous magmatism triggered by crustal thickening, the Pyrenean orogeny, and/or the counter-clockwise movement of Iberia, eventually related to the Pyrenean orogeny (Pais et al., 2012).

3 Materials and methods

3.1 Stalagmite

Stalagmite GH-13-6 from Buraca Glorioso (Figure 2-3) has a total length of 43.7 cm and was growing in an upper loft room about 30 meters from the entrance to the cave and 3-4 meters higher than the main cave chamber. This stalagmite was chosen due to its cylindrical geometries and apparent high crystal density. The upper 10 cm of the stalagmite has been sampled at 1 mm and 200 μm resolution along the vertical growth axis, perpendicular to the layers of growth. The uppermost 5 cm will be the focus of this manuscript. The remaining 5 cm of micromilled samples will be the focus of future work and is discussed in Chapter 3 of this manuscript.

Figure 2-3. Stalagmite GH-13-6 from Buraca Glorioso. Note change in calcite texture (arrow).

3.2 Cave monitoring

Monitoring of the cave and surrounding area near Buraca Glorioso began in August 2013 with temperature, relative humidity, and pressure sensors (Onset HOBO data loggers, see appendix B) being installed at two locations inside the cave and one location directly outside the entrance to the cave. Data have been and continue to be collected every 2 hours. Additional monitoring devices were installed in June 2014 with an additional temperature, relative humidity, and pressure sensor installed inside the cave and a drip counting device (Stalagmate, see appendix B) installed in the location formerly occupied by GH-13-6, the stalagmite of interest in this research. Drip counts are collected every thirty minutes and drip water is collected in a 2-L beaker, outfitted with 6 liters of storage capacity. This drip water was analyzed at the Iowa State University Stable Isotope Laboratory for oxygen and hydrogen isotopes on a Piccaro

L1102-I Isotopic Liquid Water Analyzer with autosampler. More details provided on these monitoring systems in the appendix of this manuscript.

3.3 U/Th stalagmite chronology

Sixteen samples of GH-13-6 were dated using uranium-thorium disequilibrium methods following the methods of Denniston et al. (2013). These sixteen samples were analyzed with a Thermo-Neptune multi-collector inductively coupled plasma mass spectrometer (MC-ICP-MS) at the University of New Mexico Radiogenic Isotope Laboratory. Samples, ranging from 102 to 116 mg in size, were hand milled along a growth band to minimize time-averaging of the sample. Once milled, samples were transferred to Teflon beakers. Powders were dissolved in 15N nitric acid, spiked with a ^{229}Th-^{233}U-^{236}U tracer, and the solution was dried on a hot plate. Samples were re-dissolved in 15N nitric acid and standard column chemistry methods were performed to isolate uranium and thorium. The isolated uranium and thorium samples were redissolved in nitric acid. Thirty-two samples (sixteen of U, sixteen of Th) were aspirated into the MC-ICP-MS using a Cetac Aridus II low flow desolvating nebulizer system. An age-depth model was calculated following the method of Edwards et al. (1986). Uncertainty is given as two standard deviations and ages are adjusted to the year AD 2013 as present. Decay constants are those given by Cheng et al. (2000) and unsupported ^{230}Th was corrected by applying an initial ^{230}Th/^{232}Th value of 10ppm+/-5ppm, higher than the average crustal silicate ^{230}Th/^{232}Th value of 4.4ppm+/-4.4ppm. The level of uranium in these samples is quite low (~60-110 ppb) and leads to large age

uncertainties relative to the age of these young samples (approximately +/-100 years for most samples).

3.4 Stable isotope analyses

The stalagmite was sectioned along the vertical growth axis using a water-cooled saw, polished and labeled. Hand (1 mm resolution) samples were obtained with a Dremel dental drill using Dremel bit (#105). Stable isotope data were collected from GH-13-6 by first hand milling powder at 1 mm resolution for the top 10 cm of the stalagmite along the central growth axis and every 10 mm over the rest of the stalagmite. Stable isotope ratios were obtained from these milled powder samples at the Stable Isotope Laboratory within the Department of Geological and Atmospheric Sciences at Iowa State University.

Sample sizes of 0.15 to 0.25 mg were analyzed in a ThermoFinnegan Delta Plus XL mass spectrometer coupled with a Gas Bench II and a CombiPal autosampler at the Stable Isotope Laboratory at Iowa State University. All oxygen and carbon isotopic values are presented in per mil (‰) relative to the Vienna PeeDee Belemnite carbonate standard. Precision was determined by analysis of standards (NBS-18, NBS-19, and LSVEC) interspersed among the samples. Approximately 1 standard was run for every 5 carbonate samples. Long term precision is less than 0.1‰ for oxygen and 0.06 ‰ for carbon.

3.5 Micromill sampling

Stable isotope data were also collected from micromilled samples collected every 200 µm across the top 10 cm of the stalagmite along the central growth axis. The

samples were milled using a Merchatek micromill outfitted with a Brasseler (835.11.010 medium flat end parallel diamond) milling bit. Micromill carbonate samples were analyzed following the procedure used with the 1 mm resolution samples.

3.6 Modern climate comparison

The Water Resources Programme of the IAEA (International Atomic Energy Agency) and the World Meteorological Organization (WMO) have been surveying stable hydrogen and oxygen isotopes and tritium composition in precipitation around the globe since 1961 (IAEA/WMO, 2004). Eight locations in mainland Portugal (plus 2 more in Azores) have been a part of the Global Network of Isotopes in Precipitation (GNIP) study and the results can be generally applied to determine relationships between hydrogen and oxygen isotopes and temperature and/or precipitation amounts. Lisbon was the site of collection by events from October 2002 to March 2003 – potentially indicative of longer-term winter relationships between isotopes and precipitation amounts and/or temperature. Monthly-binned records of various lengths of time are available for Lisbon as well as other GNIP sites in Portugal, the closest sites to Buraca Glorioso being Lisbon (115 km; 1 year record), Portalegre (139 km; 16 year record), Porto (208km; 16 year record), Penhas Douradas (248 km; 16 year record), Beja (257 km; 4 year record), and Vila Real (275 km; 4 year record).

4 Results

4.1 Cave monitoring

The temperature throughout the observation period inside the cave ranges from 13.9 ^{o}C in late winter (Feb-Mar) to 14.6 ^{o}C in late summer/fall (October). Outside the

cave, temperatures range from 32 ^{o}C (late summer) to 5 ^{o}C (winter). Outside the cave relative humidity varies seasonally, with lower values generally in the summer, over a yearly range from 25 to near 100 percent. Inside the cave, the variability in relative humidity is small or non-existent. Over the 15-month monitoring period, the cave relative humidity has remained at 100% with one small excursion to ~98% during December of 2013.

Drip counts have been measured in Buraca Glorioso for six months, beginning June 2014 with data collected in November 2014. The minimum in drip counts occurred in late summer/early fall with daily drip counts near 277 drips per day. The peak during this six month monitoring period occurred in late November with a drip count of 787 drips per day.

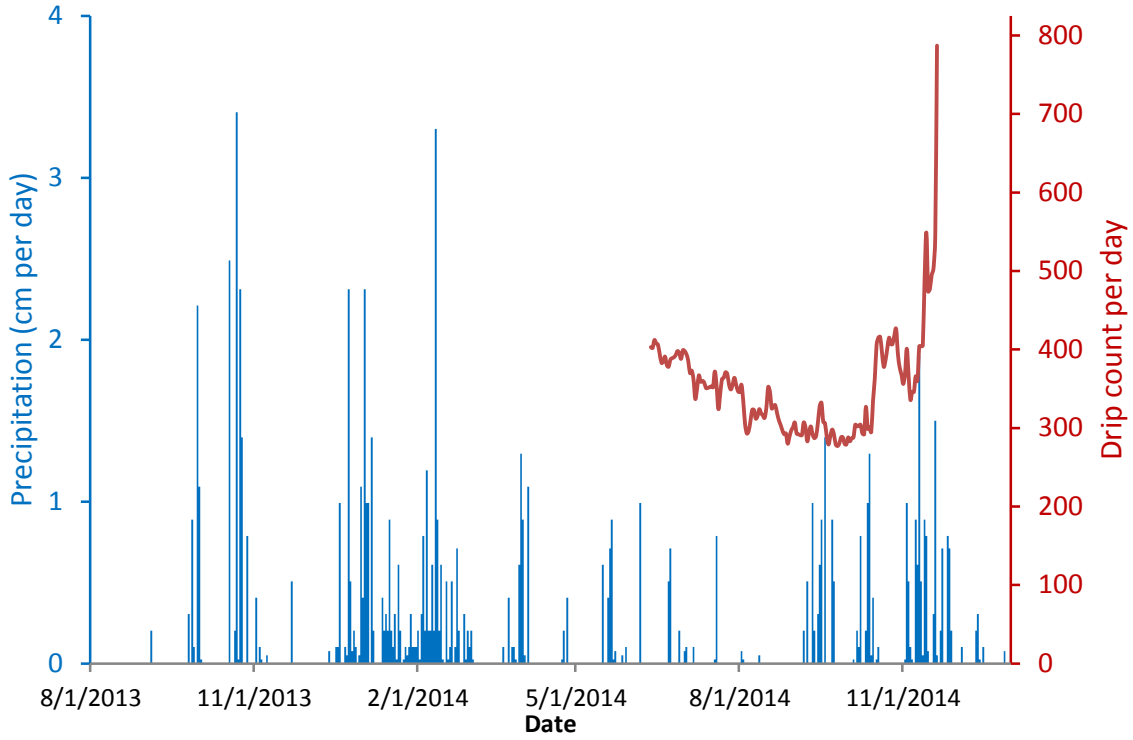

Figure 2-4. Local precipitation amounts (shown in blue) from Monte Real, Portugal (57 km from cave), August 2013 to December 2014, and Buraca Glorioso drip counts (shown in red), June 2014 to November 2014. (Monte Real precipitation data – www.wunderground.com)

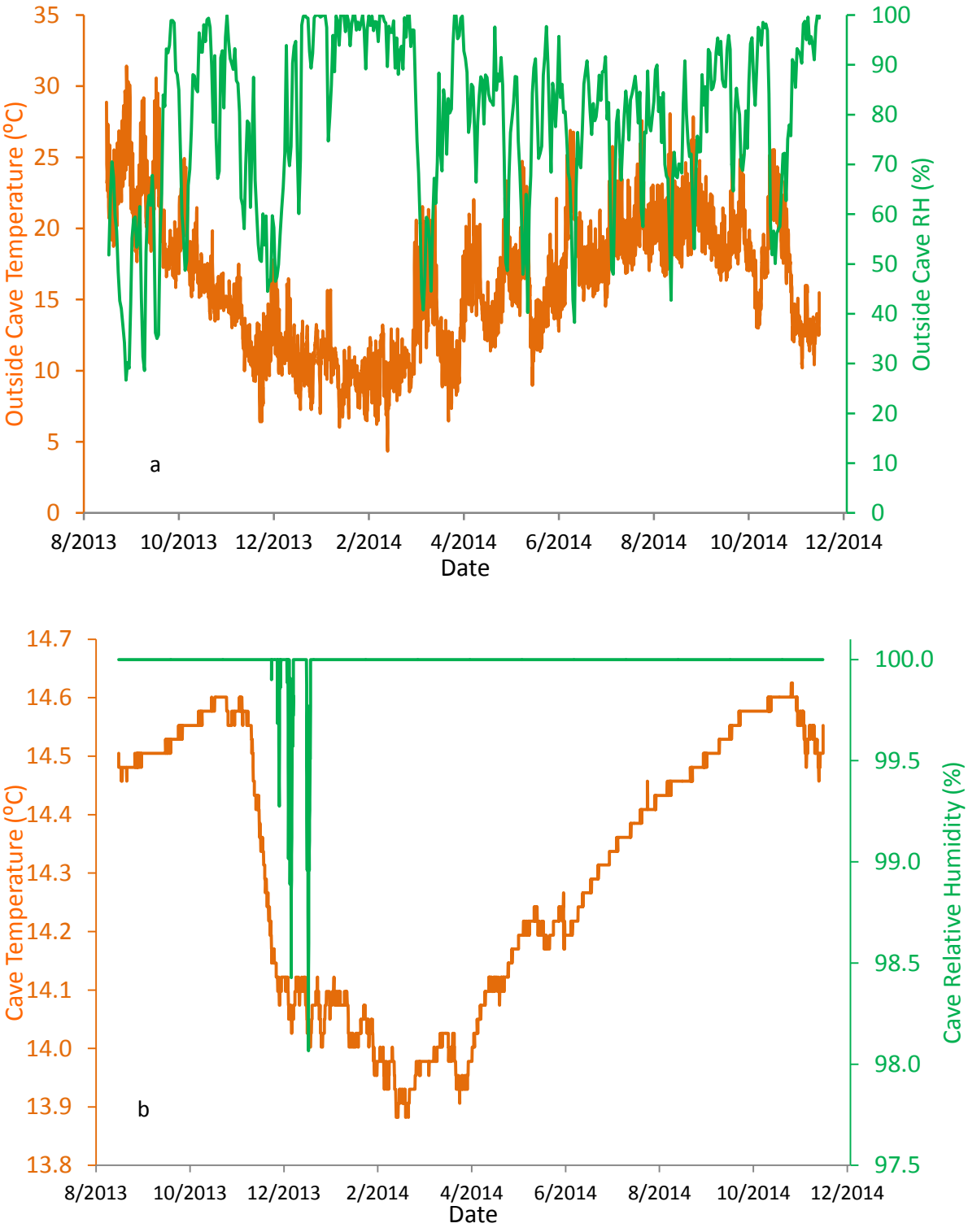

Figure 2-5. Outside (a) and inside (b) of Buraca Glorioso temperature (orange) and relative humidity (green), August 2013 to November 2014.

4.2 Age-depth model

Stalagmite GH-13-6 was wet and was actively being dripped on at the time collection in August 2013. However, sixteen U-Th dates, including one sample 5 mm from the top of the stalagmite, do not strongly indicate modern growth of the stalagmite. The linear-fit age-depth model presented in Figure 2-6 indicates the top is 223 yrs BP (present = 2013), approximately 1790 AD.

Growth rates are determined from the resolution of micromilled samples and uranium-thorium age-model data. Assuming linear growth, ages can be assigned to each 200 µm micromill samples. The growth rate over the 2337 year (2616 yr BP-223 yr BP, from the oldest U-Th date obtained and linear fit y-intercept of the age model indicating the age of the stalagmite top, respectively) period of study averages 40 µm/year. A high density of high-precision dates defines this nearly linear growth history, but two dates fall outside of the error window and were not used in the age-depth model (Figure 2-6).

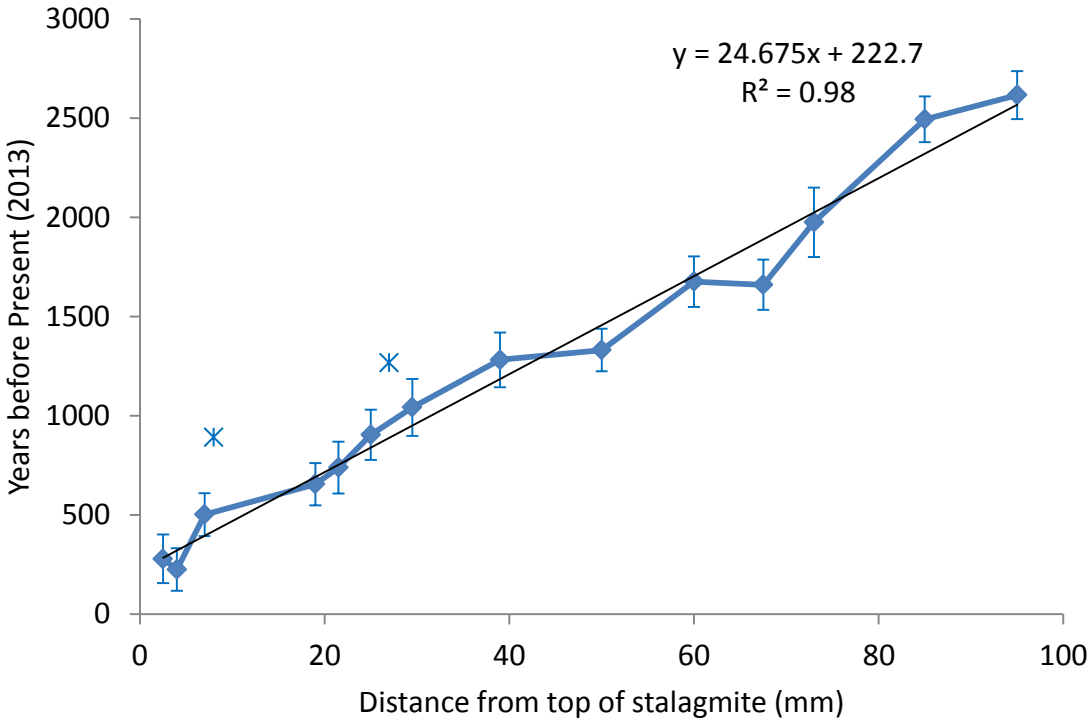

Figure 2-6. Buraca Glorioso GH-13-6 age-model (blue) derived from Uranium-Thorium disequilibrium methods. A linear fit model (black) was used providing a y-intercept of 223 years before present as the age of the stalagmite top (1790 AD). Two ages were not used in the linear fit (star symbols).

4.3 Stable isotopes

The temporal resolution for the micromilled samples is decadal to sub-decadal, generally 5 years of time-averaged growth per micromill sample. Over the entire record, the average $\delta^{18}O$ value is -2.44 ‰ and the average $\delta^{13}C$ value is -3.04 ‰. The complete record is characterized by many small (< 1.0‰) variations with several large (≥ 2.0‰) changes in both oxygen and carbon isotopes, occurring 100 BC to 0, 1200 to 1300 AD, and 1700 to 1800 AD. The $\delta^{13}C$ record shows additional large changes, not seen in the oxygen record, during the LIA interval. During one of these large isotopic changes (both $\delta^{18}O$ and $\delta^{13}C$), 1200 to 1300 AD, there is also a visual change in the calcite

composition (Figure 2-1). Some correlation exists between the oxygen and carbon records and some large changes occur in both records at approximately the same time (R^2=0.38; p-value < 0.001). 10-year averaged values of $\delta^{18}O$ and $\delta^{13}C$ have an R^2 value of 0.39 (p-value = 0.0016) and 20-year averaged values have an R^2 value of 0.42 (p-value <0.001).

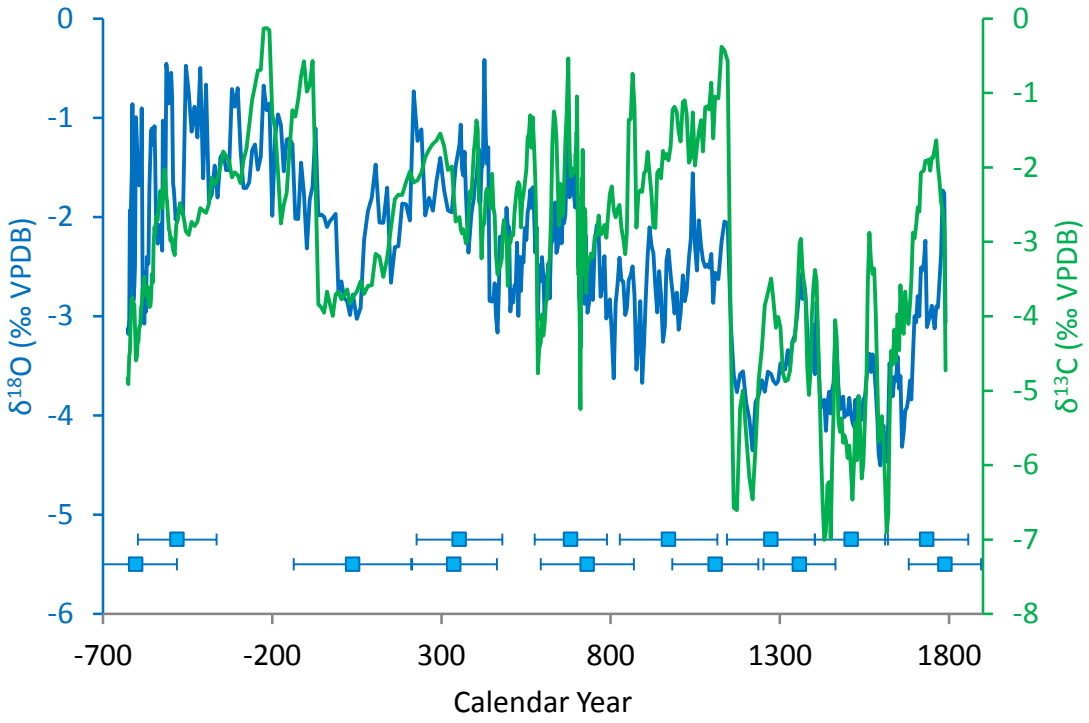

Figure 2-7. Micromill $\delta^{18}O$ (blue) and $\delta^{13}C$ (green) data from Buraca Glorioso (stalagmite GH-13-6) covering the entire speleothem record, 653 BC to 1790 AD. Ages and uncertainties determined by U-Th methods are indicated by blue box plots.

The oxygen isotope data during Medieval times (800-1300 AD) ha an average value of -2.90 ‰ with lowest values of -4.35 ‰ and highest values during the MCA of -1.56 ‰. The carbon isotopes show an average value of -2.72 ‰ during the MCA with the highest $\delta^{13}C$ value of -0.39 ‰ and the lowest $\delta^{13}C$ value of -6.61 ‰. The $\delta^{18}O$ and $\delta^{13}C$ record during the MCA and LIA is shown in Figure 2-8.

Micromilled data for the time period covering the MCA and LIA show two distinct regimes of $\delta^{18}O$ values and variability within each regime. The Little Ice Age (1450-1850 AD) average values for $\delta^{18}O$ and $\delta^{13}C$ are -3.53‰ and -4.21‰, respectively, significantly different from the average values of $\delta^{13}C$ and $\delta^{18}O$ for the MCA (-2.90 ‰ and -2.72 ‰, respectively).

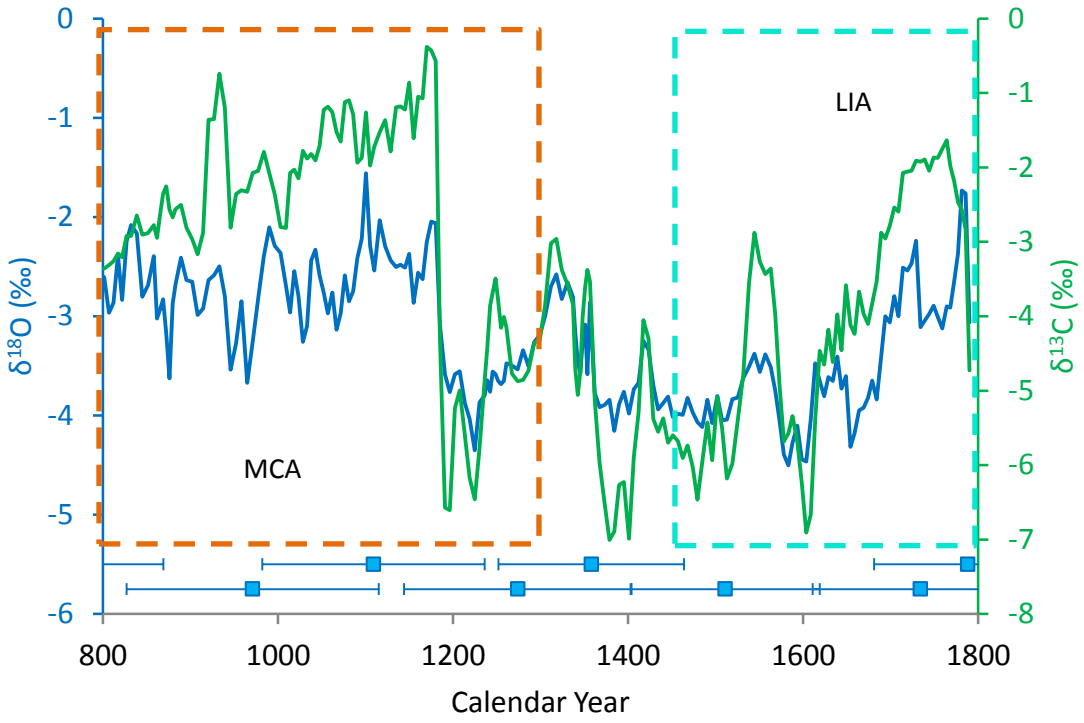

Figure 2-8. MCA and LIA $\delta^{18}O$ (blue) and $\delta^{13}C$ (green) micromill data – subset of all data. Climate intervals shown are those defined by Trouet et al., 2009.

4.4 Controls on $\delta^{18}O$ of precipitation/Precipitation Isotopes

Precipitation isotopes were recorded at numerous locations in Portugal over the past 30 years. At the two closest GNIP sites to Buraca Glorioso, Porto and Lisbon, monthly–averaged precipitation was collected for 16 years and 1 year, respectively. At Lisbon, precipitation event data was also collected daily for 6 months between 2002 and 2003.

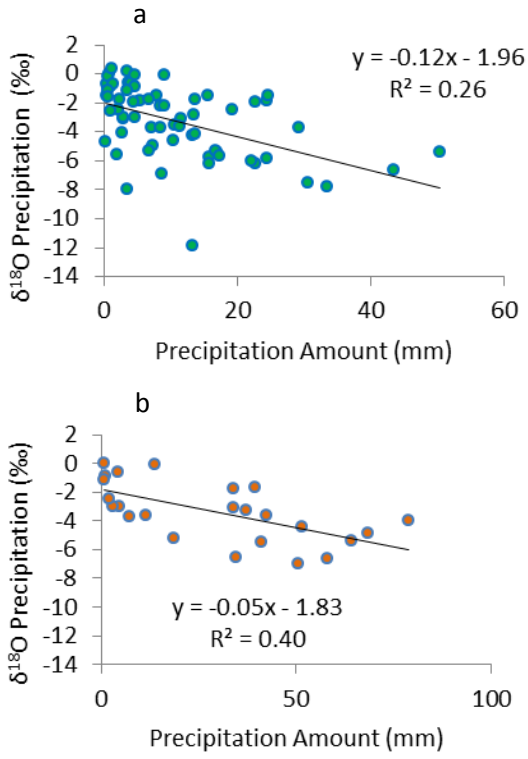

Figure 2-9. (a) Daily-binned precipitation amount data for Lisbon and (b) Event-binned precipitation amount data for Lisbon – correlations between $\delta^{18}O$ of precipitation and amount of precipitation. Precipitation events October 2002-March 2003 (GNIP data source – IAEA) (p-values < 0.001 for both relationships).

Rainfall in Porto, collected for 16 years, provides a relationship between $\delta^{18}O$ and precipitation amount (Figure 2-9a) which implies that a 16mm increase in monthly precipitation would decrease the $\delta^{18}O$ monthly value by 0.2 ‰ or -0.0125 ‰/mm. Similarly, a 1 ^{o}C decrease in temperature (at which the precipitation is falling) leads to a 0.2 ‰ decrease in $\delta^{18}O$ values. Since most of the precipitation in Portugal falls at the time of the year when temperatures are the lowest, it is difficult to be certain which factor (precipitation amount or temperature) is influencing the $\delta^{18}O$ values most significantly. In Porto, the relationship between $\delta^{18}O$ and precipitation amount and the relationship between $\delta^{18}O$ and temperature give similar R^2 values (Figure 2-10).

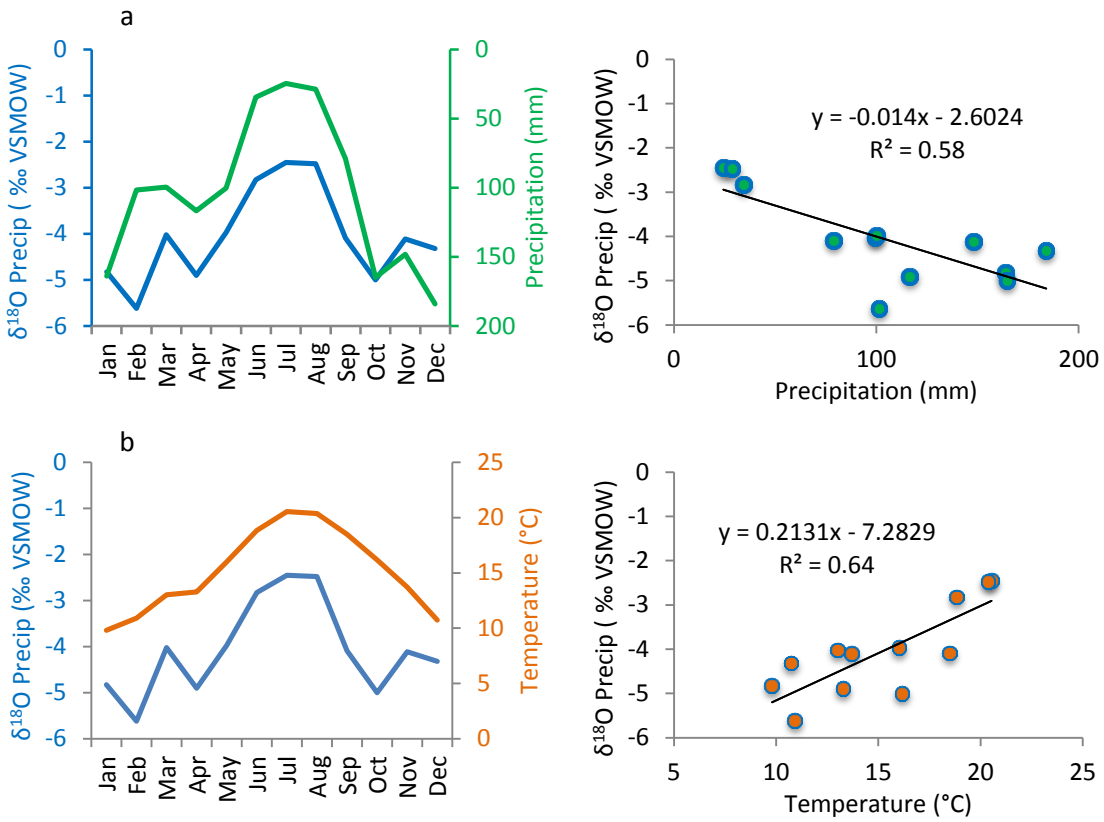

Figure 2-10. Plots of 16 years of monthly averaged GNIP data for Porto (monthly data) showing the relationship between (a) precipitation amount (p-value = 0.00039) and $\delta^{18}O$ of precipitation; (b) temperature and $\delta^{18}O$ of precipitation (p-value = 0.000019).

Precipitation was collected from the cave on one summer day (June 6, 2014 – ave. $\delta^{18}O$ value = -1.46 ‰; average daily temp = 17.2 ^{o}C) and one day in late fall (November 19, 2014 – ave. $\delta^{18}O$ value =-6.22 ‰; average daily temp= 14.4 ^{o}C).

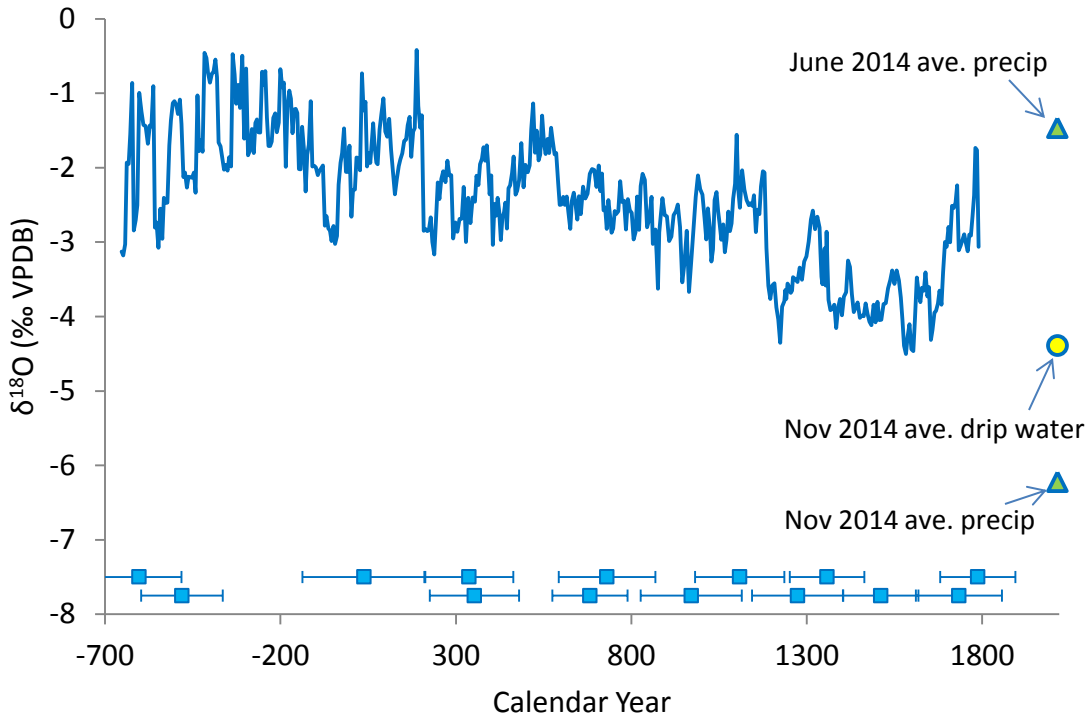

Figure 2-11. All micromill $\delta^{18}O$ (blue) data with isotopes of precipitation (indicated by triangles, June and November 2014) collected near Buraca Glorioso. $\delta^{18}O$ of drip water (collected November 2014) is indicated by circle.

5 Climate Implications, Comparison with regional proxy records, and Discussion

5.1 Cave monitoring

In the relatively short collecting time, it is apparent that the drip counts of the cave are reflecting changes in precipitation outside of the cave. The drip counts remained steady throughout the summer, increasing slightly in September due to several days of precipitation, but did not increase dramatically until additional days of heavier precipitation in late October and early November (Figure 2-4). The response time to precipitation appears to be on the order of 10-14 days or less once the outside soils become saturated. If the travel time for water between top of the rock and the cave is approximately 10 days and the distance traveled is 40 meters, the average

velocity of the water is 4 meters/day. There are likely multiple ways that water is traveling through the rock – through conduits, through fractures, and through the rock matrix (Worthington, 2007). Different types of flow likely dictate different travel speeds and residence times through the rock. A thorough investigation of rock geometry and flow speeds using environmental and injected tracer studies is needed to fully understand the flow speeds and residence times of this particular cave system.

5.2 Stable Isotopes

Correlation exists between the oxygen and carbon record (R^2= 0.38) and covariance between $\delta^{13}C$ and $\delta^{18}O$ can indicate that the calcite precipitation process is driven by kinetic effects (Hendy, 1971). In Portugal and the rest of the Iberian Peninsula, it is likely that the kinetic effects of precipitation are driven by processes ultimately related to climate (Mattey et al., 2008). Warmer/drier (cooler/wetter) climates would cause more evaporation during precipitation events and lead to higher (lower) $\delta^{18}O$ values. Warmer/drier (cooler/wetter) climates would also cause a shift towards C_4 (C_3) plants and $\delta^{13}C$ values to increase (decrease).

5.3 Modern Climate Comparison

Lisbon monthly-averaged GNIP data did not include precipitation amount measurements. This fact and the short length of time (1 year) that precipitation was measured make drawing conclusions from this data set difficult. From the longer data set, Porto (16 years), correlations between the $\delta^{18}O$ of precipitation and temperature or precipitation amount can be determined. Precipitation, temperature, and $\delta^{18}O$ of the precipitation vary throughout the year. Highest temperatures occur in summer, highest

values of $\delta^{18}O$ occur in the summer and peaks in precipitation amount occur in winter. Peak values of isotopic fractionation in the precipitation occur at the time of the year with the most precipitation and the lowest temperatures.

Event data was collected for Lisbon and correlations between precipitation $\delta^{18}O$ values and precipitation amounts were determined (Figure 2-9). Most precipitation occurs in the winter months (>75-80% of yearly total occurs October through April) and the typical event lasts for 2-4 days (www.wetterzentrale.de/topkarten/tkfaxbraar.htm). Precipitation data binned by storm event gives a R^2 value of 0.40 – increased precipitation results in decreased $\delta^{18}O$ values. As precipitation persists throughout a storm, the $\delta^{18}O$ values decreased due to less evaporation occurring while the precipitation is falling (Dansgaard, 1964; Sharp, 2007).

Calcite $\delta^{18}O$ values are a function of temperature at calcite formation and $\delta^{18}O$ of the source water. Since temperature inside the cave remains relatively constant, the variability of the calcite $\delta^{18}O$ values is primarily a function of the variability of the $\delta^{18}O$ of the precipitation in the region. The climate of the Iberian Peninsula region dominated by winter precipitation and cave drip water is also likely dominated by winter precipitation. $\delta^{18}O$ values of winter precipitation are much lower than that of less intense, summer precipitation, thus the $\delta^{18}O$ values of the calcite reflect the winter $\delta^{18}O$ precipitation signal. The $\delta^{18}O$ values of the calcite are all below the $\delta^{18}O$ value of June precipitation during the MCA and LIA thus it is unlikely that summer precipitation is a dominant contributor to the $\delta^{18}O$ of the calcite.

5.4 Calibration with precipitation model

According to uranium-thorium dating methods, the top of this stalagmite from Buraca Glorioso is not modern and dates to 1790, so calibration with instrumental records is not possible. Validation from a model of Portugal precipitation (Santos et al., 2015) from 1600 to 1790 will take the place of the instrumental calibration. The Santos et al. (2015) model (CalPT) reconstructs autumn, winter, and spring precipitation since 1600 (Santos et al., 2015). Summer precipitation is ignored because it is irregular and scarce. Past climate (precipitation) is reconstructed from instrumental data (for certain time periods and locations), documentary evidence (diaries, memoires, weather logs, ship logbooks, administrative and ecclesiastic archives, among others) and natural proxies, such as tree rings, boreholes, and ice-cores (Alcoforado et al., 2000; Bradzil et al., 2005, 2010; Camuffo et al., 2010). General trends between the two data sets exist (Figure 2-12). Trends are more apparent with slights shifts in $\delta^{18}O$ data possible due to age uncertainties.

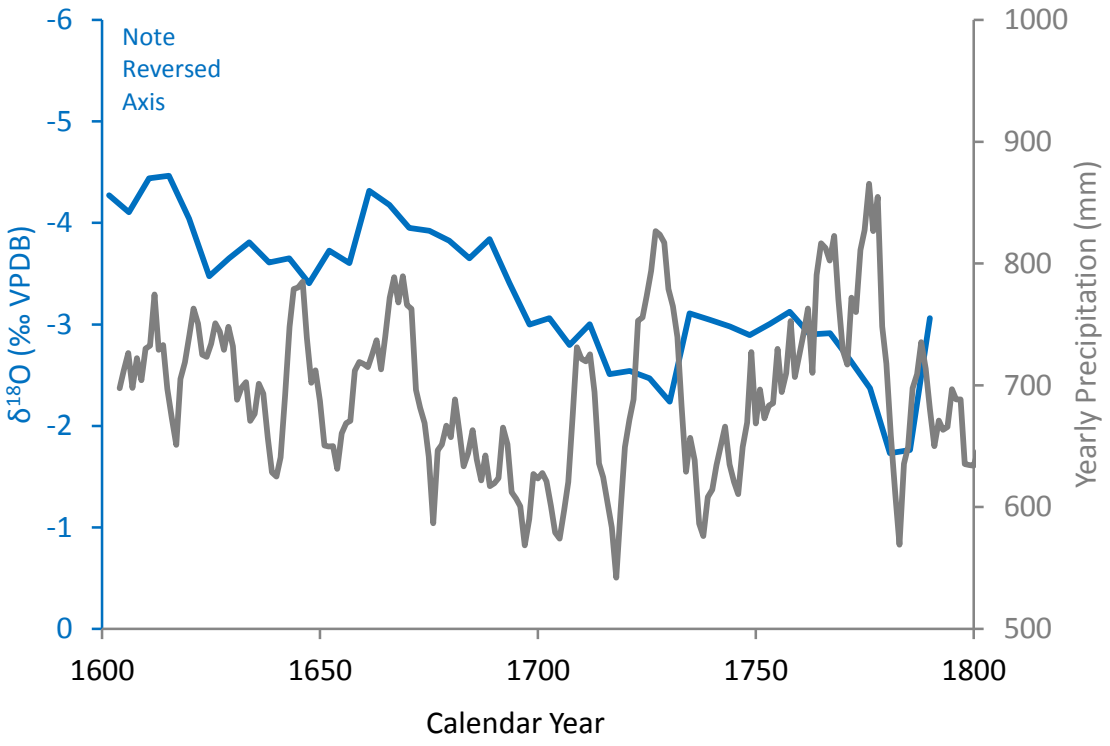

Figure 2-12. Comparison of Portugal $\delta^{18}O$ record (blue) with 5 year average CalPT (grey) precipitation model (Santos et al., 2015). Note reversed axis of Portugal $\delta^{18}O$ values. Increased precipitation is towards the top of the graph for both values.

5.5 Comparison with other proxies

Comparison with other proxy data is beneficial for at least two reasons. Finding similar patterns from other proxies in the Iberian Peninsula region allows for confidence in the ability of the proxy presented here to be representative of regional climate changes. Another reason to compare with other proxy data is to look for anti-phase behavior with regions of the world that would be expected to be out of phase with Portugal with respect to precipitation patterns and the NAO. Looking for the role of NAO dynamics, the logical location to look for anti-phase behavior would be someplace consistently under the influence of the northern node of the NAO. High correlations with precipitation and winter NAO (wNAO) index occur in regions of northern Europe

such as Norway, Sweden, and Scotland. Finding inverse precipitation behavior at these locations will give us confidence that the proxy presented here is linked to climate dynamics beyond regional and may give evidence of the behavior of the wNAO system back in time.

Northern NAO node data comes from the Scottish stalagmite presented in the Trouet et al. (2009) reconstruction which was initially presented by Proctor et al. (2000). Regional data for comparison comes from the work of Martín-Chivelet et al. (2011) who examined the $\delta^{13}C$ values over the last 4000 years from three stalagmites from Kaite Cave, Cueva del Cobre, and Cueva Mayor in northern Spain and tree-ring and speleothem Mg and Sr values from Morocco (Wassenburg et al., 2013) over the last 1000 years. The tree-ring data presented by Wassenburg et al. (2013) is an updated version of that used for the Trouet et al. (2009) reconstruction.

5.5.1 Scotland

If the stalagmite from Buraca Glorioso was indeed recoding hydroclimate changes resulting from larger-scale NAO dynamics, we would expect locations from near the northern NAO node to show inverse behavior at the same time, if that proxy were also recording NAO-derived hydroclimate variability. The Scottish stalagmite used in the Trouet et al. (2009) reconstruction is claimed be recording NAO hydroclimate behavior and is located near the northern node of the NAO system. When paired with the Portugal data, the Scottish $\delta^{18}O$ values are showing mostly opposite behavior, although the response is muted in Scotland compared to that in Portugal. The Trouet et al. (2009) reconstruction used lamina widths as the precipitation proxy of the northern

node instead of $\delta^{18}O$ values, as Baker et al. (2011) concluded that $\delta^{18}O$ and $\delta^{13}C$ data were too noisy and correlations between $\delta^{18}O$ and atmospheric pressure over long time scales were not observed.

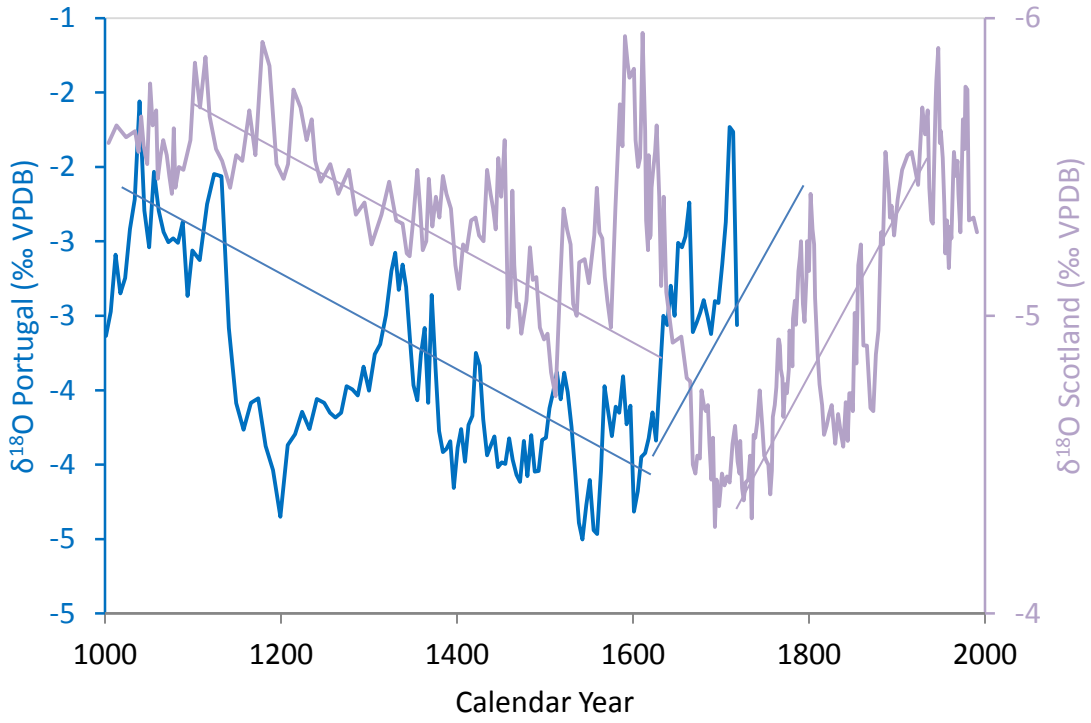

Figure 2-13. Scotland (purple) $\delta^{18}O$ and Portugal (blue) $\delta^{18}O$ values (Proctor et al., 2000; Proctor et al., 2002; Trouet et al., 2009). Note reversed axis for Scotland data and different ranges on axes. Lines drawn show general trends in the two data sets.

5.5.2 Spain

The isotope data contained within the speleothem, GH-13-6, from Buraca Glorioso in central Portugal is consistent with other proxy data from the region, including northern Spain. Similar patterns of $\delta^{13}C$ isotopic variability exist at similar time periods. Substantial isotopic changes occurred 1150-1200 AD, 1340-1400 AD, and 1580-1640 AD in both the Spain and Portugal records (Martín-Chivelet et al., 2011). This $\delta^{13}C$ record was initially presented as a temperature reconstruction over the last 4000 years

but was criticized as a temperature proxy due to the fact that the $\delta^{13}C$ values are responding to a series of factors and not under a single control (Domínguez-Villar, 2013). The multiple controls present in the Spain system appear to be also at work in the Portugal system, indicating that regional climate variability is present in both records. The data presented in Figure 2-14 are smoothing curves based on adjacent averaging (n=5, Portugal; n=11 for Spain) using different filters due to differing resolution in the two data sets (Portugal resolution = ~5 years; Spain resolution = ~1 year). The smoothing curves are overlaid on top of the raw data from Portugal and the raw data of the average from the three Spanish stalagmites.

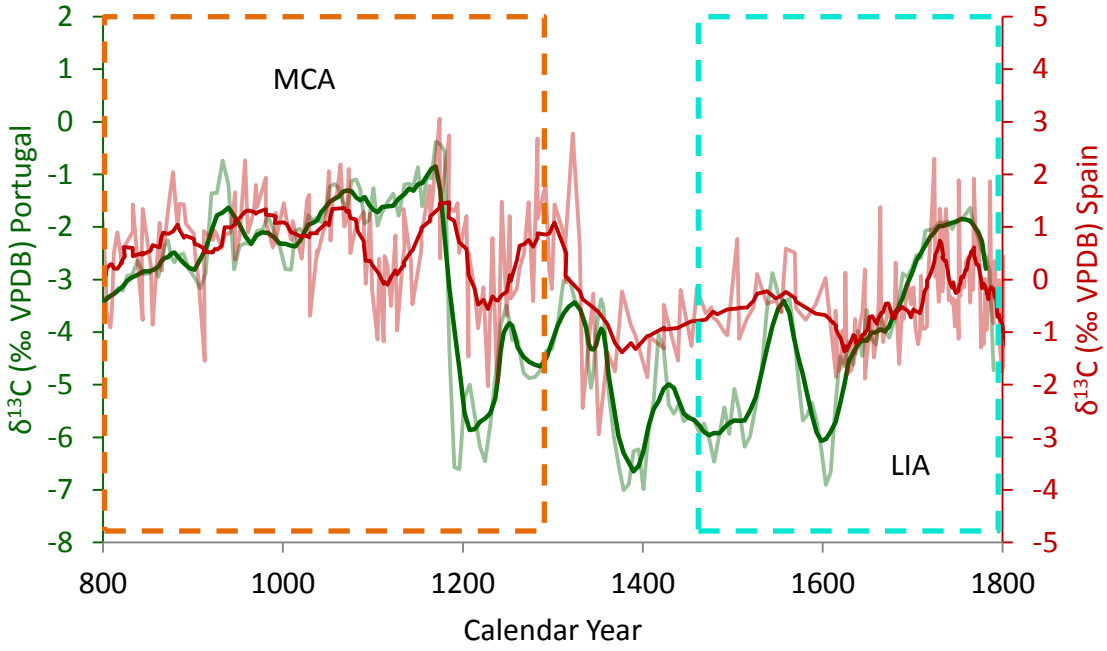

Figure 2-14. Spain $\delta^{13}C$ (red) and Portugal $\delta^{13}C$ (green) records (Martín-Chivelet et al., 2011) during the MCA and LIA. Climate intervals of MCA and LIA are those defined by Trouet et al., 2009.

5.5.3 Morocco

The data presented from central Portugal cave, Buraca Glorioso, is consistent with other proxy data from the region, including Morocco. The tree ring record from the Atlas Mountains of Morocco (approx. 1100 km from Buraca Glorioso) presented by Wassenburg et al. (2012) is an updated version of the Moroccan tree ring record used by Trouet et al. (2009) and Esper et al. (2007) and similar patterns exist between Portugal $\delta^{18}O$ variability and the Morocco tree ring PDSI reconstruction. The signal is likely different at times due to the fact that Morocco is not as consistently under the influence of the NAO as Portugal is. The same long-term trends exist, however, indicating that larger scale processes are at work in both locations, at least at times. Both records show precipitation variability within the MCA and not the same level of positive persistency in the behavior of the NAO as indicated by the Trouet et al. (2009) NAO reconstruction. The age uncertainty with the Portugal record is generally +/- 100 years. Shifting the Portugal record slightly in time allows for even better agreement between the Portugal and Morocco records.

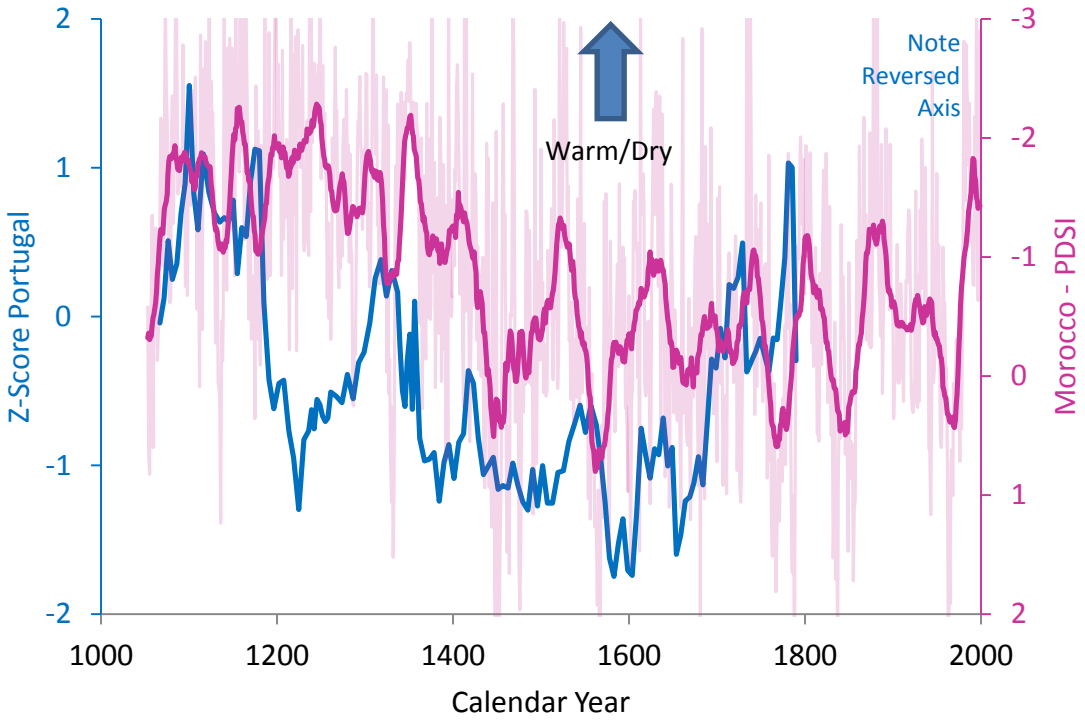

Figure 2-15. Portugal $\delta^{18}O$ z-score (blue) compared to Morocco reconstructed PDSI index (purple). (Wassenburg et al., 2013). Note reversed axis for Morocco PDSI data. Drier climate is indicated by upward trending data in both data sets.

Also presented by Wassenburg is a speleothem study of magnesium and strontium variability from Morocco. Wassenburg et al. suggest that from stalagmite and multiple proxy records that considerable rainfall variability occurred during the MCA/MWP, implying a more variable NAO than previously suggested (Wassenburg et al., 2013). The $\delta^{18}O$ record from Buraca Glorioso presented here shows a variable climate in Portugal during the MCA as well.

5.6 NAO Reconstruction

Higher values of $\delta^{18}O$ contained within the Portugal stalagmite are a result of higher $\delta^{18}O$ values of the precipitation falling above the cave. These higher values occur when there is more evaporation as the precipitation is falling, indicative of a drier

climate. SLP gradients associated with higher NAO index leads to drier conditions in Portugal, thus, higher values of $\delta^{18}O$ from the stalagmite are associated with positive NAO modes. The record presented here shows generally positive NAO indices (indicated by higher $\delta^{18}O$ values) during the MCA compared to the lower NAO indices (lower $\delta^{18}O$ values) during LIA.

Trouet et al. (2009) argue that the nodes used in the reconstruction lie under the influence of the NAO at all times and that stationarity is not a concern for these locations. Due to the slight movement of the centers of action of the NAO, Morocco might not be consistently under the influence of the NAO but Portugal consistently is under the influence of the NAO. Portugal, therefore, is an ideal location for a NAO southern node. Future reconstructions might benefit from using the $\delta^{18}O$ isotopic values of the Portuguese stalagmite as the southern node dataset or pairing the Portugal record with another record from the region to better account for the non-stationarity.

An alternate NAO reconstruction, as proposed by Lehner et al. (2012), would use the Portugal data presented together with the existing Scotland and Morocco data, and paired with another precipitation-sensitive northern NAO node. This 4-site proxy reconstruction (2 sites from each node) would help account for some of the non-stationarity of the NAO system. Some of the pseudo-proxy locations (Iceland, Norway, Sweden) chosen by Lehner et al. (2012) might make ideal additions for real proxies in this proposed reconstruction.

Although the MCA was characterized by generally drier conditions in Portugal, indicating positive NAO conditions in Portugal as shown by the $\delta^{18}O$ isotopic values in the stalagmite from Buraca Glorioso, the persistence of positive NAO conditions for 400 years during the MCA, as suggested by Trouet et al. (2009), is not verified with these data and remains a topic of interest to the paleoclimate community, requiring further studies from locations sensitive to NAO behavior. Significant changes in the isotopic values of both carbon and oxygen during the MCA in Portugal, especially 1200-1300 AD, indicate that either the climate of Portugal was not persistently dry throughout the entire MCA or the LIA in Portugal began earlier than the 1450 AD timeframe specified by Trouet et al., (2009) and earlier than the LIA start as defined by others as well – 1300 AD (Fagan, 2000) and 1450 AD (IPCC, 2013).

6 Conclusions

The $\delta^{18}O$ and $\delta^{13}C$ records from a stalagmite from Buraca Glorioso, a cave in central Portugal, indicate that the hydroclimate in Portugal during the MCA was variable and wetter than what would be indicated by the Trouet et al. (2009) reconstruction. Significant changes in the isotopic values of both carbon and oxygen around 1200 AD indicate that either the climate of Portugal was not persistently dry throughout the entire MCA or the LIA in Portugal began earlier than the 1450 AD timeframe specified by Trouet et al., (2009). This variable hydroclimate in Portugal indicates that the Medieval Climate Anomaly (MCA) was characterized by a generally positive, yet variable, North Atlantic Oscillation mode compared to the less positive, yet still variable, mode of the Little Ice Age (LIA).

These changes in $\delta^{18}O$ and $\delta^{13}C$ indicate a shift to wetter/cooler conditions in Portugal during the end of the defined MCA, with a visual change in the calcite composition (Figure 2-1) occurring at this time as well. All three of these changes are likely the result of this shift to wetter/cooler conditions. This signal indicating a shift to wetter/cooler conditions is not confined to Buraca Glorioso. There is a substantial shift in the $\delta^{13}C$ values from the speleothem record from Spain, indicating a shift to wetter/cooler conditions across the Iberian Peninsula.

When compared to previously-published records, the record presented here (from Portugal) is from a location more consistently under the influence of the NAO system and is therefore a more suitable southern node for future NAO reconstructions. Modeling results (Lehner et al., 2012) have not been able to replicate the persistently positive NAO mode published in the Trouet et al. (2009) study. Similarly, the record from Portugal presented here also does not indicate a persistently positive NAO mode during the 400+ years of Medieval times.

References

Alcoforado, M.–J., Nunes, M., García, J.C., Taborda, J.P., 2000. Temperature and precipitation reconstruction in southern Portugal during the late Maunder Minimum (AD 1675-1715). Holocene 10, 333-340.

Almeida, C., Silva, M.L., and J.A. Crispim, 1995. Hydrogeological aspects of groundwater protection in karstic areas. Final Report, Dir-General Science. 211-220.

Baker, A., Wilson, R., Fairchild, I., Franke, J., Spotl, C., Mattey, D., Trouet, V., Fuller, L., 2011. High resolution $\delta^{18}O$ and $\delta^{13}C$ records from an annually laminated Scottish stalagmite and relationship with last millennium climate. Global Planet. Change 79, 303-311.

Bradzil, R., Dobrolny, P., Luterbacher, J., Moberg, A., Pfister, C., Wheeler, D., Zorita, E., 2010. European climate of the past 500 years: new challenges for historical climatology. Clim. Change 101, 7-40.

Camuffo, D.,Bertolin, C., Barriendos, M., Dominguez-Castro, F., Cocheo, C., Enzi, S., Sghedoni, M., della Valle, A., Garnier, E., Alcoforado, M.-J., Xoplaki, E., Luterbacher, J., Diodato, N., Maugeri, M., Nunes, M.F., Rodriguez, R., 2010. 500-year temperature reconstruction in the Mediterranean Basin by means of documentary data and instrumental observations. Clim. Change 101, 169-199.

Cheng, H., Edwards, R.L., Hoff, J., Gallup, C.D., Richards, D.A., Asmerom, Y., 2000. The half-lives of U-234 and Th-230. Chem. Geol. 169, 17-33.

Dansgaard, W., 1964. Stable isotopes in precipitation. Tellus 16, 436-468.

Denniston, R., Wyrwoll, K.-H., Polyak, V., Brown, J., Asmerom, Y., Wanamaker, A., LaPointe, Z., Cleary, D., Cugley, J., Woods, D., 2013. A Stalagmite record of Holocene Indonesian-Australian summer monsoon variability from the Australian tropics. Quat.Sci. Rev. 78, 155-168.

Domínguez-Villar, D., 2013. Comment on "Land surface temperature changes in Northern Iberia since 4000 yr BP, based on $\delta^{13}C$ of speleothems". Global Planet. Change 100, 291-294.

Edwards, R.L., Chen, J.H., Wasserburg, G.J., 1986. 238U-234U-230Th-232Th systematics and the precise measurement of time over the past 500,000 years. Earth Planet. Sci. Lett. 81, 175-192.

Esper, J., Frank, D., Buntgen, U., Verstege, A., Luterbacher, J., 2007. Long-term drought severity variations in Morocco. Geophys. Res. Lett. 34, 5.

Fagan, B., 2000. The Little Ice Age: How Climate Made History. Basic Books, New York.

Hendy, C., 1971. The isotopic geochemistry of speleothems – I. The calculation of the effects of different modes of formation on the isotopic composition of speleothems and their applicability as palaeoclimatic indicators. Geochim. Cosmochim. Acta 35, 801-824.

Hurrell, J.,1995. Decadal Trends in the North Atlantic Oscillation: Regional Temperatures and Precipitation. Science.269, 676-679.

Hurrell, J., Kushnir, Y., Ottersen, G., Visbeck, M., 2003. An Overview of the North Atlantic Oscillation. Geophys. Monograph 134, 1-35.

Hurrell, J., Van Loon, H., 1997. Decadal trends in climate associated with the North Atlantic Oscillation. Clim. Change. 36, 301-326.

IAEA/WMO, 2004. Global network of isotopes in precipitation. The GNIP Database. Accessible at: http://isohis.iaea.org.

IPCC, 2013. Fifth Assessment Report (AR5), Climate Change 2013: The Physical Science Basis. Contribution of Work Group I to the Fifth Assessment Report of the Intergovernmental Panel on Climate Change, Cambridge Press, Cambridge, United Kingdom and New York, NY, USA. 1552 pp.

LeGrande, A.N., Schmidt, G.A., 2006. Global gridded data set of the oxygen isotopic composition in seawater. Geophys. Res. Lett. 33, L12604, doi:10.1029/2006GL026011.

Lehner, F., Raible, C., Stocker, T., 2012. Testing the robustness of a precipitation proxy-based North Atlantic Oscillation reconstruction. Quat. Sci Rev. 45, 85-94.

Martín-Chivelet, J., M.B. Muñoz-García, R.L. Edwards, M.J. Turrero, and A.I. Ortega. 2011. Land surface temperature changes in Northern Iberia since 4000 yr BP, based on $\delta^{13}C$ of speleothems. Global Planet. Change, 77, 1-12.

Mattey, D., Lowry, D. Duffet, J., Fisher, R., Hodge, E., Fisia, S., 2008. A 53 year seasonally resolved oxygen and carbon isotope record from a modern Gilbraltar speleothem: reconstructed drip water and relationship to local precipitation. Earth Planet. Sci. Lett. 269, 80-95.

Pais, J., Cunha, P., Pereira, D., Legoinha, P., Dias, R., Moura, D., Brumda Silveira, A., Kullberg, J.C., Gonzalez-Delgado, J.A., 2012. The Paleogene and Neogene of Western Iberia (Portugal). Springer, Heidelberg.

Pinto, J., Raible, C., 2012. Past and recent changes in the North Atlantic Oscillation. Clim. Change 3, 79-90.

Proctor, C., Baker, A., Barnes, W., Gilmore, M., 2000. A thousand year speleothem proxy record of North Atlantic climate. Clim. Dyn. 16, 815-820.

Proctor, C., Baker, A., Barnes, W., 2002. A three thousand year record of north Atlantic climate. Clim. Dyn. 19, 449-454.

Rodrigues, M., Fonseca, A., 2010. Geoheritage assessment based on large-scale geomorphological mapping: contributes from a Portuguese limestone massif example. Geomorphologie: relief, processus, environnement. 2, 189-198.

Rogers, J., 1984. The Association between the North Atlantic Oscillation and the Southern Oscillation in the Northern Hemisphere. Mon. Weather Rev. 112, 1999-2015.

Santos, J., Carneiro, M., Alcoforado, M., Leal, S., Luz, A., Camuffo, D., Zorita, E., 2015. Calibration and multi-source consistency analysis of reconstructed precipitation series in Portugal since the early 17th century. The Holocene 25, 663-676.

Sharp, Z., 2007. Principles of Stable Isotope Geochemistry. Pearson Prentice Hall, Upper Saddle, NJ.

Thompson, D., Wallace, J., 2000. Annular modes in the extratropical circulation, Pt I: Month-to-month variability. J. Clim 13, 1000–1016.

Trouet , V., Esper, J., Graham, N.E., Baker, A., Scourse, J.D., Frank, D.C., 2009. Persistent positive North Atlantic Oscillation mode dominated the Medieval climate anomaly. Science 324, 78-80.

Wassenburg, J.A., Immenhauser, A., Richter, D.K., Niedermayr, A., Riechelmann, S., Fietzke, J., Scholz, D., Jochum, K.P., Fohlmeister, J., Schroder-Ritzrau, A., Sabaoui,A.,Riechelmann, D.F.C., Schneider, L., Esper, J., 2013. Moroccan speleothem and tree ring records suggest a variable positive state of the North Atlantic Oscillation during the Medieval Warm Period. Earth Planet. Sci. Lett. 375, 291-302.

Worthington, S., 2007. Groundwater residence times in unconfined carbonate aquifers. J. Cave Karst Studies 69, 94-102.

CHAPTER 3: STABLE ISOTOPE RECORD OF HYDROCLIMATE OF THE IBERIAN PENINSULA SINCE 2600 YEARS BP

Abstract

Oxygen and carbon isotope data from calcite stalagmites from a Portuguese cave (Buraca Glorioso, 39^{o}N, 8^{o}W) show variability that is inferred to be due to hydroclimatic changes in the region. Long-term (greater than millennial-scale) changes in calcite $\delta^{18}O$ values at this location are dependent on long-term solar insolation changes due to orbital parameters, while shorter-term variability is a result of Total Solar Irradiance (TSI) variability, volcanic forcing, and temperature and precipitation changes, due, in part, to internal modes of variability such as the North Atlantic Oscillation (NAO). Variability in carbon isotopes ($\delta^{13}C$) appear to be dependent on volcanic forcing and temperature and precipitation variability. The $\delta^{18}O$ and $\delta^{13}C$ record from Portugal is compared with other relevant proxy records from stalagmites in Spain, Sweden, and Scotland, multi-proxy Northern Hemisphere temperature reconstructions, and pollen records from the Iberian Peninsula. The $\delta^{13}C$ record from Buraca Glorioso is strikingly similar to records of other locations in the region, suggesting that Buraca Gloriso is recording regional climate variability. The main driver of isotopic variability on long time scales is insolation changes due to variability in the Earth orbital parameters. The $\delta^{18}O$ and $\delta^{13}C$ records from Buraca Glorioso both respond to large volcanic forcing events. Some small-scale variability is linked to changes in TSI and changes in temperature and precipitation as a result of internal climate mode (e.g. NAO) variability.

1 Introduction

Climate reconstructions can be used to understand the dynamics of the climate system and can provide a more complete representation when integrated with other published, existing proxy data, such as those from stalagmites, lake and ocean sediments, and tree rings (Li et al., 2010). $\delta^{18}O$ records from speleothems are used as a proxy to reconstruct elements of the climate system such as hydroclimate, which may be related to internal climate modes, such as the North Atlantic Oscillation. $\delta^{13}C$ records are also used as a proxy to reconstruct temperature or other elements of the climate system (Martín-Chivelet et al., 2011). Here we compare the Portugal record presented in this document from a stalagmite from central Portugal to other proxy data for the past 2600+ years. During the Medieval Climate Anomaly and Little Ice Age, variable hydroclimate in Portugal likely was changing the $\delta^{18}O$ and $\delta^{13}C$ signals contained within the stalagmite. Looking at the $\delta^{18}O$ and $\delta^{13}C$ records on longer time scales allows for a more detailed analysis of all short- and long-term drivers of the Iberian Peninsula climate system – forcing from insolation changes, total solar irradiance, and volcanoes, and internal forcing, such as the NAO, are all variables that affect precipitation and temperature in this region and the isotopic signal recorded in the cave.

As was shown in chapter 2 of this manuscript, stalagmites from Buraca Glorioso are likely recording hydroclimate and are able to indicate past changes in the climate system of the Iberian Peninsula. The isotope record contained within GH-13-6 illustrates several thousands of years of climate in the region. The full isotope ($\delta^{18}O$ and

$\delta^{13}C$) record will be examined in this chapter. $\delta^{18}O$ and $\delta^{13}C$ records such as this, tied with U-Th dates, allow for a very rich and meaningful record during the time periods of interest going back as far as the stalagmite allows and within the useful limits of U-Th dating methods. This longer record allows for interpretation of the longer-term drivers of the climate system.

Other research from this cave, Buraca Glorioso, has demonstrated the ability of isotope records from this cave to record broader climate signals (Houts et al., 2014). Fluctuations in the $\delta^{18}O$ values in Buraca Glorioso correspond to the millennial-scale variability recorded in NGRIP as well as Iberian margin and north Atlantic sediment cores. There are shifts to higher $\delta^{18}O$ values that correspond with dry periods during Dansgaard-Oeschger stadials and Heinrich events. Hiatuses in stalagmite growth during Heinrich events number 1, 4, 5, and 6 agree with this correlation (Houts et al., 2014).

Figure 3-1 depicts relationships between factors that are potentially important causes of changing $\delta^{18}O$ values in the calcite. Some of these factors and their contributions to this $\delta^{18}O$ record from the Buraca Glorioso cave system will be explored in this chapter. Figure 3-2 depicts relationships between factors likely contributing to the $\delta^{13}C$ record in Buraca Glorioso.

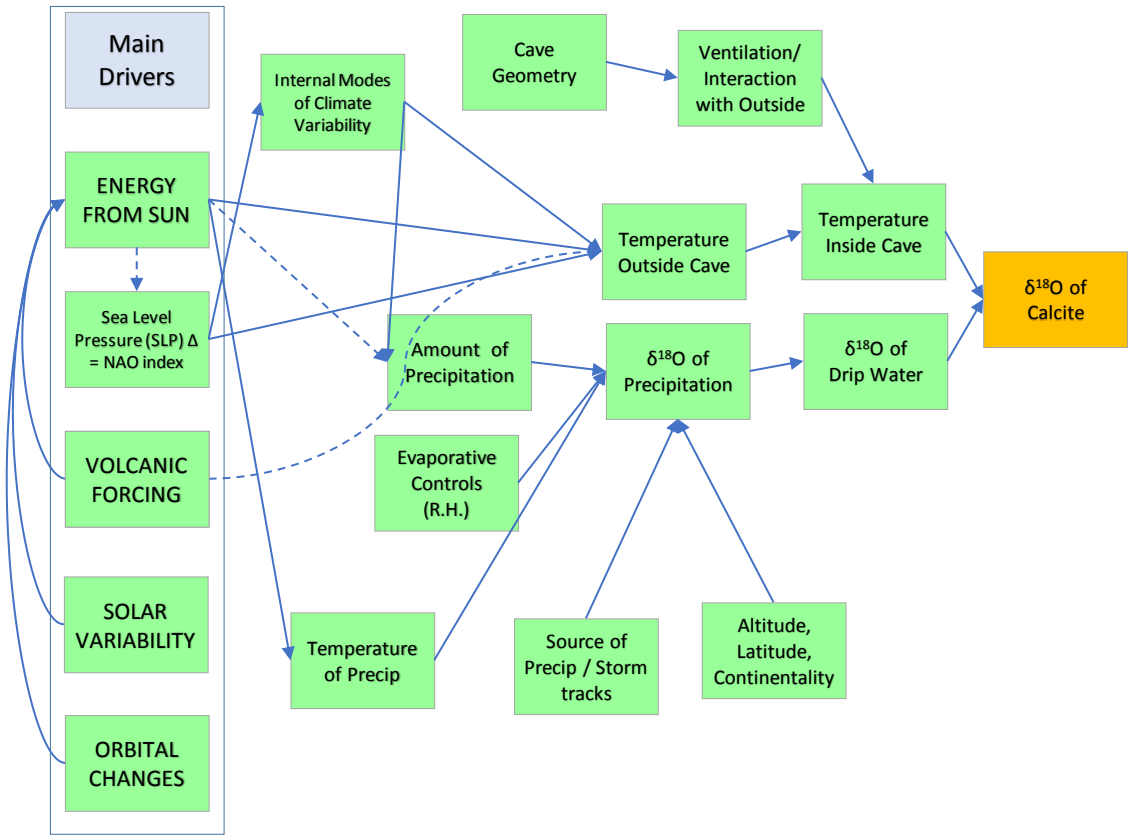

Figure 3-1. Climate drivers and other factors influencing the $\delta^{18}O$ of the calcite in Buraca Glorioso.

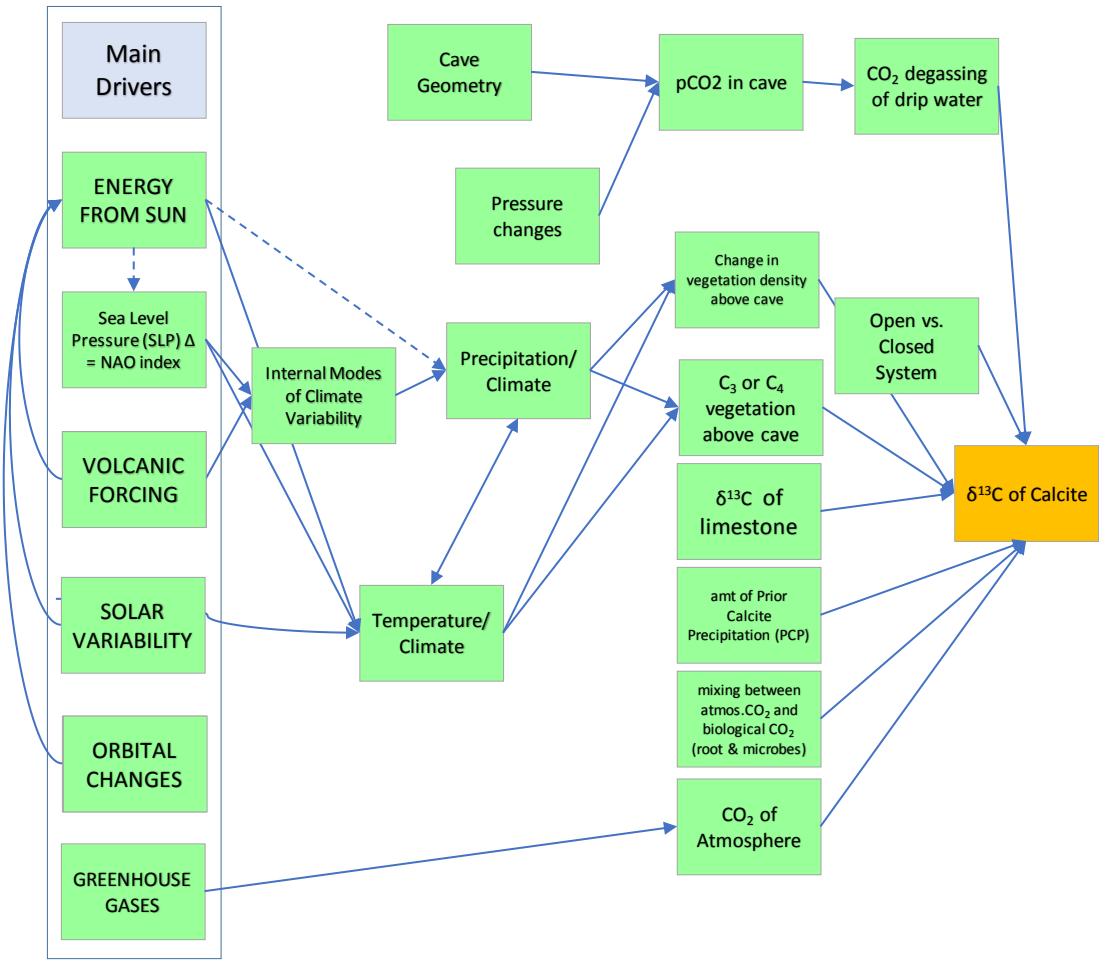

Figure 3-2. Climate drivers and other factors influencing the $\delta^{13}C$ of the calcite in Buraca Glorioso.

The hypotheses that will be considered in this chapter include: 1. the main driver of the longer scale variability of the Buraca Glorioso $\delta^{18}O$ record is solar insolation changes due to changes in the Earth's orbital parameters. 2. Shorter-term, yet still important, factors driving the stable isotopes in the Buraca Glorioso system – both $\delta^{18}O$ and $\delta^{13}C$ values - are solar irradiance variability, volcanic forcing, and internal modes of variability, such as the NAO, which impact temperature and precipitation patterns in the region.

2 Case setting

2.1 Present day climate of the Iberian Peninsula

The Iberian Peninsula (approx. 38-42^{o}N latitude, 2-10^{o}W longitude) is principally comprised of the countries Spain and Portugal and is bounded by the Atlantic Ocean to the west and the Mediterranean Sea to the east. The Iberian Peninsula is situated in close proximity to other European countries as well as those of northern Africa, allowing for comparisons between the record from Portugal and that of other, long-term proxy records.

Buraca Glorioso is located in the hot summer Mediterranean climate (Csa, koeppen-geiger.vu-wien.ac.at) which indicates average temperature in the warmest month above 22 ^{o}C and at least four months averaging above 10^{o}C. There is a strong seasonal component to the climate of Portugal, with dry summers and wet winters (October-April). Annual rainfall averages (30-year average) range from 660 mm in Monte Real (56 m asl) and 697mm in Santarem (107 m asl) to 840mm in Alcobaça (38 m asl), three of the nearest precipitation recording locations. Rainfall is seasonal in central Portugal, with > 77% of rainfall occurring from October to March. This strong seasonality in precipitation gives rise to winter being the rainiest season while the transitional seasons, spring and fall, are the most irregular (Santos et al., 2015). Summer precipitation is irregular and scarce (Santos et al., 2015) and, for this cave location, may not contribute to cave drip water at all.

2.2 Cave Setting

The principal speleothem in this study is GH-13-6 and was collected from Buraca Glorioso in August 2013. Buraca Glorioso is located at an altitude of 425 m asl above sea level. Buraca Glorioso is a cave formed in Mesozoic limestone, located in west central Portugal (see Figure 2-2) in a topographically distinctive area known as the Estremadura Limestone Massif (ELM) that makes up the center portion of the country (Rodrigues and Fonseca, 2010). Rodrigues and Fonseca (2010) consider it the most important karst relief in Portugal. The ELM is 20 km from the Atlantic Ocean and about 100 km from Lisbon. The most important topographical features of the area are formed by mainly compact limestones, oolitic limestones, and dolomitic limestones (Almeida et al., 1995). These limestones are mid-Jurassic in age and were formed by a shallow, epicontinental sea (Almeida et al., 1995). The highly soluble limestone rock is a large groundwater reservoir and contains abundant fossils, active conduits, and both surface and underground karst formations (Rodrigues and Fonseca, 2010). This entire region underwent an important and long-lasting uplift (beginning approximately 100 Mya) during the late Cretaceous to Paleogene (Pais et al., 2012). The mechanism of this uplift is likely related to the Pyrenean orogeny (Pais et al., 2012).

3 Methods

The stalagmite from Buraca Glorioso was sectioned, polished, labeled, and hand-milled every 1 mm over the top 10 cm and every 10 mm for the remainder of the stalagmite. These hand-milled samples were analyzed for carbon and oxygen isotopes at the Iowa State University Stable Isotope Laboratory. Sixteen ages over the top 10 cm

of the stalagmite were determined using uranium-thorium disequilibrium methods at the University of New Mexico. 496 micromill (200 µm wide) samples were collected from the top 10 cm of the stalagmite and analyzed for carbon and oxygen isotopes at the Iowa State University Stable Isotope Laboratory. A comparison of the oxygen and carbon isotopes from the 1 mm samples and the corresponding micromill samples is shown in Appendix A.

To better understand the processes occurring near and in the cave, temperature, relative humidity, and pressure sensors were installed inside and outside of the cave. An acoustic drip counter and drip water collection system was installed within the cave. Precipitation from the cave area has been collected for isotopic analysis and precipitation isotopes from Portugal GNIP data have been analyzed for general trends.

Large changes (~4 ‰ oxygen, VPDB and ~7 ‰, carbon, VPDB) are observed in the 2300+ year time series of oxygen and carbon isotopes from stalagmite GH-13-6 from Buraca Glorioso. Some time periods, 1150-1300 AD for example, demonstrate large changes in oxygen isotopes over a short period of time, changing from -2.0 to -4.4 ‰ in just 45 years. In order to verify that the signal contained within these changes is a result of climate change and not instrumental noise, an investigation was performed to see if the large changes occurred within an instrumental run (intra-run variability) or if the changes were occurring between runs (inter-run variability) on the mass spectrometer. The results of this work are shown in Appendix A.

To address the question about factors driving climate in this area and driving changes in isotopes inside the cave, other proxy records were compared to the Buraca

Glorioso data. Insolation values from Earth's orbital changes (Berger and Loutre, 1991) and total solar insolation (TSI) values (Bard et al., 1997; Bard et al., 2000; Bard et al., 2007) were compared to the Buraca Glorioso $\delta^{18}O$ record. Volcanic forcing is considered for the entire record and compared to both $\delta^{18}O$ and $\delta^{13}C$ values. Further refinement of the likely climate drivers comes from comparisons of the Buraca Glorioso record with the widely accepted Northern Hemisphere temperature reconstructions of Moberg et al. (2005) and Mann and Jones (2003). Temperature reconstructions from Iberian Peninsula pollen data (Desprat et al., 2003) and the Spain stalagmite record of Martín-Chivelet et al. (2011) are compared to the record from Buraca Glorioso. Temperature-proxy data from Sweden (Sundqvist et al., 2010) and precipitation reconstructions from Scotland (Proctor, 2000; Proctor, 2002; Trouet et al., 2009) are also compared to the Buraca Glorioso record to help refine climate drivers in the larger European region.

4 Results

4.1 Cave monitoring

The temperature throughout the observation period inside the cave ranges from 13.9 ^{o}C in late winter (February-March) to 14.6 ^{o}C in late summer/fall (October). Outside the cave, temperatures range from 32 ^{o}C (late summer) to 5 ^{o}C (winter). Outside the cave relative humidity varies seasonally, with lower values generally in the summer, with a yearly range from 25 to near 100 percent. Inside the cave, the variability in relative humidity is small or non-existent. Over the 15-month monitoring

period, the cave relative humidity remained at 100% with one small excursion to ~98% during December of 2013.

Drip counts have been measured in Buraca Glorioso for six months, beginning June 2014 with data collected in November 2014. The minimum in drip counts occurred in late summer/early fall with daily drip counts near 277 drips per day. The peak during this six month monitoring period occurred in late November with a drip count of 787 drips per day.

4.2 Age-depth model

Stalagmite GH-13-6 was wet and was actively being dripped on at the time collection in August 2013. However, sixteen U-Th dates, including one sample 5 mm from the top of the stalagmite, do not strongly indicate modern growth of the stalagmite. The linear-fit age-depth model presented in Figure 2-6 indicates the top is 223 yrs BP (present = 2013), approximately 1790 AD.

4.3 Stable isotopes

The temporal resolution for the micromilled samples is decadal to sub-decadal, generally 5 years of time-averaged growth per micromill sample. Over the entire record, the average $\delta^{18}O$ value is -2.44 ‰ and the average $\delta^{13}C$ value is -3.04 ‰. The complete record is characterized by many small (< 1.0‰) variations with several large (≥ 2.0‰) changes in both oxygen and carbon isotopes, with the large changes occurring 100 BC to 0, 1200 to 1300 AD, and 1700 to 1800 AD. The $\delta^{13}C$ record shows additional large changes, not seen in the oxygen record, during the LIA interval. Some correlation exists between the oxygen and carbon records and some large changes occur in both

records at approximately the same time (R^2 = 0.38, p-value < 0.001). The full $\delta^{18}O$ and $\delta^{13}C$ record is shown in Figure 3-3.

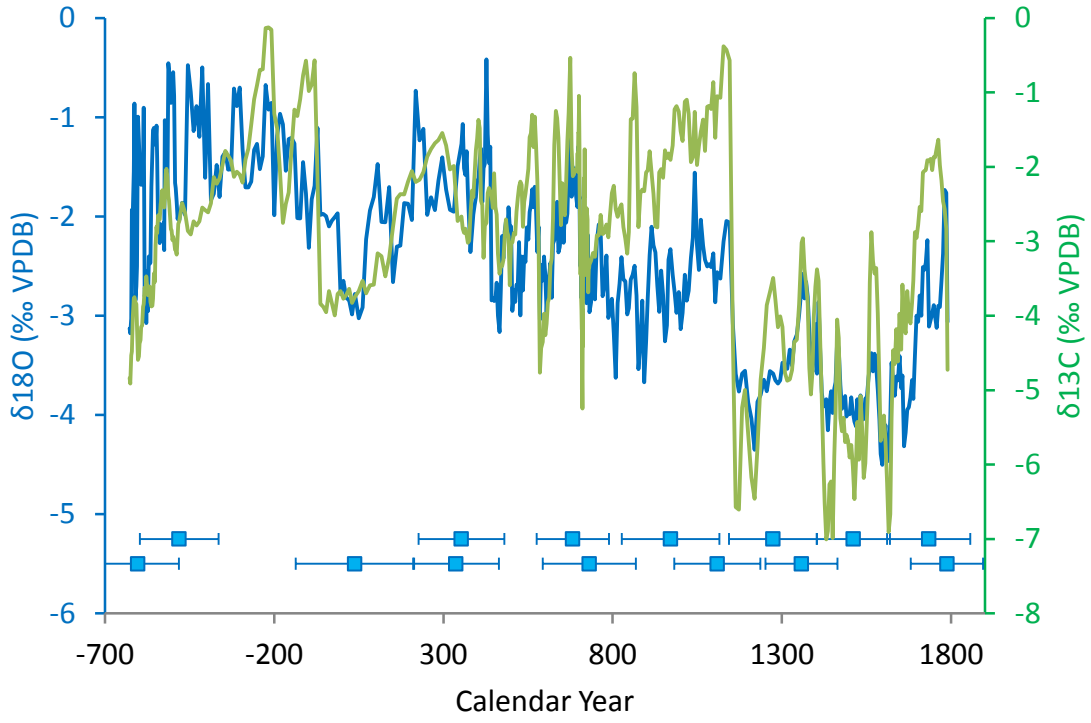

Figure 3-3. $\delta^{18}O$ (blue) and $\delta^{13}C$ (green) record from Buraca Glorioso, Portugal.

4.4 Controls on $\delta^{18}O$ of precipitation/Precipitation Isotopes

Precipitation isotopes were recorded at numerous locations in Portugal over the past 30 years. At the two closest GNIP sites to Buraca Glorioso, Porto and Lisbon, monthly–averaged precipitation was collected for 16 years and 1 year, respectively. At Lisbon, precipitation event data were also collected daily for 6 months between 2002 and 2003.

Rainfall in Porto, collected for 16 years, provides a relationship between $\delta^{18}O$ and precipitation amount which implies that a 16 mm increase in monthly precipitation would decrease the $\delta^{18}O$ monthly value by 0.2 ‰ or -0.0125 ‰/mm. Similarly, a 1 ^{o}C

decrease in temperature (at which the precipitation is falling) leads to a 0.2 ‰ decrease in $\delta^{18}O$ values. Since most of the precipitation in Portugal falls at the time of the year when temperatures are the lowest, it is difficult to be certain which factor (precipitation amount or temperature) is influencing the $\delta^{18}O$ values most significantly. In Porto, the relationship between $\delta^{18}O$ and precipitation and the relationship between $\delta^{18}O$ and rainfall amount give similar R^2 values (Figure 2-10).

Precipitation was collected from the cave on one summer day (June 6, 2014 – ave. $\delta^{18}O$ value = -1.46 ‰; average daily temp = 17.2 ^{o}C) and one day in late fall (November 19, 2014 – ave. $\delta^{18}O$ value =-6.22 ‰; average daily temp= 14.4 ^{o}C). Drip water was collected from inside the cave in November and that sample had an average value of -4.39 ‰.

5 Climate Implications and Discussion

5.1 Earth Orbital Parameters

Considering the entirety of the Buraca Glorioso GH-13-6 $\delta^{18}O$ record, the trend from 2600 years BP to 223 years BP (1790 AD, the calculated top of the stalagmite) is decreasing $\delta^{18}O$ values. A cause of this decreasing trend is likely the overall decreasing June solar insolation values in the Northern Hemisphere (values shown at 40^{o}N latitude) during the last half of the Holocene (Berger and Loutre, 1991). This is consistent with many other studies, including records from Sanboa Cave, China (Wang et al., 2008), Dongge Cave, China (Wang et al., 2005), and Botuvera Cave, Brazil (Cruz et al., 2005) that show isotopic changes which reflect changes in insolation.

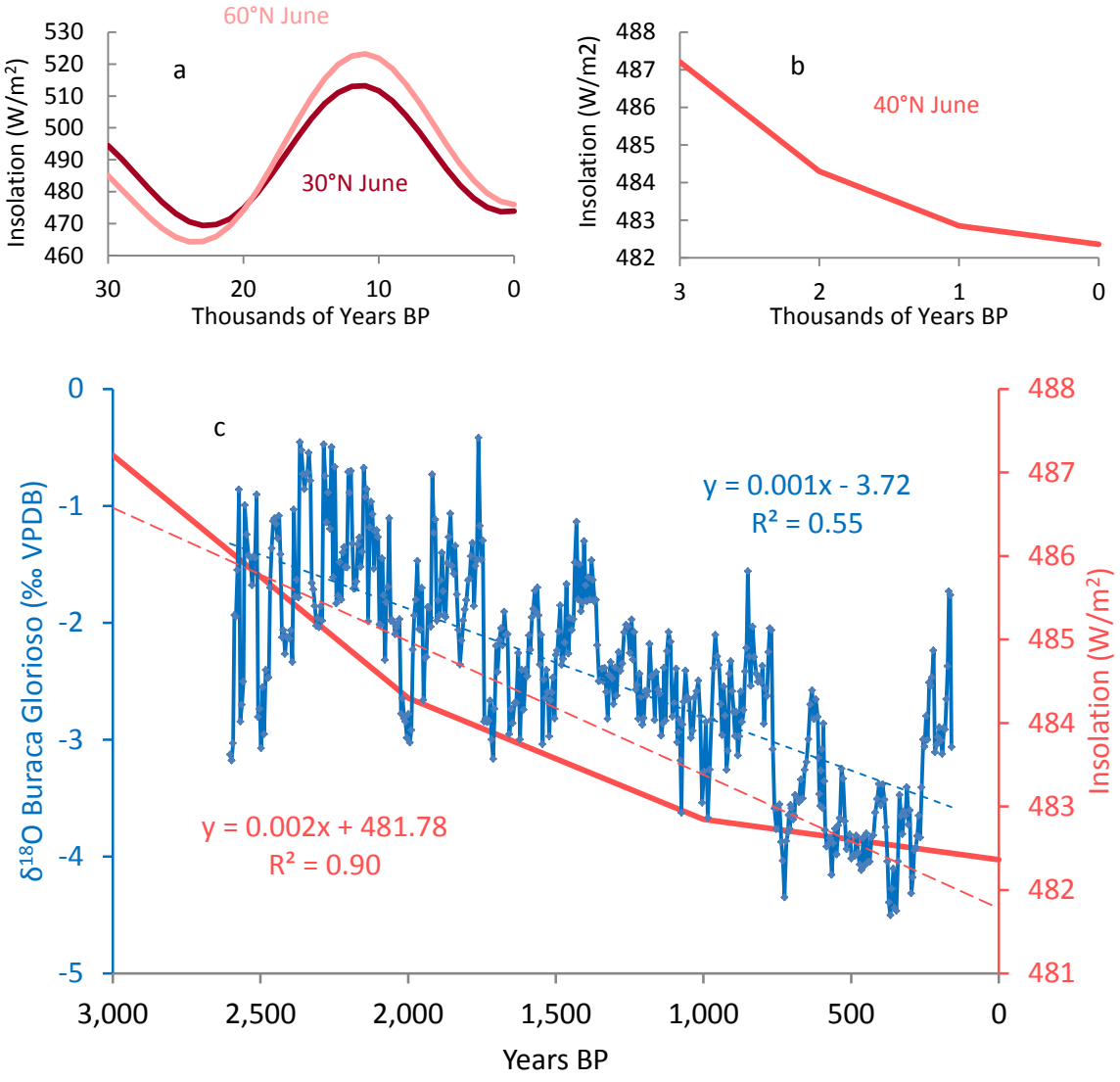

Figure 3-4. Berger and Loutre (1991) insolation data. (a) Long-term mid-latitude (30°N and 60°N) Northern Hemisphere insolation changes. (b) Insolation changes at 40°N latitude over the last 3000 years. (c) 3000 years of insolation changes at 40°N and $\delta^{18}O$ variability from Buraca Glorioso in central Portugal (latitude 39°N).

5.2 Total solar irradiance (TSI)

Looking at the smaller scale variability of solar variability at this latitude over the Late Holocene allows for more accurate assessment of the small-scale variability of the Buraca Glorioso record and will help determine if this record is primarily driven by changes in solar output. The larger-scale insolation changes due to orbital parameters

were previously considered. In order to look for shorter-term variability, the $\delta^{18}O$ record from Buraca Glorioso was detrended to remove the longer scale variability due to insolation changes. A linear fit to the $\delta^{18}O$ data was derived (blue dotted line in Figure 3-4c) and each data point was subtracted from the linear fit model for that point. The detrended $\delta^{18}O$ data will be used for future comparisons with other records in this chapter.

The work of Bard et al. (1997, 2000, 2007) considers the smaller scale variability in irradiance due to changes in the output from the sun. This reconstructed Total Solar Irradiance (TSI) record is based on variations in the cosmogenic nuclides ^{14}C and ^{10}Be (Bard et al., 1997). The data are further refined by assuming a 0.25% reduction in TSI during the Maunder Minimum (after Lean et al., 1995) and normalized to a TSI value of 1367 W/m^2 from the year 1950 AD (Bard et al., 2000). Additional corrections to the TSI reconstruction involve the same assumptions as before plus small long-term geomagnetic modulation (after Korte & Constable, 2005) and a polar enhancement factor (PEC = 0.8 according to Field et al., 2006) (Bard et al., 2007). These slight variations in TSI reconstruction are plotted separately in Figure 3-5a. Increases in TSI correspond with decreases in ^{10}Be values (Figure 3-5b). Increases in TSI are due to additional energy output from the sun. This additional energy into the Earth's atmosphere is one factor that causes warming just as a decrease in TSI (for example, low values such as during the Maunder Minimum) is a cause for cooling (Crowley et al., 2000). Surface air temperatures are generally expected to increase in response to

higher values of TSI, which causes drier air near the cave and more evaporation as precipitation is falling and $\delta^{18}O$ values of the precipitation (and cave calcite) to increase.

Over the 2300 year record from Buraca Glorioso, there are time periods when the variability in the Portugal record suggests coupling with the TSI reconstruction and other times when they diverge. Both records (TSI and $\delta^{18}O$ Portugal) increase from 840 until roughly 1040 AD, exhibit divergent behavior until approximately 1350 AD and then both show generally increasing trends through the end of the records. If one considers that the $\delta^{18}O$ record from Portugal has +/- 100 years age uncertainty from U-Th dating, the records more closely match yet still not a perfect match. This indicates that solar irradiance variability is a dominant factor, at times, in the shorter-term variability in the Buraca Glorioso record but is not the only driver of climate in the region.

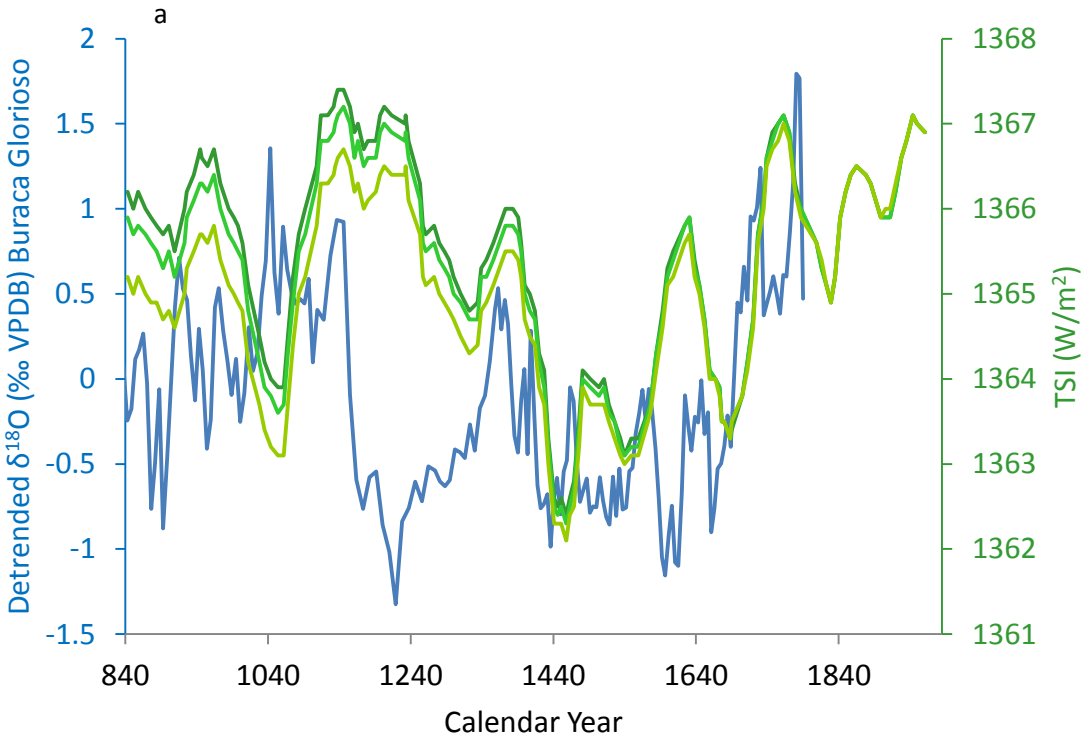

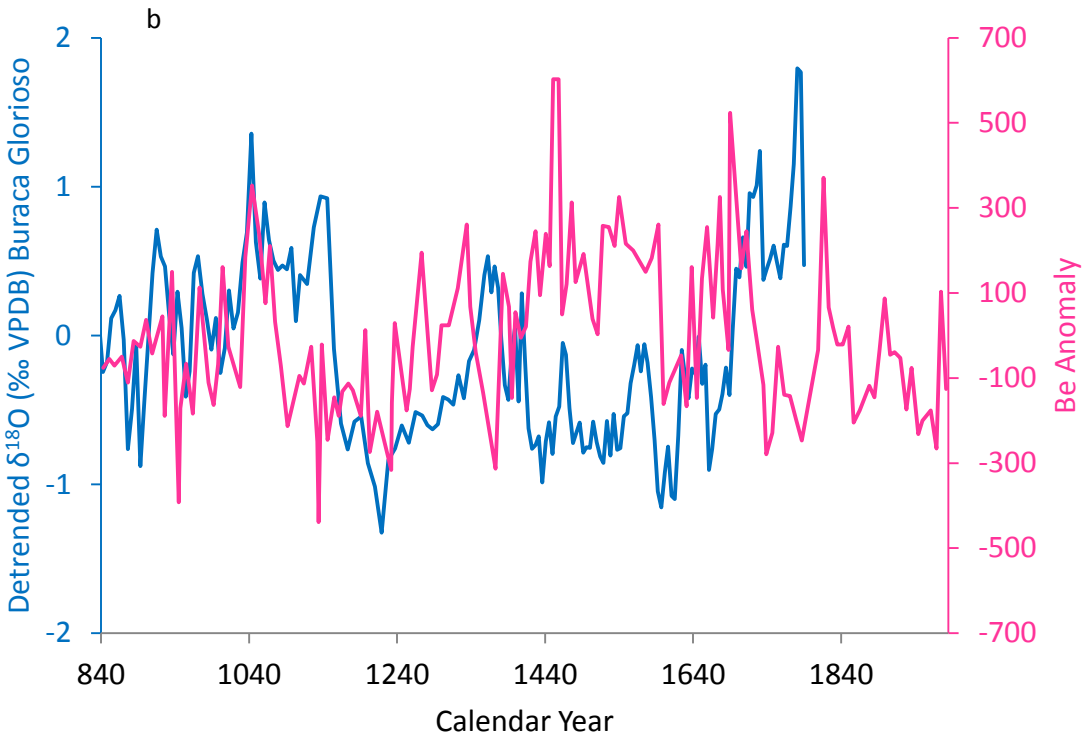

Figure 3-5. Solar irradiance data and Portugal detrended $\delta^{18}O$ values (blue) with (a) TSI data (green); (b) Be anomalies (pink) (Bard et al., 2000). Be-10 production is expected to be higher during time periods of lower TSI.

5.3 Temperature- or precipitation-proxy

Proxy records – speleothems, tree rings, sediment cores and others – can be thought of as a temperature proxy and/or a precipitation proxy. Each data point could be precipitation-influenced or temperature-influenced or it is possible for a record to be more influenced by precipitation at times and more influenced by temperature at other times or for the record to be influence by both temperature and precipitation at all times. Precipitation and temperature are obviously linked - warmer air can have more moisture, cooler air can hold less.

Comparison of the speleothem proxy data with instrumental data allows for a certain level of confidence when determining the major drivers of the cave system. In

situations where there is no overlap with instrumental data (such as the record thus far from Buraca Glorioso), comparison with temperature and precipitation proxies will help tease apart whether the Portugal record is a temperature proxy, precipitation proxy, or a combination of both and determine if internal modes of climate variability, such as the NAO, are driving these temperature and precipitation changes.

5.3.1 Temperature

Comparison with Northern Hemisphere temperature reconstructions

If the Buraca Glorioso record is recording larger-scale temperature changes, it would be expected to correlate with other proxy-based temperature reconstructions from the Northern Hemisphere, including those of Mann and Jones (2003) and Moberg et al. (2005), assuming that local and hemispheric temperature variations are driven by the same processes.

The Northern Hemisphere temperature reconstruction by Moberg et al. (2005) analyzed lake and ocean sediment cores (low resolution) and dendrochronological (high resolution) evidence to reconstruct temperatures in the Northern Hemisphere over the past 2000 years. This reconstruction agrees well with borehole measurements and temperature data from Global Climate Models (Moberg et al., 2005). Maximum temperatures were recorded from 1000 to 1100 AD and minimum temperatures were recorded around 1600 AD, closely aligned with some of the highest and lowest values, respectively, in the detrended $\delta^{18}O$ data from Portugal (Figure 3-6). In the detrended $\delta^{18}O$ record from Portugal, higher values are indicating warmer/drier conditions and lower values indicating cooler/wetter conditions. In the Moberg record, large,

multicentennial variability is evident and it appears that the hydroclimate record from Portugal loosely follows this same pattern of variability.

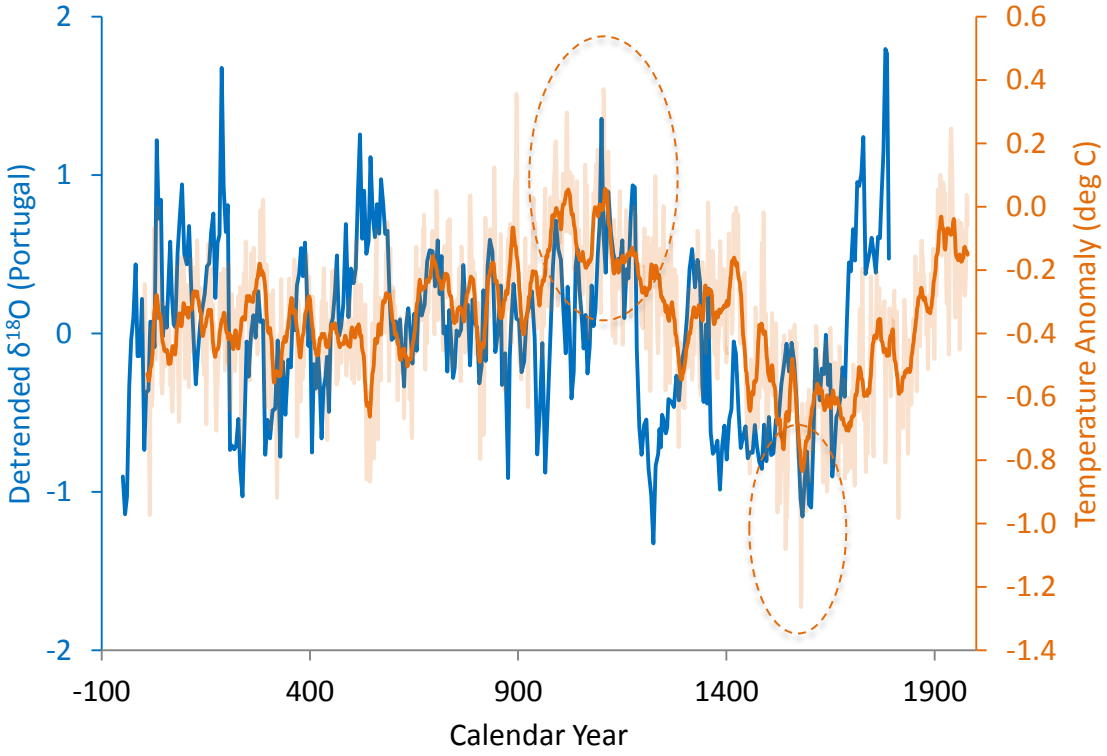

Figure 3-6. Moberg NH temperature reconstruction (orange) and Portugal $\delta^{18}O$ detrended (blue) values (Moberg et al., 2005). Highest and lowest values of the Moberg NH temperature reconstruction are circled.

Another high-resolution proxy reconstruction of Northern and Southern Hemisphere temperature over the last 2000 years is that of Mann and Jones (2003). This reconstruction uses 23 individual proxy records from 8 distinct regions in the Northern Hemisphere and data from 5 regions in the Southern Hemisphere and includes historical data, lake sediments, ice cores, tree rings, and fossil shells (Mann and Jones, 2003). Data are presented by Mann and Jones (2003) either as Southern Hemisphere only, Northern Hemisphere only, or Global Temperature Anomalies. Figure 3-7 shows

the Northern Hemisphere temperature reconstruction with the detrended $\delta^{18}O$ record from Portugal.

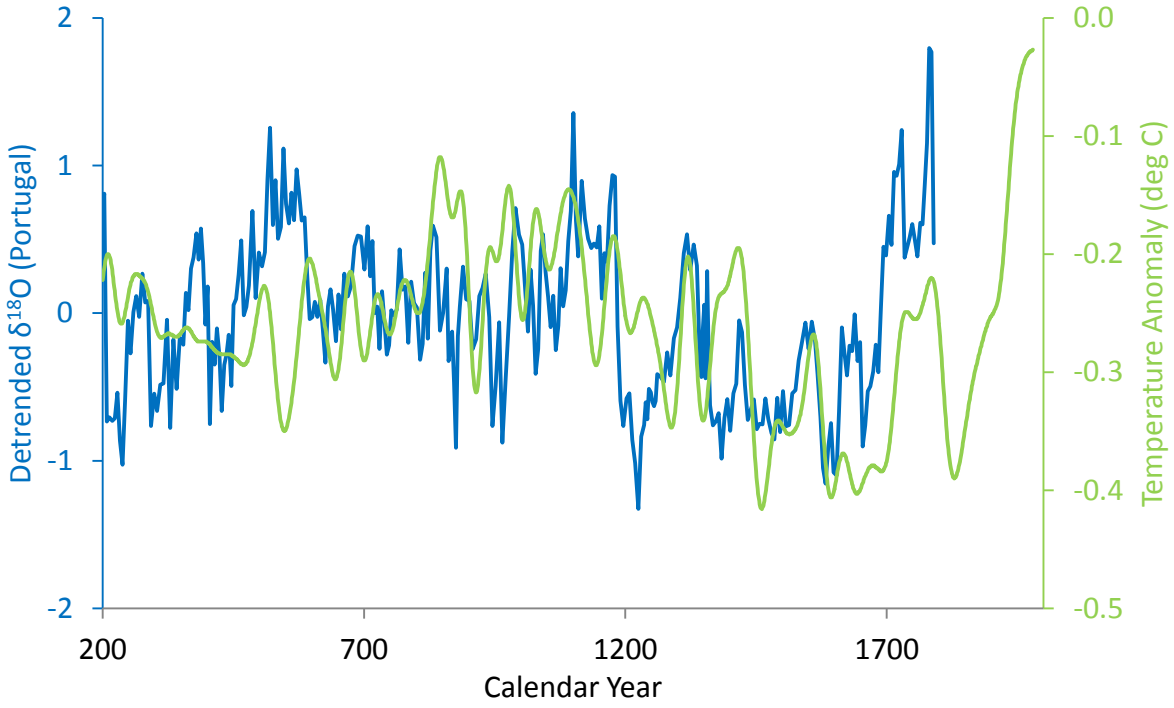

Figure 3-7. Mann and Jones NH temperature reconstruction (green) and Portugal $\delta^{18}O$ detrended (blue) values (Mann and Jones, 2003).

General patterns of data from the Mann and Jones (2003) and Moberg (2005) Northern Hemisphere temperature reconstructions agree quite well (r^2=0.37; p-value=0) with each other, even though the absolute values of these changes are slightly different due to the average nature (40-year smoothed) of the Mann and Jones reconstruction. This correlation is expected due to the fact that these reconstructions use some of the same data. Both temperature patterns agree fairly well with the detrended $\delta^{18}O$ data from Portugal. The detrending process in essence removes the effects of the long-term insolation decrease taking place in the Holocene. This detrended $\delta^{18}O$ time series

reflects similar variability to temperature reconstructions yet not all of the variability is captured by these temperature reconstructions. 5 year correlation of $\delta^{18}O$ from Portugal with the Mann and Jones NH temperature reconstruction yields an r^2 value of 0.16 (10 year, r^2=0.17; 20-year, r^2=0.18; p-values all < 0.001) and $\delta^{18}O$ Portugal record correlated with the Moberg reconstruction yields an r^2 value of 0.05 (10 year, r^2=0.06; 20-year, r^2=0.06; p-values all <0.001).

There are also time periods when the $\delta^{13}C$ values for the Buraca Glorioso record match up well with the temperature reconstructions of Mann and Jones (2004) and Moberg (2005). Since the $\delta^{13}C$ and $\delta^{18}O$ record from Buraca Glorioso are well correlated, this result is not surprising. The comparison plots for carbon isotopes are presented in Appendix E.

Although the $\delta^{18}O$ record from Portugal matches up well with the NH temperature reconstruction of Mann and Jones and matches up not as well with the Moberg NH temperature reconstruction, hemispheric or global mean temperature reconstructions do not accurately reflect the century-scale variability due to changes in oceanic and atmospheric processes, such as the NAO (IPCC, 2013; Keigwin and Pickart, 1999). Regional changes in oceanic and atmospheric processes, such as those that may be driving the temperature and/or precipitation patterns which are impacting the isotope records in Portugal, may be diminished or absent in global or hemispheric reconstructions such as those presented by Moberg (2005) and Mann and Jones (2003) (IPCC, 2013). Comparison with regional records will allow for a better understanding of the regional-scale processes impacting temperature and precipitation at this location.

Comparison with Sweden $\delta^{18}O$ record

In order to fully reconstruct NAO behavior back in time, a northern node of the system will need to be identified to pair with the record from Portugal. Figure 2-1 highlights regions of Europe that have statistically significant correlations of wNAO index with winter precipitation amounts. Portugal exhibits a strong negative correlation while regions of northern Europe – Scotland, Sweden, and Norway – exhibit strong positive correlations. These regions experience higher precipitation amounts during winters with higher, more positive wNAO indices. A hydroclimate proxy from one of these locations might be the ideal complement to the Portuguese hydroclimate record presented in this manuscript for studying the behavior of the NAO and its importance on the variability observed in Buraca Glorioso.

Temperature effects of the NAO are more obvious in northern Europe than in southern Europe (Portugal). In addition or instead of a precipitation-sensitive proxy from the northern node of the NAO, it is possible that a temperature-sensitive proxy could indicate NAO variability when paired with the Portugal precipitation-sensitive record presented in this manuscript.

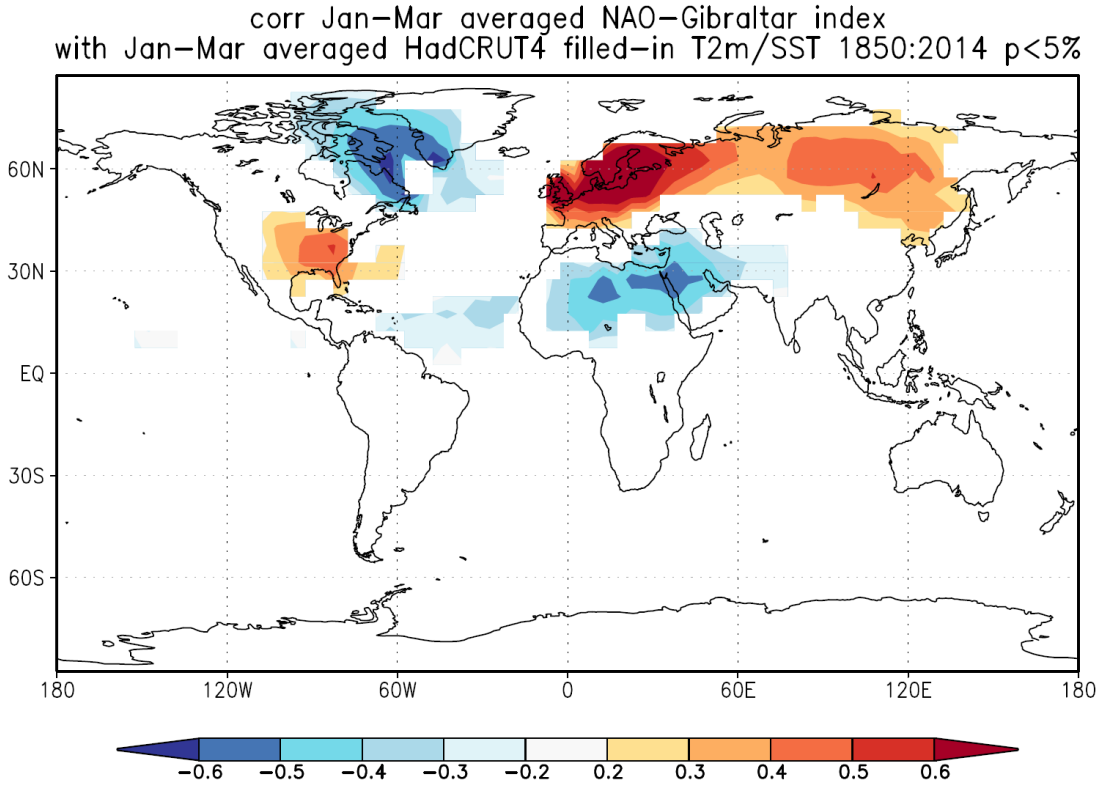

Figure 3-8. Correlation of January-March winter NAO index and January-March temperature anomalies. (KMNI Climate Explorer - climexp.knmi.nl)

Sweden is located within the area of highest correlation between winter temperature anomalies and wNAO index (Figure 3-8). $\delta^{18}O$ data (Figure 3-9) from Korallgrotten cave in northwestern Sweden (Sundqvist et al., 2010), at times, exhibit anti-phase behavior with the record from Portugal. It would be expected that, for the same NAO index, the locations in Portugal and Sweden would experience opposite hydroclimate reactions (Sweden = NAO+, increase temp. anomaly, decrease $\delta^{18}O$; Portugal = NAO+, drier conditions, increase $\delta^{18}O$). This inverse behavior is indicated at times in these two records (light blue boxes in Figure 3-9). At other times (light pink boxes in Figure 3-9), the two records show similar behavior. This could be indicative of

times when the NAO is not a dominating factor in the isotopic signal of one or both of these records.

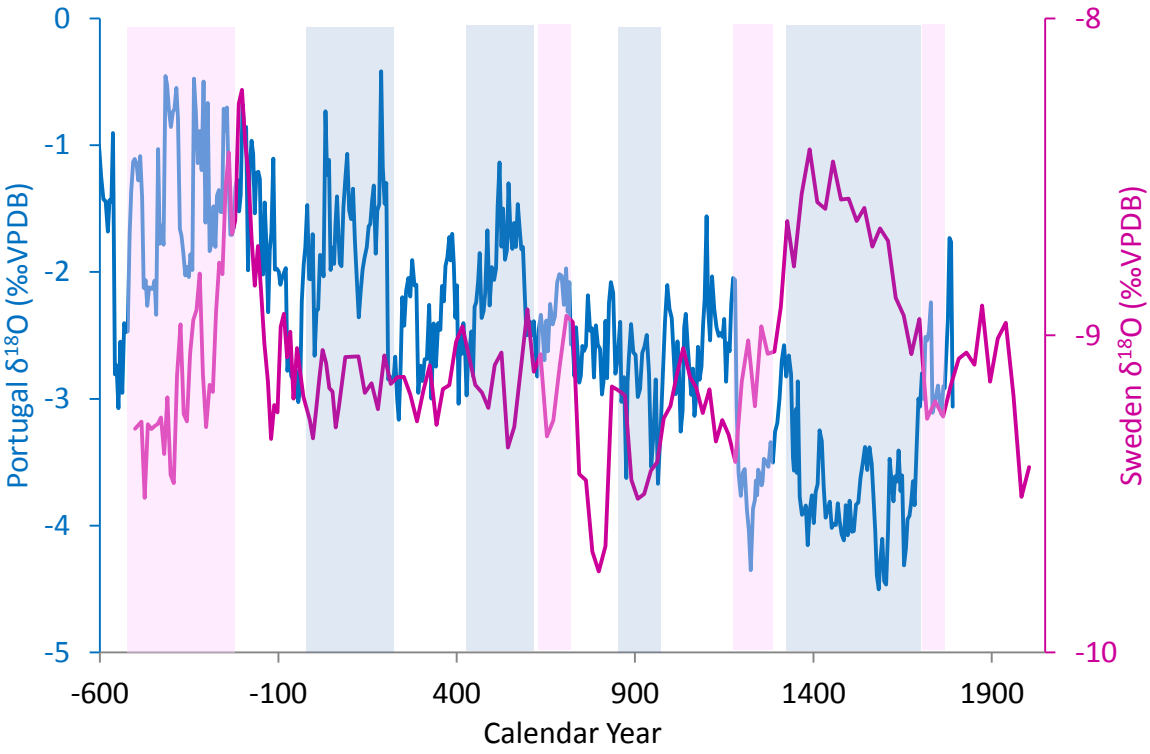

Figure 3-9. Comparison of Buraca Glorioso, Portugal micromill $\delta^{18}O$ *data (blue) with Korallgrotten (pink) cave, Sweden* $\delta^{18}O$ *data. The Korallgrotten record is a temperature record from near the northern node of the NAO system. Light blue boxes indicate times when opposite behavior is observed between Buraca Glorioso and Korallgrotten. Light pink boxes indicate times when similar behavior is observed between the two locations.*

Comparison with Spain $\boldsymbol{\delta^{13}C}$ ***Record***

The isotope data contained within the speleothem, GH-13-6, from Buraca Glorioso in central Portugal are consistent with other proxy data from the region, including northern Spain. Similar patterns of $\delta^{13}C$ isotopic variability exist at similar time periods. Interpretation of the $\delta^{13}C$ signal in a speleothem is not a simple task as there are many factors that influence the $\delta^{13}C$ signal, including changes in atmospheric CO_2, change fromC_3 to C_4 plants in the region, changes in vegetation density above the cave,

and changes in the air pCO_2 in the cave (Zhang et al., 2015; Dorale et al., 1998; Fairchild and Baker, 2012). Martín-Chivelet et al. (2011) have determined that the basic conditions in the karst systems overlaying the three studied caves in Spain have stayed the same over the last 4000 years and the medium- and long-term changes in the $\delta^{13}C$ record can be attributed to changes in surface temperature. This $\delta^{13}C$ record was initially presented as a temperature reconstruction over the last 4000 years but has been criticized as a temperature proxy due to the fact that the $\delta^{13}C$ values are responding to a series of factors and are not under a single control (Domínguez-Villar, 2013). The two Iberian Peninsula records presented (Portugal and Spain) likely are responding to the same regional changes in precipitation and temperature. These changes likely are influencing the vegetation above all of the caves and impacting the $\delta^{13}C$ records contained within the caves.

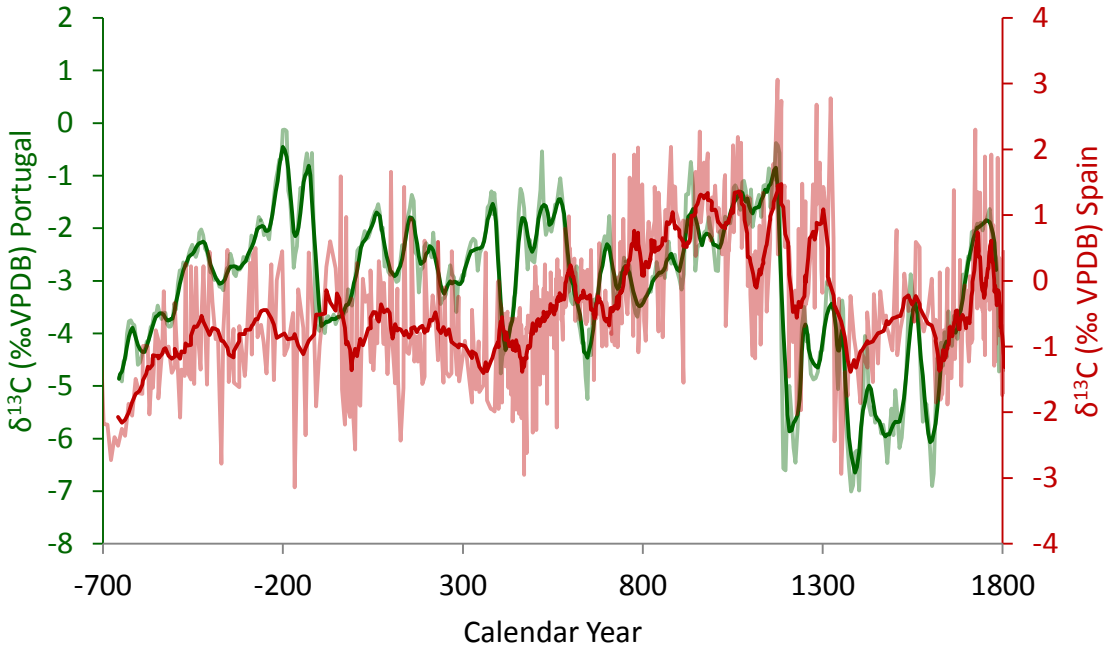

Figure 3-10. $\delta^{13}C$ records from Portugal (green) and Spain (red), both Iberian Peninsula records, from 700 BC to 1800 AD.

The apparent high correlation of the record from Buraca Glorioso and the records from Spain allows for high confidence in the age models of each record. The age models used, which both contain error, are independent of each other. The correlation between records also indicates that both of these records are responding to regional climate variability and not local conditions in or near the respective cave locations. The presence of a regional response has substantial implications for future use of both of these records as proxies for climate reconstruction.

Temperature fluctuations, solar variability, and changes in earth's orbital parameters do not account for all of the variability within this record. Precipitation variability is likely a major part of the climate system as well.

5.3.2 Precipitation

Comparison with Scotland record

Another location that would appear to be in a potentially desirable location for studying the northern node of the North Atlantic would be Scotland (See Figure 2-1). A cave in northwest Scotland, Uamh an Tartair, has been extensively studied. The $\delta^{18}O$ values from this stalagmite have not been the main focus of climate studies but instead the lamina widths of the stalagmite have been used as a proxy for past precipitation. Annual layer lamina counting allows for accurate dating and the laminae from three stalagmites from this cave are combined to produce a hydroclimate record spanning

3000 years (Proctor et al., 2000).

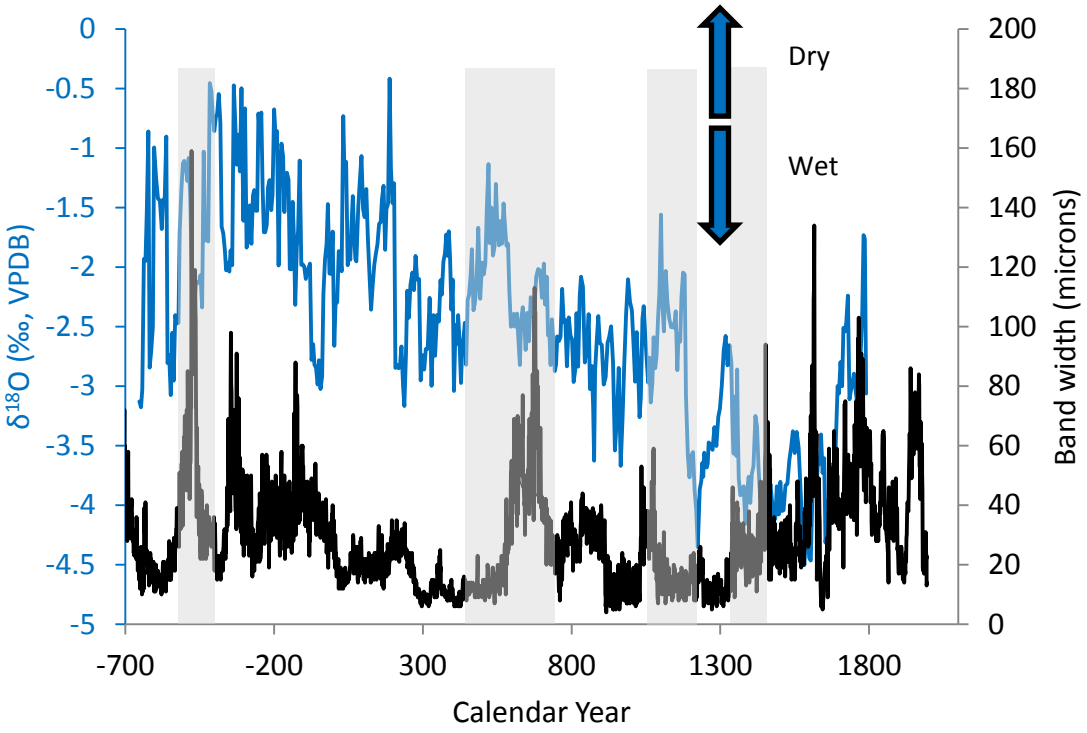

Figure 3-11. Lamina width from Scotland (black) versus $\delta^{18}O$ from Portugal (blue). Wetter Scotland = smaller bandwidth; Drier Portugal = higher $\delta^{18}O$ values (Proctor et al., 2000; Proctor et al., 2002; Trouet et al., 2009). Opposite hydroclimate behaviors would be expected in these two systems as a result of the same NAO mode (light grey boxes).

The lamina width record from Scotland does not match up well with the $\delta^{18}O$ record from Portugal (Figure 2-13). The $\delta^{18}O$ Scotland record matches up much better with the Portugal $\delta^{18}O$ record but the Scotland $\delta^{18}O$ record does not go back in time as far as the lamina widths. Times of opposite hydroclimate are indicated by the light grey boxes in Figure 3-11. A positive NAO mode would indicate wet conditions in Scotland and dry in Portugal, which NAO negative conditions would favor dry conditions in Scotland and wetter conditions in Portugal.

Comparison with Iberian Peninsula Pollen Record

Comparison of the Portugal stalagmite record with other records from the Iberian Peninsula is important to do to look for regional behavior of the climate system. Desprat et al. (2003) developed a pollen record from the Ria de Vigo, NW Iberia for the last 3000 years. Ria de Vigo is a fluvial system with a large hydrologic basin and the pollen record is sensitive to climatic changes and changes due to humans influencing the plant type and density. Changes in the types of pollen, from temperate species to steppic species, may indicate changes in the climate of the region. Pollen changes may also show changes from woodlands to pasturelands or deforestation, for example. The pollen record of Desprat et al. (2003) indicates that there was a cold phase around 975-250 BC, followed by a warm period 250 BC to 450 AD, a cold period from 450-950 AD. These events were then followed by the MCA (950-1400 AD) and the LIA (1400-1850 AD). Data from Buraca Glorioso are incomplete from the first cold period indicated by Desprat et al. (2003), but there is some indication that the Buraca Glorioso record could have recorded a cooler period leading up to 250 BC. A warm period 250 BC to 450 AD is indicated in both records. The Buraca Glorioso record does not indicate a cold period during the Dark Ages (450-950 AD) but does show a warmer period corresponding to the MCA, culminating with a cooler period during the LIA in both records.

5.4 Volcanic forcing

Four of the largest volcanic events over the past 2800 years match up with some of the largest changes in the Buraca Glorioso $\delta^{13}C$ and $\delta^{18}O$ records. Volcanic sulfate records from the GISP2 ice core record show large volcanic events around 52 BD, 640

AD, 1176 and 1258 AD, and 1782 AD and these match up with isotopic changes in the Buraca Glorioso record (Zielinski et al.,1997). These changes imply that the Buraca Glorioso $\delta^{13}C$ and $\delta^{18}O$ record is likely impacted by large volcanic events, possibly due to temperature and precipitation changes that also led to vegetation changes above the cave caused by these volcanic events.

A possible explanation for the large decreasing isotope excursion in the 13th century in both the $\delta^{18}O$ and $\delta^{13}C$ Portugal record, unexplained by variations in orbital parameters, TSI, precipitation and temperature, is volcanic activity. Sulfate aerosols from volcanic forcing affects global climate by changing the atmospheric radiative inputs and outputs (IPCC, 2013; Jones et al., 2009). Somewhere in the tropical regions of the planet, according to sulfate records from Greenland ice cores, in or around the year 1258, a large volcanic explosion occurred (Stothers, 2000). This was likely one of the largest volcanic eruptions of the last two millennia and had far-reaching effects, spreading sulfuric acid aerosols and shards of glass across the planet as far as both the North and South Poles (Stothers, 2000). This particular volcanic eruption and/or others could have had a substantial impact on the climate of the world, including Portugal, and may be detected in the $\delta^{18}O$ and $\delta^{13}C$ records of Buraca Glorioso. It is possible that volcanic forcing is not only forcing the $\delta^{18}O$ and $\delta^{13}C$ records in this cave, but forcing the entire NAO system in the region (Breitenbach et al., 2015). If this large decreasing isotope excursion seen in the Buraca Glorioso record is the result of volcanic forcing the NAO into a negative mode, this would be correlated with higher amounts of

precipitation to Portugal and lower $\delta^{18}O$ values to the study site. Further study is obviously needed to understand the role of volcanic forcing on this and other records.

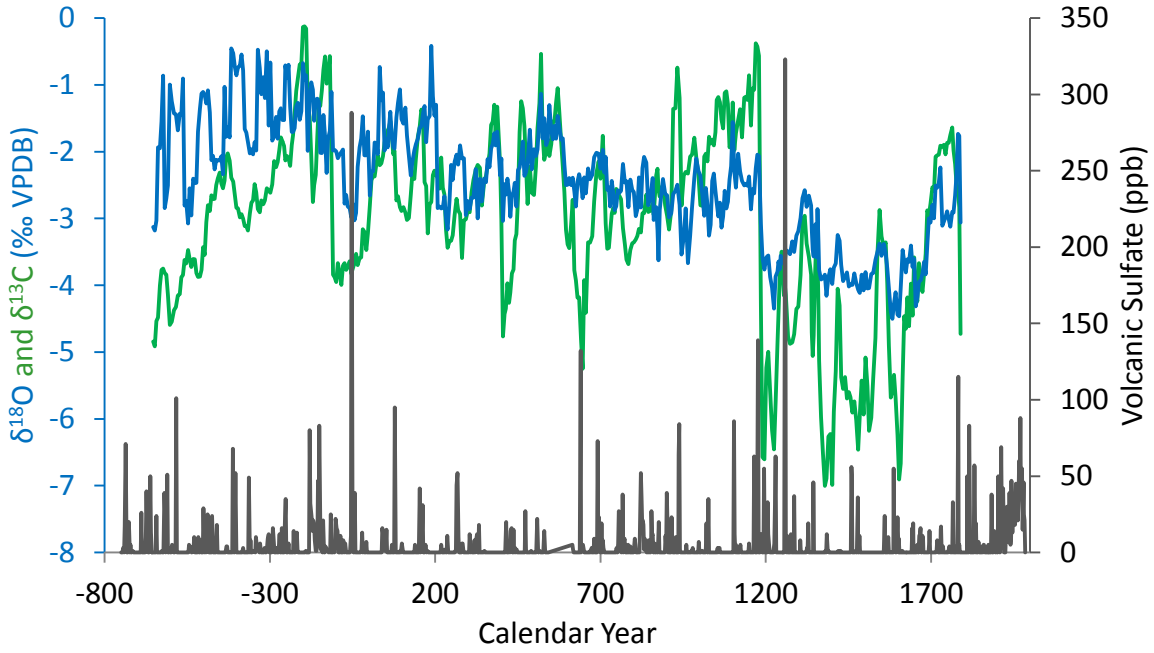

Figure 3-12. Volcanic forcing (grey) and Portugal $\delta^{18}O$ (blue) and $\delta^{13}C$ (green). Volcanic forcing is given by sulfate concentrations (grey) measured from GISP2 (Greenland) ice core (Zielinski et al., 1997).

6 Conclusions

Each pathway in Figures 3-1 and 3-2 can be studied to further understand the behavior of the isotopic signals from calcite from Buraca Glorioso. Once we know the relationship between variables and the results, we can fully understand the climate signal contained within the cave.

Variability in Earth's orbital parameters driving insolation changes is the main mechanism forcing climate in this area on longer timescales. Total solar irradiance variability and volcanic forcing are other major influences, at least at certain times during this record, and drive some of the shoter-term variability. Temperature and

precipitation changes are occurring as well during this 2300 year record and influence the $\delta^{18}O$ and $\delta^{13}C$ record contained in the stalagmite from Buraca Glorioso and these changes could be due to changes in internal modes of climate variability, such as the NAO.

A notable feature of the $\delta^{18}O$ and $\delta^{13}C$ Portugal record is the large decreasing isotope excursion around 1200-1220 AD, in the heart of the Medieval Climate Anomaly, which is not adequately explained by changes in solar variability, Earth's orbital parameters, and precipitation and temperature changes. It is possible that this large decreasing $\delta^{18}O$ and $\delta^{13}C$ excursion around 1200-1220 AD is a result of volcanic forcing that caused changes in temperatures and/or precipitation in the region and around the world.

References

Bard, E., Raisbeck, G., Yiou, F., Jouzel, J., 1997. Solar modulation of cosmogenic nuclide production over the last millennium: comparison between ^{14}C and ^{10}Be records. Earth Planet. Sci. Lett. 150, 453-462.

Bard, E., Raisbeck, G., Yiou, F., Jouzel, J., 2000. Solar irradiance during the last 1200 years based on cosmogenic nuclides. Tellus 52B, 985-992.

Bard, E., Raisbeck, G., Yiou, F., Jouzel, J., 2007. Comment on "Solar activity during the last 1000 yr inferred from radionuclude records" by Muscheler et al. (2007). Quat. Sci. Rev. 26, 2301-2308.

Berger and Loutre, 1991. Insolation values for the climate of the last 10 million years. Quat. Sci. Rev. 10, 297-317.

Breitenbach, F., Ridley, H., Lechleitner, F., Asmerom,Y., Rehfeld, K., Prufer, K., Kennett, D., Aquino, V., Polyak, V., Goswami, B., Marwan, N., Haug, G., Baldini, J. Volcanic forcing of the North Atlantic Oscillation over the last 2,000 years. 2015 EGU Abstract #6541. Geophysical Research Abstracts. European Geophysical Union General Assembly 2015. Vol. 17.

Crowley, T., 2000. Causes of Climate Change over the past 1000 Years. Science 289, 270-277.

Cruz, F., Burns, S., Karmann, I., Sharp, W., Vuille, M., Cardoso, A., Ferrari, J., Dias, P., Viana, O., Insolation-driven changes in atmospheric circulation over the past 116,000 years in subtropical Brazil. Nature 343, 63-65.

Denton, G., Broecker, W., 2008. Wobbly ocean conveyor circulation during the Holocene? Quat. Sci. Rev. 27, 1939-1950.

Desprat, S., Goni, M.F.S., Loutre, M.-F., 2003. Revealing climatic variability of the last three millennia in northwestern Iberia using pollen influx data. Earth Planet. Sci. Lett. 213, 63-78.

Domínguez-Villar, D., 2013. Comment on "Land surface temperature changes in Northern Iberia since 4000 yr BP, based on $\delta^{13}C$ of speleothems". Global Planet. Change 100, 291-294.

Dorale, J., Edwards, R.L., Ito, E., Gonzalez, L., 1998. Climate and Vegetation History of the Midcontinent from 75 to 25 ka: A Speleothem Record from Crevice Cave, Missouri, USA. Science 282, 1871-1874.

Fairchild, I., A. Baker, 2012. Speleothem Science: From Process to Past Environments. Wiley-Blackwell, Oxford.

Field, C., Schmidt, G., Koch,D., Salyk, C., 2006. Modeling production and climate-related impacts on ^{10}Be concentration in ice cores. J. Geophys. Res. 111, 1-13.

Houts, A., Denniston, R., Aserom, Y., Polyak, V., Wanamaker, A., Haws, J., Thatcher, D., 2014. A high-resolution record of continental climate variability over the last 90,000 years from Buraca Glorioso cave, Western Portugal. GSA Abstract #43-5. Geological Society of America Abstract with Programs. Vol. 46, No. 6, p. 127.

IPCC, 2013. Fifth Assessment Report (AR5), Climate Change 2013: The Physical Science Basis. Contribution of Work Group I to the Fifth Assessment Report of the Intergovernmental Panel on Climate Change, Cambridge Press, Cambridge, United Kingdom and New York, NY, USA. 1552 pp.

Jones, P., Briffa, K., Osborn, T., Lough, J., van Ommen, T., Vinther, B., Luterbacher, J., Wahl, E., Zwiers, F., Mann,M., Schmidt, G., Ammann, C., Buckley, B., Cobb, K., Esper, J., Goosse, H., Graham, N., Jansen, E., Kiefer, T., Kull, C., Kuttel, M., Mosley-Thompson, E., Overpeck, J., Riedwyl, N., Schulz, M., Tudhope, A., Villalba, R., Wanner, H., Wolff, E., Xoplaki, E., 2009. High-resolution palaeoclimatology of the last millennium: a review of current status and future prospects. Holocene 19, 3-49.

Keigwin, L., Pickart,R., 1999. Slope Water Current over the Laurentian Fan on Interannual to Millennial Time Scales. Science 286, 520-523.

Korte, M., Constable, C., 2005. Continuous geomagnetic field models for the past 7 millennia: 2.CALS7K. Geochem., Geophys., Geosystems 6,1-18.

Lean, J., Beer, J., Bradley, R., 1995. Reconstruction of solar irradiance since 1610: implications for climate change. Geophys. Res. Lett. 22, 3195-3198.

Li, B., Nychka, D., Ammann, C., 2010. The Value of Multiproxy Reconstruction of Past Climate. J. Am. Stat. Assoc. 105, 883-911.

Mann, M.E., Jones, P.D., 2003. Global Surface Temperatures over the Past Two Millennia. Geophys. Res. Lett. 30, 1820.

Martín-Chivelet, J., Muñoz-García, M., Edwards., L., Turrero, M., Ortega, A., 2011. Land surface temperature changes in Northern Iberia since 4000 yr BP, based on $\delta^{13}C$ of speleothems. Global Planet. Change 77, 1-12.

Moberg, A., Sonechkin, D., Holmgren, K., Datsenko, N., Karlen, W., 2005. Highly variable Northern Hemisphere temperatures reconstructed from low- and high-resolution proxy data. Nature 433, 613-617.

Pais, J., Cunha, P., Pereira, D., Legoinha, P., Dias, R., Moura, D., Brumda Silveira, A., Kullberg, J.C., Gonzalez-Delgado, J.A., 2012. The Paleogene and Neogene of Western Iberia (Portugal). Springer, Heidelberg.

Proctor, C., Baker, A., Barnes, W., Gilmore, M., 2000. A thousand year speleothem proxy record of North Atlantic climate. Clim. Dyn. 16, 815-820.

Proctor, C., Baker, A., Barnes, W., 2002. A three thousand year record of north Atlantic climate. Clim. Dyn. 19, 449-454.

Rodrigues, M., Fonseca, A., 2010. Geoheritage assessment based on large-scale geomorphological mapping: contributes from a Portuguese limestone massif example. Geomorphologie: relief, processus, environnement. 2, 189-198.

Santos, J., Carneiro, M., Alcoforado, M., Leal, S., Luz, A., Camuffo, D., Zorita, E., 2015. Calibration and multi-source consistency analysis of reconstructed precipitation series in Portugal since the early 17^{th} century. Holocene 25, 663-676.

Stothers, R., 2000. Climatic and demographic consequences of the massive volcanic eruption of 1258. Clim. Change 45, 361-374.

Sundqvist, H.S., K. Holmgren, A. Moberg, C. Spötl, and A. Mangini, 2010. Stable isotopes in a stalagmite from NW Sweden document environmental changes over the past 4000 years. Boreas 39, 77-86.

Trouet , V., Esper, J., Graham, N.E., Baker, A., Scourse, J.D., Frank, D.C., 2009. Persistent positive North Atlantic Oscillation mode dominated the Medieval climate anomaly. Science 324, 78-80.

Wang, Y., Cheng, H., Edwards, R.L., He, Y., Kong, X., An, Z., Wu, J., Kelly, M., Dyoski, C., Li, X., 2005. The Holocene Asian Monsoon: Links to Solar Changes and North Atlantic Climate. Science 308, 854-857.

Wang, Y., Cheng, H., Edwards, R.L., Kong, X., Shao, X., Chen, S., Jiang, X., Wang, X., An, Z., 2008. Millennial- and orbital-scale changes in the East Asian monsoon over the past 224,000 years. Nature 451, 1090-1093.

Zhang, H., Cai, Y., Tan,L., Cheng, H., Qin, S., An, Z., Edwards, R.L., Ma, L., 2015. Large variations of $\delta^{13}C$ values in stalagmites from southeastern China during historical times: implications for anthropogenic deforestation. Boreas 44, 1-15.

Zielinski, G., Mayewski, P., Meeker, D., Whitlow, S., Twickler, M., 1997. A 110,000-Yr Record of Explosive Volcanism from the GISP2 (Greenland) Ice Core. Quat. Res. 45, 109-118.

Zorita, E., Gonzalez-Rouco, F., 2002. Are temperature-sensitive proxies adequate for North Atlantic Oscillation reconstruction? Geophys. Res. Lett. 29, 1-4.

CHAPTER 4: GENERAL CONCLUSIONS and FUTURE WORK

1 General Conclusions

Stalagmites from Buraca Glorioso record Portuguese hydroclimate of the Iberian Peninsula. Hydroclimate is mostly a measure of precipitation in the region but since the link between precipitation and temperature is strong, this record could reflect changes in temperature as well. Drier times of the year correspond with warmer times of the year in Portugal and wetter conditions prevail at cooler times of the year, complicating the interpretation of $\delta^{18}O$ values from the speleothem calcite.

The potential of speleothems as climate proxies is apparent. There are situations where the data is difficult to interpret (due to the multiplicity of interrelated inputs) and calibration is often difficult or impossible, as is the case with this research (due to nonexistent instrumental records for the time period and location covered by the speleothem record). However, sensitivity to climate and climate changes makes speleothems an excellent proxy, one that warrants additional research.

In order to interpret isotopic changes contained within stalagmites, some assumptions and testing of those assumptions must take place. If the isotopic composition of the calcite is a function of the temperature at formation, this quantity must be determined. From this study, it was determined that the temperature in the cave likely only varies by approximately 0.6 ^{o}C on an annual basis. This small change in temperature would reflect a small change in $\delta^{18}O$, less than 0.14 ‰. Temperature at calcite formation in this study, therefore, is assumed to be constant and variability of $\delta^{18}O$ in the calcite is reflecting variability in $\delta^{18}O$ of precipitation.

The results of this study add to the collective understanding of the climate system in the Atlantic region, specifically the North Atlantic Oscillation. Changes in $\delta^{18}O$ and $\delta^{13}C$ in the calcite during the MCA and LIA show a variable hydroclimate in Portugal with generally warmer/drier conditions, yet still variable, during the MCA and cooler/wetter conditions during the LIA.

Considering the entire Buraca Glorioso record, longer-term drivers of the climate in the region can be studied. Solar insolation changes due to orbital parameters are important factors controlling the $\delta^{18}O$ values of the calcite. Other factors that cause isotopic changes on shorter timescales include changes in TSI, precipitation and temperature changes, in part due to internal climate mode variability, and volcanic forcing.

Speleothems, due to their widespread nature across a variety of terrestrial areas and their ability to be precisely and absolutely dated, will continue to be studied for use as a climate proxy. The Iberian Peninsula will continue to attract attention for these types of studies due to its location - in a position consistently under the influence of the NAO and near the Atlantic Ocean. Results from climate proxy studies such as these will help researchers better understand the NAO and the entire climate system.

2 Future Work

2.1 Instrumentation

While much work has been done to learn about this cave, cave environment, and the results from the stalagmite, there is much more to study. Further understanding of the cave system will better constrain the $\delta^{18}O$ data recorded in stalagmite. There are

still several parts to the cave system that could be better constrained to better use the isotopic changes indicated by the stalagmites to deduce past climatic conditions in the region and world. Additional work to understand the Buraca Glorioso cave system include installation of a pCO_2(to measure the partial pressure of carbon dioxide) meter inside the cave to confirm that conditions within the cave are stable throughout the year and a meteorological station at or near the cave that records temperature, humidity, and precipitation. There are few sites that record temperature and relative humidity within 50 km and the nearest meteorological station that records daily precipitation is 58 km away (Monte Real, Portugal). It is assumed that quantities and time of precipitation at Monte Real closely match those at the cave and residence time of water within the cave is calculated from these precipitation data. The cave is located at a higher elevation than any of the nearby precipitation monitoring stations. Likely this difference in altitude affects the amount of precipitation received, but likely not the timing of such events.

2.2 Isotopes of local precipitation and dripwater

In addition to more accurate meteorological data, additional isotopes of precipitation from the area is critical to further understanding the isotopic changes seen within the calcite. Citizen scientists, including high school students and teachers and owners of the nearby tourist cave, will be involved in collecting precipitation throughout the year to see how precipitation isotopes vary with time, with precipitation amounts, and within a storm. Concurrent measurements of precipitation isotopes and temperature would allow us to be able to decompose the relationship with $\delta^{18}O$ of

precipitation and temperature and precipitation amount and determine which (temperature or precipitation amount) is the dominant control of the $\delta^{18}O$ of precipitation in the cave area. Portugal's distinct wet and dry seasons allow for simpler climatic interpretations of this record. Precipitation amount increases and temperature decreases at the same time of the year in Portugal (winter). Both increased amount and decreased temperature drive $\delta^{18}O$ precipitation values lower but which factor is more important?

Currently, dripwater in the cave is being collected in 3 collection containers that very roughly separate different time periods of drip water. As we collect more detailed yearly precipitation, collecting dripwater in monthly or weekly time steps would allow for direct comparison of the precipitation falling outside the cave and how the isotopes of that water changes during transit into the cave. An automated collected device would be the most practical way of sampling due to the remote nature of the cave.

2.3 Elements

In calcitic speleothems, there exists a positive correlation between higher magnesium and strontium concentrations and lower effective rainfall, determined by prior calcite precipitation (PCP) or Prior Aragonite Precipitation (PAP) (Wassenburg et al, 2013). Future work will involve elemental analysis of the stalagmite and of the drip water from the cave. Analysis of elements will allow us to begin to determine if the Buraca Glorioso record is precipitation-driven or temperature-driven. If the elemental ratios remain unchanged during periods of large isotopic changes, we can infer that the isotopic changes are due to precipitation amount effects. Trace element analysis will be

done on the same portions of the same as the isotopes were measured to allow for direct comparison of the two results (Fairchild et al., 2006).

For much of the last 2600 years, stalagmite GH-13-6 has been growing fairly slowly. It is also a fairly small (approx. 43 cm by 4 cm) stalagmite. Annual layers are impossible to discern with the naked eye. Examining the stalagmite with fluorescent light under a microscope may indicate annual and/or seasonal banding. If annual banding exists, the age model could be further calibrated using layer counting techniques paired with uranium-thorium disequilibrium methods. Another benefit to microscopic analysis of laminae is to analyze seasonal changes in annual growth layers (Mattey et al., 2008).

2.4 Replication

During the trip to Buraca Glorioso in August 2013, other stalagmites were collected that would make possibly good replicates of GH-13-6. GH-13-13 and GH-13-2 have been dated and have dates that overlap the time period of interest. One mm resolution stable isotope data have been obtained during these overlapping time periods to allow for comparison of oxygen and carbon isotopes. These data show similar trends over the same time periods, considering the errors in the U-Th ages. Stalagmite GH-13-13 was obtained near the loft area of the cave but was on the floor of the cave. It has a dirtier appearance. Stalagmite GH-13-2 was obtained from the loft area near the primary stalagmite of interest. The top of this stalagmite is dated at 1848 years before 2013 and has 23 mm and 768 years of overlap with GH-13-6.

Replication is essential to determining with certainty that the isotopic changes contained within the stalagmite are a result of climate changes in the region. Fortunately, there are three other lower resolution records with U-Th dates from Buraca Glorioso stalagmites to compare to our high resolution record. Two of the stalagmites are small and have dated growth intervals in the late Holocene. One of these two stalagmites was collected from the loft area of the cave, just as GH-13-6 was collected. One of the stalagmites was collected just under the loft area, within 5 meters of GH-13-6. A third stalagmite (GH-12-LowRM) was collected from 7-8 meters away, is much larger, and the bottom of the stalagmite has been dated to 120,000 yr BP. Figure 4-1 presents $\delta^{18}O$ data from each of these stalagmites as well as GH-13-6 during the overlapping time periods of the late Holocene.

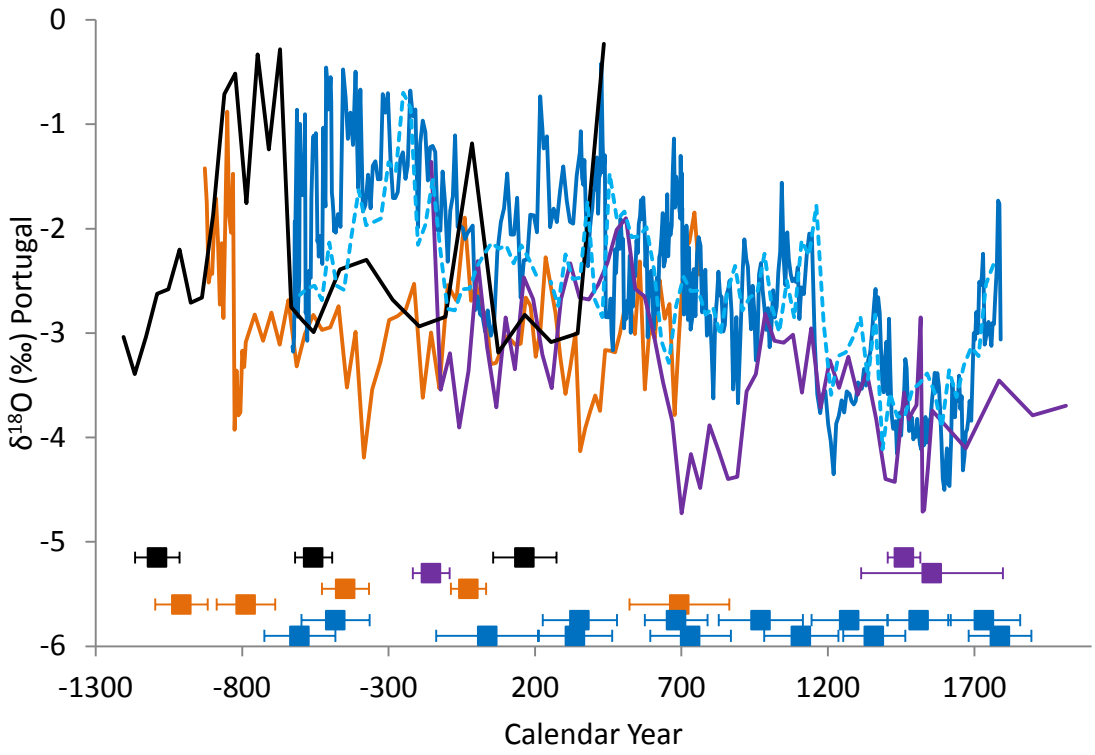

Figure 4-1. Four stalagmites containing late Holocene data from Buraca Glorioso. GH-13-6 (1mm resolution = dashed blue; micromill = solid blue), GH-13-13 (purple), GH-13-2 (black), and GH-12-LowRM (orange). U-Th dates for each stalagmite are indicated in the corresponding color with errors as shown. Figure 4-2. Plot of variability contained within each Buraca Glorioso stalagmite – GH-13-6 (1 mm = blue on right; micromill = blue on left), GH-13-13 (purple), GH-13-2 (black), and GH-12-LowRM (orange).

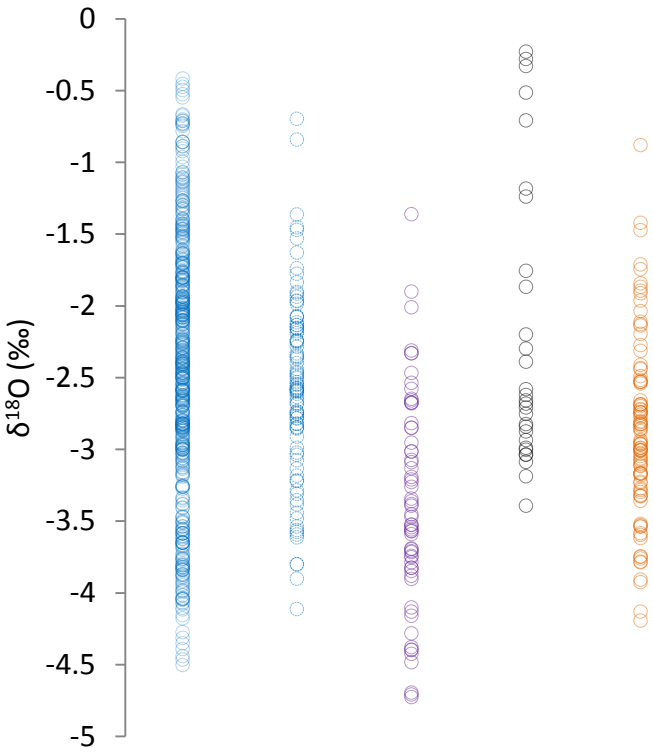

Figure 4-2. Plot of variability contained within each Buraca Glorioso stalagmite – GH-13-6 (1 mm = blue on right; micromill = blue on left), GH-13-13 (purple), GH-13-2 (black), and GH-12-LowRM (orange).

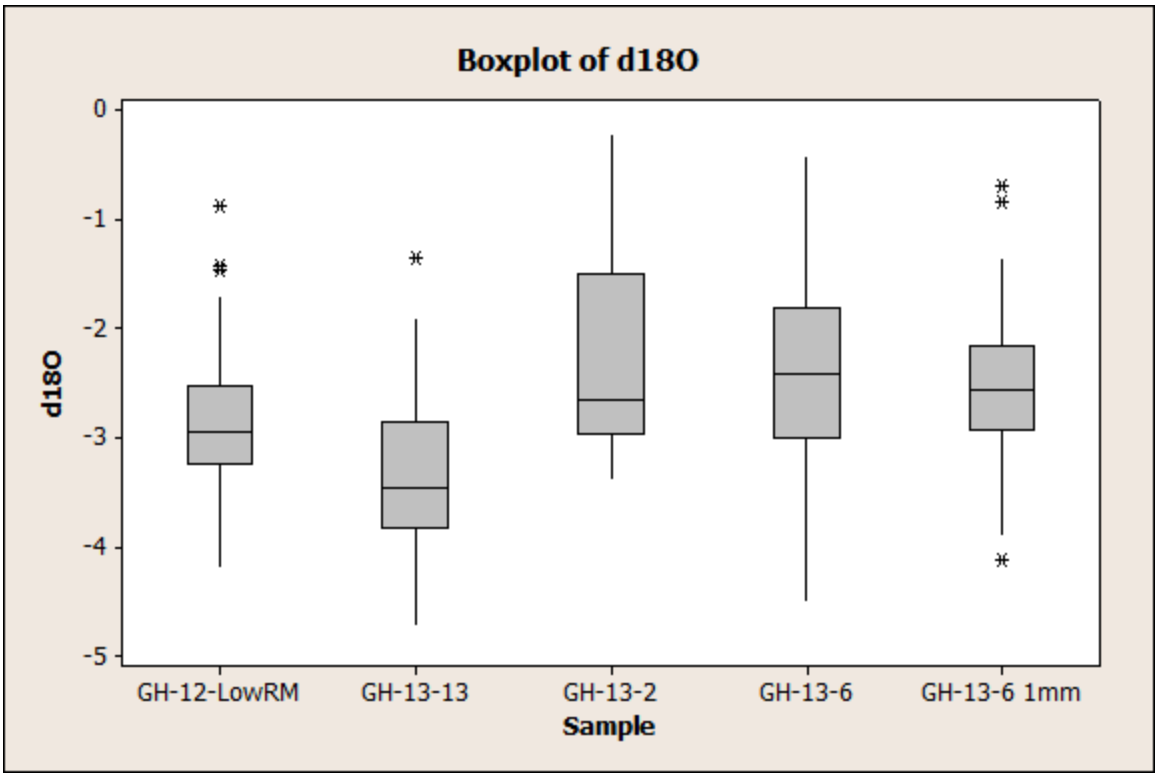

Figure 4-3. Box and whiskers plot showing variability of $\delta^{18}O$ *values for each stalagmite from Buraca Glorioso. The line in the middle of the box is the median, the top and bottom of the box are the third (Q3) and first (Q1) quartile lines, respectively, and the vertical lines indicate the range of the data. The stars are statistical outliers identified as observations that are greater than 1.5 times the Q3-Q1 range outside of the box.*

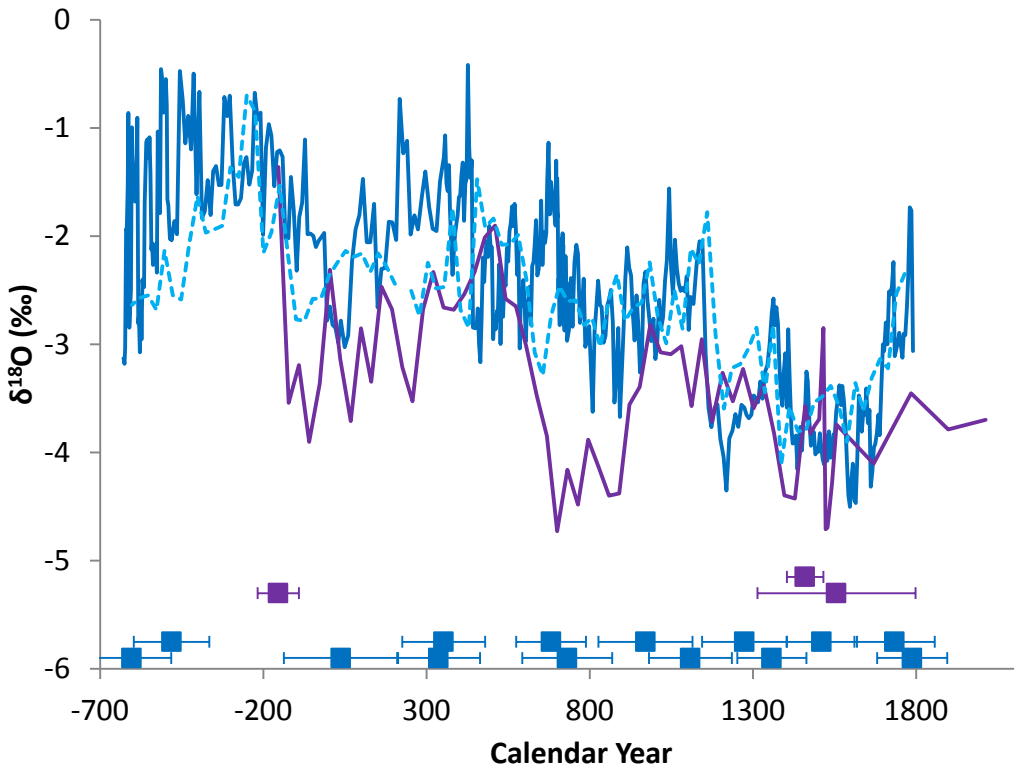

Figure 4-4. Plot of two Buraca Glorioso stalagmites with dates and isotopes from same time period – GH-13-6 (1mm resolution = dashed blue; micromill = solid blue) and GH-13-13 (purple).

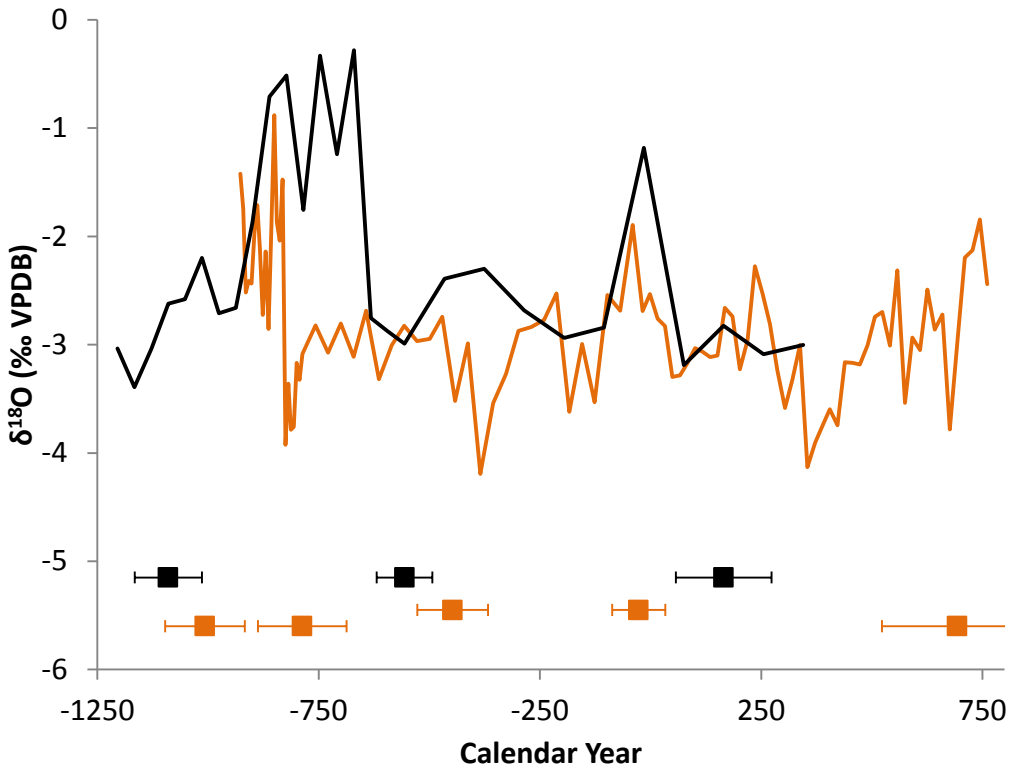

Figure 4-5. Plot of two Buraca Glorioso stalagmites with dates and isotopes from same time period – GH-12-LowRM (orange) and GH-13-2 (black).

Two other stalagmites were collected from the loft area but do not have U-Th dates presently. Stalagmites GH-13-3 and GH-13-4 were both growing near GH-13-6 in the loft area of the cave and have potential to be good replicates. Ideally, one or both of these stalagmites will have overlapping growth periods with GH-13-6 and overlapping growth periods with the instrumental period, allowing for direct comparison of measured climate data with measured $\delta^{18}O$ changes in the calcite.

Replication is critical to the success of this project to show that the isotopic changes measured in the stalagmites are as a result of regional climatic changes and not variability within the stalagmite and its micro-environment (cave dynamics). If we see similar patterns in two or more stalagmites from the same cave, changes can be more

confidently attributed to changes in regional climate. Another step beyond replication within the cave is replication from the same area in Portugal but in a different cave. This has been done by comparing the Buraca Glorioso data with those of the three caves from Spain (Martín-Chivelet et al., 2011). The record from GH-13-6 and the three Spanish caves are remarkably similar, indicating that the processes controlling the carbon isotopes, and likely the oxygen isotopes as well, are related to regional climate changes.

Hand milling of stalagmites is common practice, yielding large amounts of data for analysis. To look for finer scale changes in the climate system, finer scale sampling is necessary. Although the general trends remain the same, the ability to micromill sections of the stalagmite allows for closer inspection of decadal (or smaller) scale changes. Having several other specimens to accurately date and sample at 1 mm resolution will allow us to pinpoint several other stalagmites on which to do micromill sampling for further comparison with GH-13-6.

Additionally, in order to study other Holocene Rapid Climate Changes (as described by Mayewski et al., 2004), micromilling of GH-13-6 paired with additional U-Th dates on the sample would allow this record to be compared with other records dating further back into the Holocene. The record presented in this work ends at 2600 years BP, during the Rapid Climate Change event of 3500-2500 years BP (Mayewski et al., 2004). The stalagmite, GH-13-6 is approximately 43 cm long and only the top 10 cm have been dated and micromilled, so there is potentially much more to learn about Holocene climate variability from this one particular record.

2.5 Earthquake

A linear fit to the dates given by uranium-thorium disequilibrium methods give a date for the top of the stalagmite of 1790 AD. It is possible that the stalagmite has not grown at all since the late 1700s. Although this does not change the wealth of information to be gained from these stalagmites prior to the 1700s, it does limit our ability to calibrate these data with instrumental data. Many places in the cave show large stalactites that appear to have been broken off with smaller soda straws growing from the broken off portion of the stalactite (Figure 4-6). Many factors could have caused this breakage but an event coincidental with the slowing or ceasing of growth in the cave seems like a likely scenario.

In 1755, much of Lisbon and much of Portugal was destroyed by the Great Lisbon Earthquake of November 1, 1755 (Gutscher, 2004; Pro et al.,2013; Vilanova et al., 2003). Could this earthquake have caused the damage to the stalactites and also caused a shift in drip patterns within the cave? Additional dating of the ends of these large stalactites and the entirety of the small soda straws would inform us about the timing of potentially large changes in the cave dynamics coincident with the Great Lisbon Earthquake.

Figure 4-6. Stalagmite GH-13-6 (left) with large stalactite (right) from Buraca Glorioso with end broken off. New soda straw growing at the base of the broken stalactite.

2.6 Additional proxy for northern node of NAO

The Trouet et al. (2009) NAO reconstruction used a climate proxy from each of the NAO nodes (Scottish speleothem and Moroccan tree ring record). Ideally, this research aims to develop a northern node to compare with the Portugal Buraca Glorioso cave data to use for reconstructing past NAO behavior. Existing data have allowed (see Chapter 2 and 3) for comparison of stalagmite $\delta^{18}O$ data from Portugal with $\delta^{18}O$ data from Sweden (Koralgrotten, Sundqvist et al., 2010), $\delta^{18}O$ data and lamina width from Scotland (Proctor et al., 2000; Proctor et al., 2002; Trouet et al., 2009), two areas with high positive correlations between winter precipitation and winter North Atlantic Oscillation indices (see Chapter x, Figure x). Further development of these locations and/or the development of a different, second study site (possibly in Scotland, Sweden, and/or Norway) would further this research by allowing for comparisons of changes seen at the two nodes of the NAO system. We would expect to see opposite changes on similar timeframes. Continued collaborations and synthesis of paleoclimate records will

allow for better understanding of the climate system and the mechanisms that drive climate.

References

Almeida, C., Silva, M.L., and J.A. Crispim, 1995. Hydrogeological aspects of groundwater protection in karstic areas. Final Report, Dir-General Science. 211-220.

Baker, A., Smith, C., Jex, C., Fairchild, I., Genty, D., Fuller, L., 2008. Annually laminated speleothems: a review. Int. J. Speleol., 37, 193-206.

Baker, A., Wilson, R., Fairchild, I., Franke, J., Spotl, C., Mattey, D., Trouet, V., Fuller, L., 2011. High resolution $\delta^{18}O$ and $\delta^{13}C$ records from an annually laminated Scottish stalagmite and relationship with last millennium climate. Global Planet. Change 79, 303-311.

Fairchild, I., Smith, C., Baker, A., Fuller, L., Spotl, C., Mattey, D., McDermott, F., 2006. Modification and preservation of environmental signals in speleothems. Earth Sci. Rev. 75, 105-153.

Mayewski, P., Rohling, E., Stager, J., Karlen, W., Maasch, K., Meeker, L., Meyerson, E., Gasse, F., van Kreveld, S., Holmgren, K., Lee-Thorp, J., Rosqvist, G., Rack, F., Staubwasser, M., Schneider, R., Steig, E., 2004. Holocene Climate Variability. Quat. Res. 62, 243-255.

Pro, C., Burorn, E., Bezzeghoud, M., Udias, A., 2013. The earthquakes of 29 July 2003, 12February 2007, and 17 December 2009 in the region of Cape Saint Vincent (SW Iberia) and their relation with the 1755 Lisbon earthquake. Tectonophysics 583, 16-27.

Gutscher, M.-A.., 2004. What Caused the Great Lisbon Earthquake? Science 305, 1246-1248.

Mattey, D., Lowry, D. Duffet, J., Fisher, R., Hodge, E., Fisia, S., 2008. A 53 year seasonally resolved oxygen and carbon isotope record from a modern Gilbraltar speleothem: reconstructed drip water and relationship to local precipitation. Earth Planet. Sci. Lett. 269, 80-95.

Proctor, C., Baker, A., Barnes, W., Gilmore, M., 2000. A thousand year speleothem proxy record of North Atlantic climate. Clim. Dyn. 16, 815-820.

Proctor, C., Baker, A., Barnes, W., 2002. A three thousand year record of north Atlantic climate. Clim. Dyn. 19, 449-454.

Sundqvist, H.S., K. Holmgren, A. Moberg, C. Spötl, and A. Mangini, 2010. Stable isotopes in a stalagmite from NW Sweden document environmental changes over the past 4000 years. Boreas 39, 77-86.

Trouet , V., Esper, J., Graham, N.E., Baker, A., Scourse, J.D., Frank, D.C., 2009. Persistent positive North Atlantic Oscillation mode dominated the Medieval climate anomaly. Science 324, 78-80.

Vilanova, S., Nunes, C., Fonseca, J., 2003. Lisbon 1755: A Case of Triggered Onshore Rupture? B. Seismol. Soc. Am. 93, 2056-2068.

Wassenburg, J.A., Immenhauser, A., Richter, D.K., Niedermayr, A., Riechelmann, S., Fietzke, J., Scholz, D., Jochum, K.P., Fohlmeister, J., Schroder-Ritzrau, A., Sabaoui,A.,Riechelmann, D.F.C., Schneider, L., Esper, J., 2013. Moroccan speleothem and tree ring records suggest a variable positive state of the North Atlantic Oscillation during the Medieval Warm Period. Earth Planet. Sci. Lett. 375, 291-302.

APPENDIX A: DATA SAMPLING

Large changes (>3-4‰,VPDB) are observed in the 2300+ year time series of oxygen isotopes from stalagmite GH-13-6 from Buraca Glorioso. Some time periods, 1150-1300 AD, for example, demonstrate large changes in oxygen isotopes over a short period of time, changing from -2.0 to -4.4 ‰ in 45 years. To determine that the signal contained within these changes is a result of climate change and not instrumental noise, an investigation was performed looking to see if the large changes occurred within an instrumental run (intra-run variability) or the changes were occurring between runs (inter-run variability) on the mass spectrometer. Figure A-1 shows that each of the large changes in isotopes occurs within a run under the same conditions (same acid, standards, etc.).

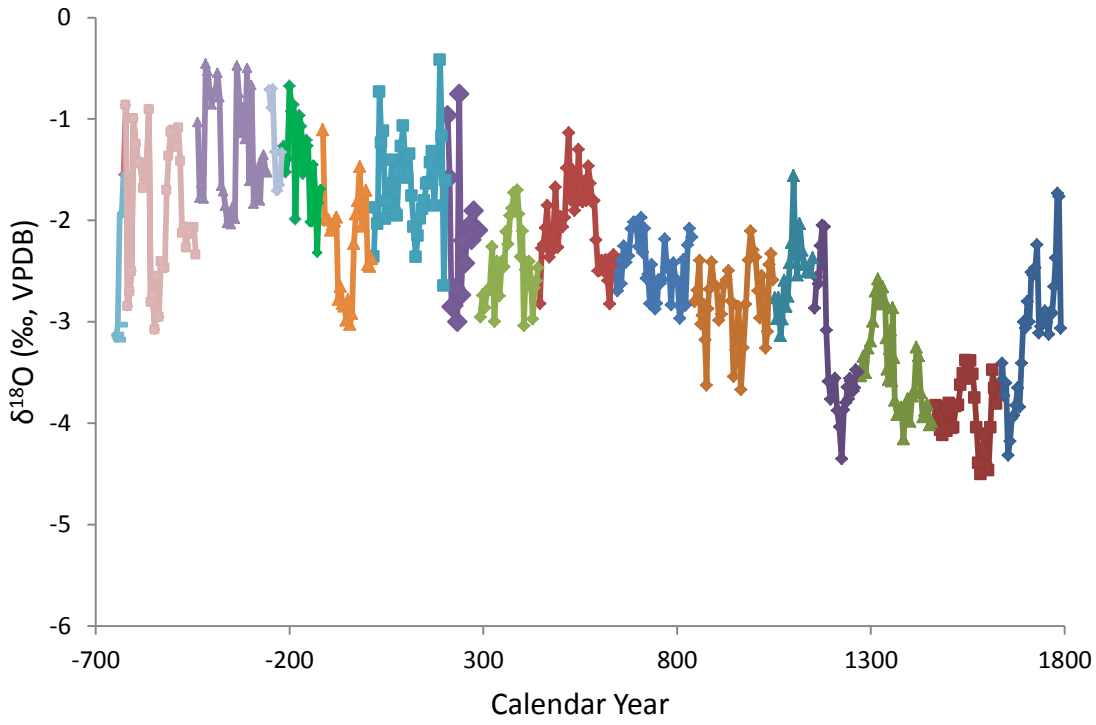

Figure A-1. Plot showing inter-run and intra-run variability for GH-13-6 micromill $\delta^{18}O$ *data. Each separate run of isotopes on the mass spectrometer is indicated by a distinct color.*

Many studies using stalagmites as a climate proxy are conducted with resolution lower than that performed in the research presented here. Initially, these stalagmites were sampled at 1 mm resolution over the likely time period of interest and, once definitive U-Th ages were obtained, micromilling began along the growth axis. These samples (1 mm and micromilled) were analyzed on the Thermo Finnegan mass spectrometer and analyzed for stable carbon and oxygen isotopes. These samples were analyzed 9-15 months apart on the same machine with different filaments in the machine and the same set of standards (NBS-18, NBS-19, LSVEC). The two suites of data were compared to determine if the high-resolution data signal was reflected in the

lower resolution data initially gathered. Figure A-2 (a) and (b) shows the 1mm versus micromilled data for oxygen and carbon isotopes, respectively.

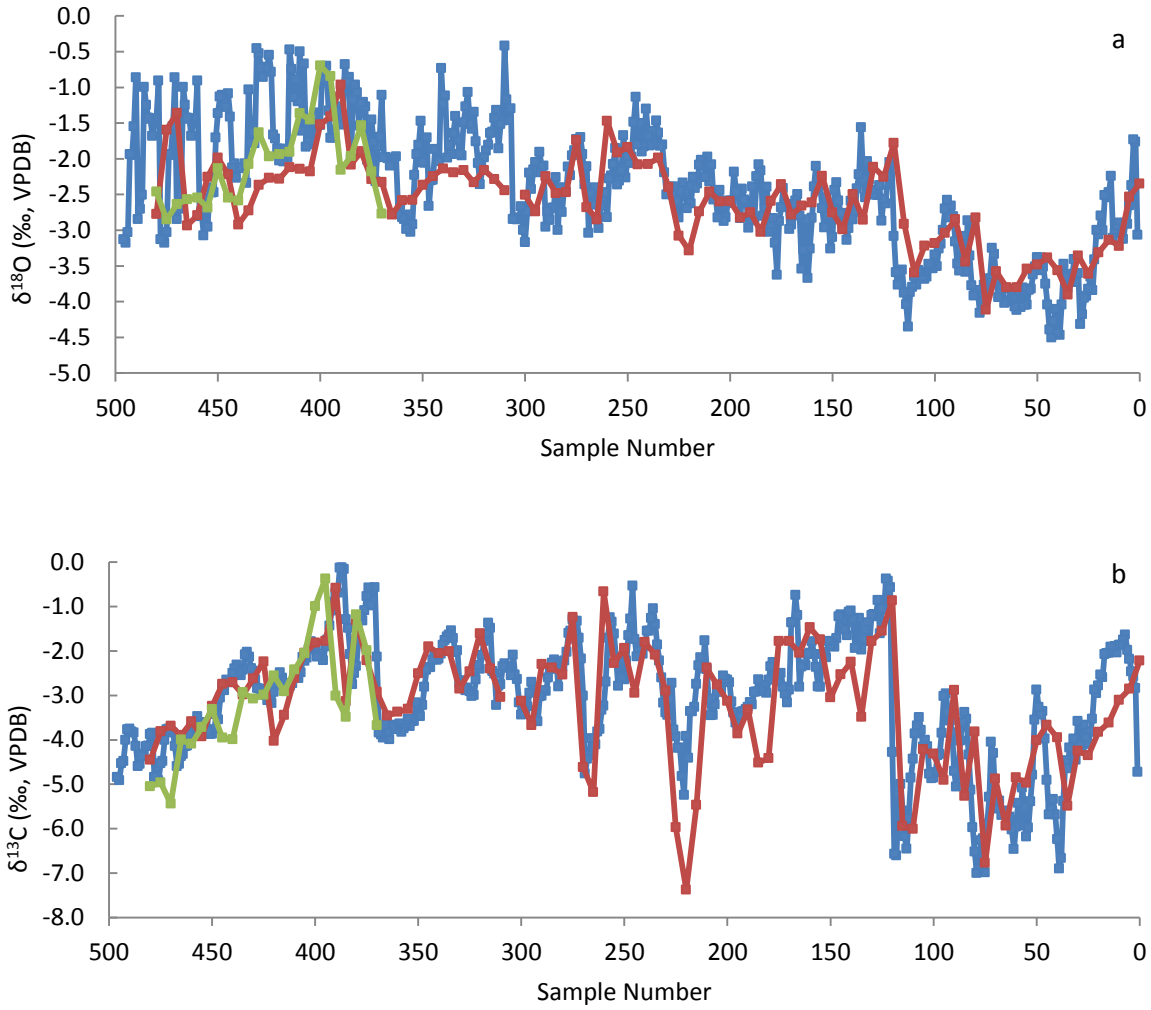

Figure A-2 (a) $\delta^{18}O$ and (b) $\delta^{13}C$. Blue indicates micromilled data, red indicates 1mm sampling. Green indicates alternate transect during a period of growth not along central axis.

The data show striking similarities in both the carbon and oxygen isotopes. General trends are evident in both records which indicate that, for many research questions, a lower resolution record will indicate broad climate changes just as well as a higher resolution record indicates.

APPENDIX B: INSTRUMENTATION IN CAVE

HOBO Data Loggers

HOBO Data Loggers are deployed inside and outside of the cave. One set of sensors records pressure, temperature, and relative humidity outside the entrance to the cave. Inside the cave, there are three sets of HOBO data loggers – one set near the entrance and two sets near the loft area of the cave where GH-13-6 was collected in August 2013. The HOBO data logger collects measurements every 30 minutes and the outside and two of the inside devices have been continuously operating since August 2013. The third inside device was installed in June 2014.

Figure A-3. HOBO data loggers inside Buraca Glorioso – recording relative humidity, temperature, and pressure.

Resources:

http://www.onsetcomp.com/products

Stalagmate

The Stalagmate acoustic drip counter was installed in Buraca Glorioso in June 2014. It counts drips every 2 hours. The drip counter and drip water collector are in the location where GH-13-6 was removed in August 2013.

Figure A-4. Stalagmate drip counting device mounted inside 2-L beaker and outfitted with 6 liters of storage for drip water inside Buraca Glorioso.

Resources:

Mattey,D., Collister, C., 2008. Controls on water drop volume at speleothem drip sites: An experimental study. J. Hydrol. 358, 259-267.

www.driptych.com

www.geminidataloggers.com/articles/caves-data-logging-climate-change

APPENDIX C: U/TH DATING INFORMATION FOR BURACA GLORIOSO STALAGMITES

Table C-1. U-Th dates from GH-13-6

Sample	Mineral	Distance to base (mm)	238U (ng/g)	232Th (pg/g)	d234U (corr'd)	error	230Th/ 238U activity	error	230Th/ 232Th (ppm)	error	uncorrected age (yr)	error (yr)	age (yr BP)	error (yr)
GH-13-6-QQQ	calcite	342	88	171	314.2	1.5	0.0323	0.001275	277	72	2713	109	2616	121
GH-13-6-RRR	calcite	352	96	196	306.2	1.3	0.0308	0.001193	249	56	2597	102	2494	116
GH-13-6-SSS	calcite	364	89	475	286.6	1.3	0.0262	0.001231	81	8	2249	107	1975	175
GH-13-6-TTT	calcite	369.5	87	220	283.4	1.3	0.0209	0.00123	136	28	1790	106	1660	127
GH-13-6-UUU	calcite	377	78	123	275.5	1.3	0.0204	0.00135	213	72	1757	118	1594	153
GH-13-6-VVV	calcite	387	108	174	296.1	1.4	0.0167	0.00112	171	49	1413	96	1331	107
GH-13-6-WWW	calcite	398	82	46	312.8	1.4	0.0157	0.00159	457	503	1311	134	1282	138
GH-13-6-XXX	calcite	407.5	79	188	324.5	1.6	0.014	0.00153	98	27	1160	127	1042	144
GH-13-6-YYY	calcite	418	113	140	345.3	1.4	0.0088	0.00121	118	48	716	99	655	106
GH-13-6-ZZZ	calcite	430	100	74	315.3	1.3	0.0065	0.00124	144	93	539	104	502	108
GH-13-6-ZZ2	calcite	434.5	80	116	287.7	1.3	0.0042	0.00135	48	23	353	114	279	123
GH-13-6-ZZ1	calcite	433	90	42	292.7	1.3	0.0029	0.00122	103	111	249	103	225	107
GH-13-6-XX1	calcite	410	61	68	332.8	1.4	0.0161	0.00168	235	131	1323	139	1267	145
GH-13-6-XX2	calcite	412	64	49	346.5	1.4	0.0116	0.00149	252	194	942	122	904	127
GH-13-6-XX3	calcite	415.5	79	85	351.4	1.4	0.0098	0.00153	149	82	792	125	739	131
GH-13-6-YY1	calcite	429	88	57	333.7	1.4	0.0112	0.00122	288	213	923	101	891	105

Notes:

- present is defined as the year 2013
- Errors are at the 2σ level
- The initial $^{230}Th/^{232}Th$ atomic ratio of 1.0×10^{-5} +/- 5.5×10^{-6} was used to correct measured $^{230}Th/^{232}Th$ ratios
- $\delta^{234}U_{meas'd} = \{(^{234}U/^{238}U)_{meas'd}/(^{234}U/^{238}U)_{eq} - 1\} \times 10^3$, where $(^{234}U/^{238}U)_{eq}$ is secular equilibrium activity ratio; $\lambda_{238}/\lambda_{234} = 1.0$. Values reported as permil.

Table C-2. U-Th dates from GH-13-13, GH-13-2, GH-12-LowRM

Sample	Distance to base (mm)	Distance to top (mm)	Age (yr BP)	Error (yr)
GH-13-13	171		457	242
GH-13-13	164		553	56
GH-13-13	113		2167	63
GH-13-2-ZZZ		4	1848	108
GH-13-2-XXX		12	2569	63
GH-13-2-VVV		26	3103	76
GH-13-2-TTT			3331	60
GH-13-2-AAA			3682	98
GH-12-LowRM	1488		1,320	170
GH-12-LowRM	1403		2,040	60
GH-12-LowRM	1350		2,800	100

APPENDIX D: MICROMILL $\delta^{18}O$ AND $\delta^{13}C$ DATA FROM GH-13-6

Table D-1. Micromill $\delta^{18}O$ and $\delta^{13}C$ data

aligns with 1 mm sampling	Micromill Identifier	Identifier	$\delta^{13}C$	$\delta^{13}C$ error	$\delta^{18}O$	$\delta^{18}O$ error	LINEAR FIT - ENTIRE WAY
437	1	GH_13_6	-4.72612	0.08	-3.06296	0.25	1790.00
	2	GH_13_6	-2.83604	0.08	-1.76293	0.25	1785.67
	3	GH_13_6	-2.56965	0.08	-1.73213	0.25	1781.33
	4	GH_13_6	-2.46723	0.08	-2.37098	0.25	1777.00
	5	GH_13_6	-2.18237	0.08	-2.65262	0.25	1772.67
	6	GH_13_6	-1.98064	0.08	-2.91427	0.25	1768.33
436	7	GH_13_6	-1.63594	0.08	-2.90091	0.25	1764.00
	8	GH_13_6	-1.75332	0.08	-3.12321	0.25	1759.00
	9	GH_13_6	-1.86969	0.08	-3.00605	0.25	1754.00
	10	GH_13_6	-1.86849	0.08	-2.89398	0.25	1749.00
	11	GH_13_6	-2.0426	0.08	-2.97841	0.25	1744.00
435	12	GH_13_6	-1.89469	0.08	-3.04428	0.25	1739.00
	13	GH_13_6	-1.92431	0.08	-3.10975	0.25	1734.00
	14	GH_13_6	-1.91096	0.08	-2.23893	0.25	1729.00
	15	GH_13_6	-2.0434	0.08	-2.46754	0.25	1724.00
	16	GH_13_6	-2.05555	0.08	-2.54055	0.25	1719.00
434	17	GH_13_6	-2.07403	0.08	-2.51078	0.25	1714.00
	18	GH_13_6	-2.59284	0.08	-3.00095	0.25	1709.00
	19	GH_13_6	-2.53631	0.08	-2.79823	0.25	1704.00
	20	GH_13_6	-2.78272	0.08	-3.06172	0.25	1699.00
	21	GH_13_6	-2.95663	0.08	-2.99942	0.25	1694.00
433	22	GH_13_6	-2.87851	0.08	-3.40791	0.25	1689.00
	23	GH_13_6	-3.53027	0.08	-3.83914	0.25	1684.00
	24	GH_13_6	-3.82638	0.08	-3.64999	0.25	1679.00
	25	GH_13_6	-4.10201	0.08	-3.82395	0.25	1674.00
	26	GH_13_6	-3.96525	0.08	-3.92265	0.25	1669.00
432	27	GH_13_6	-3.66793	0.08	-3.94906	0.25	1664.00
	28	GH_13_6	-4.23706	0.08	-4.17758	0.25	1659.00
	29	GH_13_6	-4.11466	0.08	-4.31493	0.25	1654.00
	30	GH_13_6	-3.58138	0.08	-3.60471	0.25	1649.00
	31	GH_13_6	-4.45655	0.08	-3.72799	0.25	1644.00
431	32	GH_13_6	-3.97569	0.08	-3.40648	0.25	1639.00
	33	GH_13_6	-4.6148	0.08	-3.65141	0.25	1634.00
	34	GH_13_6	-4.17952	0.08	-3.61165	0.25	1629.00
	35	GH_13_6	-4.64881	0.08	-3.80778	0.03	1624.00
	36	GH_13_6	-4.46512	0.08	-3.65244	0.03	1619.00
430	37	GH_13_6	-5.37943	0.08	-3.47383	0.03	1614.00
	38	GH_13_6	-6.66755	0.08	-4.04292	0.03	1608.80
	39	GH_13_6	-6.90553	0.08	-4.46562	0.03	1603.60
	40	GH_13_6	-6.23965	0.08	-4.44072	0.03	1598.40
	41	GH_13_6	-5.68437	0.08	-4.10402	0.03	1593.20
429	42	GH_13_6	-5.34002	0.08	-4.27369	0.03	1588.00
	43	GH_13_6	-5.57468	0.08	-4.50344	0.03	1583.00
	44	GH_13_6	-5.68296	0.08	-4.39182	0.03	1578.00
	45	GH_13_6	-4.90377	0.08	-4.04251	0.03	1573.00
	46	GH_13_6	-3.97509	0.08	-3.74811	0.03	1568.00
428	47	GH_13_6	-3.35797	0.08	-3.51358	0.03	1563.00
	48	GH_13_6	-3.43448	0.08	-3.38315	0.03	1556.75
	49	GH_13_6	-3.26759	0.08	-3.56095	0.03	1550.50

Table D-1. Micromill $\delta^{18}O$ and $\delta^{13}C$ data (continued)

	50	GH_13_6	-2.87618	0.08	-3.37888	0.03	1544.25
	51	GH_13_6	-3.55583	0.08	-3.50829	0.03	1538.00
	52	GH_13_6	-4.79117	0.08	-3.62225	0.03	1531.75
	53	GH_13_6	-5.393	0.08	-3.81947	0.03	1525.50
	54	GH_13_6	-5.98378	0.08	-3.83411	0.03	1519.25
426	55	GH_13_6	-6.17983	0.08	-4.04323	0.03	1513.00
	56	GH_13_6	-5.50671	0.08	-4.04811	0.03	1507.39
	57	GH_13_6	-5.08022	0.08	-3.803	0.03	1501.78
	58	GH_13_6	-5.93692	0.08	-4.07677	0.03	1496.17
	59	GH_13_6	-5.42799	0.08	-3.84041	0.03	1490.56
	60	GH_13_6	-5.95683	0.08	-4.11601	0.03	1484.94
	61	GH_13_6	-6.46225	0.08	-4.06844	0.03	1479.33
	62	GH_13_6	-6.02299	0.08	-3.96668	0.03	1473.72
	63	GH_13_6	-5.73785	0.08	-3.82313	0.03	1468.11
	64	GH_13_6	-5.90616	0.08	-3.99473	0.03	1462.50
	65	GH_13_6	-5.67668	0.06	-3.98519	0.1	1456.89
	66	GH_13_6	-5.59948	0.06	-4.01729	0.1	1451.28
	67	GH_13_6	-5.69706	0.06	-3.81038	0.1	1445.67
	68	GH_13_6	-5.37314	0.06	-3.8755	0.1	1440.06
	69	GH_13_6	-5.55407	0.06	-3.93817	0.1	1434.44
	70	GH_13_6	-5.3797	0.06	-3.69731	0.1	1428.83
	71	GH_13_6	-4.30258	0.06	-3.3346	0.1	1423.22
	72	GH_13_6	-4.05142	0.06	-3.24955	0.1	1417.61
422	73	GH_13_6	-5.28908	0.06	-3.67227	0.1	1412.00
	74	GH_13_6	-5.89222	0.06	-3.73401	0.1	1406.44
	75	GH_13_6	-6.98699	0.06	-3.98151	0.1	1400.89
	76	GH_13_6	-6.22603	0.06	-3.76182	0.1	1395.33
421	77	GH_13_6	-6.26619	0.06	-3.88624	0.1	1389.78
	78	GH_13_6	-6.89325	0.06	-4.15592	0.1	1384.22
	79	GH_13_6	-7.00475	0.06	-3.84197	0.1	1378.67
	80	GH_13_6	-6.52049	0.06	-3.89503	0.1	1373.11
	81	GH_13_6	-5.97083	0.06	-3.91527	0.1	1367.56
420	82	GH_13_6	-5.13156	0.06	-3.7745	0.1	1362.00
	83	GH_13_6	-4.3379	0.06	-3.35484	0.1	1359.22
	84	GH_13_6	-3.53012	0.06	-2.86128	0.1	1356.44
	85	GH_13_6	-3.37636	0.05	-3.58496	0.11	1353.67
	86	GH_13_6	-3.61105	0.06	-3.08281	0.1	1350.89
	87	GH_13_6	-4.01792	0.06	-3.26478	0.1	1348.11
	88	GH_13_6	-4.74538	0.06	-3.56738	0.1	1345.33
	89	GH_13_6	-5.0581	0.06	-3.46607	0.1	1342.56
	90	GH_13_6	-4.7031	0.06	-3.15805	0.1	1339.78
419	91	GH_13_6	-3.84274	0.06	-2.80638	0.1	1337.00
	92	GH_13_6	-3.57331	0.06	-2.65692	0.1	1330.67
	93	GH_13_6	-3.37704	0.06	-2.82488	0.1	1324.33
	94	GH_13_6	-2.96068	0.06	-2.57718	0.1	1318.00
418??	95	GH_13_6	-3.01871	0.06	-2.69883	0.1	1311.67
	96	GH_13_6	-3.84758	0.06	-2.99571	0.1	1305.33
	97	GH_13_6	-4.32277	0.06	-3.19066	0.1	1299.00
	98	GH_13_6	-4.35183	0.06	-3.25885	0.1	1292.67
417??	99	GH_13_6	-4.73186	0.06	-3.50359	0.1	1286.33
	100	GH_13_6	-4.85547	0.06	-3.34278	0.1	1280.00
	101	GH_13_6	-4.87424	0.06	-3.53508	0.1	1273.67
	102	GH_13_6	-4.77066	0.09	-3.49558	0.06	1267.33
416	103	GH_13_6	-4.14965	0.09	-3.47272	0.06	1261.00
	104	GH_13_6	-4.0067	0.09	-3.651	0.06	1257.88
	105	GH_13_6	-4.15469	0.09	-3.683	0.06	1254.75
	106	GH_13_6	-3.78522	0.09	-3.65191	0.06	1251.63

Table D-1. Micromill $\delta^{18}O$ and $\delta^{13}C$ data (continued)

415.5	107	GH_13_6	-3.49478	0.09	-3.58515	0.06	1248.50
	108	GH_13_6	-3.68058	0.09	-3.55804	0.06	1245.38
	109	GH_13_6	-3.85901	0.09	-3.76169	0.06	1242.25
	110	GH_13_6	-4.43373	0.09	-3.64417	0.06	1239.13
415	111	GH_13_6	-4.85643	0.09	-3.79523	0.06	1236.00
	112	GH_13_6	-5.76936	0.09	-3.86811	0.06	1230.33
	113	GH_13_6	-6.45789	0.09	-4.35115	0.06	1224.67
	114	GH_13_6	-6.1727	0.09	-4.0369	0.06	1219.00
414	115	GH_13_6	-5.59597	0.09	-3.87473	0.06	1213.33
	116	GH_13_6	-4.99786	0.09	-3.55437	0.06	1207.67
	117	GH_13_6	-5.23345	0.09	-3.58454	0.06	1202.00
	118	GH_13_6	-6.60568	0.09	-3.76557	0.06	1196.33
	119	GH_13_6	-6.56999	0.09	-3.58811	0.06	1190.67
413	120	GH_13_6	-4.27677	0.09	-3.08182	0.06	1185.00
	121	GH_13_6	-0.56767	0.09	-2.06313	0.06	1180.00
	122	GH_13_6	-0.42643	0.09	-2.04692	0.06	1175.00
	123	GH_13_6	-0.37865	0.09	-2.25058	0.06	1170.00
	124	GH_13_6	-1.07202	0.09	-2.62578	0.06	1165.00
412	125	GH_13_6	-1.05256	0.09	-2.56218	0.06	1160.00
	126	GH_13_6	-1.61065	0.09	-2.86614	0.06	1155.00
	127	GH_13_6	-0.85913	0.05	-2.37019	0.11	1150.00
	128	GH_13_6	-1.22442	0.05	-2.51056	0.11	1145.00
	129	GH_13_6	-1.17745	0.05	-2.48016	0.11	1140.00
411	130	GH_13_6	-1.1939	0.05	-2.50469	0.11	1135.00
	131	GH_13_6	-1.78446	0.05	-2.43636	0.11	1128.75
	132	GH_13_6	-1.36571	0.05	-2.29393	0.11	1122.50
	133	GH_13_6	-1.52699	0.05	-2.03339	0.11	1116.25
410	134	GH_13_6	-1.72312	0.05	-2.53952	0.11	1110.00
	135	GH_13_6	-1.97626	0.05	-2.29197	0.11	1105.19
	136	GH_13_6	-1.26282	0.05	-1.55891	0.11	1100.38
	137	GH_13_6	-1.87169	0.05	-2.21705	0.11	1095.57
	138	GH_13_6	-1.93717	0.05	-2.4175	0.11	1090.76
	139	GH_13_6	-1.28684	0.05	-2.74739	0.11	1085.95
	140	GH_13_6	-1.09701	0.05	-2.85014	0.11	1081.14
	141	GH_13_6	-1.12182	0.05	-2.58889	0.11	1076.33
	142	GH_13_6	-1.65262	0.05	-2.97186	0.11	1071.52
	143	GH_13_6	-1.52315	0.05	-3.13603	0.11	1066.71
	144	GH_13_6	-1.25809	0.05	-2.76203	0.11	1061.90
	145	GH_13_6	-1.18385	0.05	-2.96959	0.11	1057.10
407-408	146	GH_13_6	-1.22649	0.05	-2.76285	0.11	1052.29
	147	GH_13_6	-1.71253	0.07	-2.5875	0.09	1047.48
407.5	148	GH_13_6	-1.9063	0.07	-2.32918	0.09	1042.67
	149	GH_13_6	-1.82087	0.07	-2.43623	0.09	1037.86
	150	GH_13_6	-1.87963	0.07	-3.09575	0.09	1033.05
406-407	151	GH_13_6	-1.7788	0.07	-3.25968	0.09	1028.24
	152	GH_13_6	-2.1449	0.07	-2.79484	0.09	1023.43
	153	GH_13_6	-2.03241	0.07	-2.54593	0.09	1018.62
	154	GH_13_6	-2.07359	0.07	-2.96255	0.09	1013.81
406	155	GH_13_6	-2.81202	0.07	-2.69536	0.09	1009.00
	156	GH_13_6	-2.80076	0.07	-2.36207	0.09	1002.67
405-406	157	GH_13_6	-2.36207	0.07	-2.28966	0.09	996.33
	158	GH_13_6	-2.07666	0.07	-2.10294	0.09	990.00
	159	GH_13_6	-1.79094	0.07	-2.39016	0.09	983.67
404	160	GH_13_6	-2.04594	0.07	-2.82722	0.09	977.33
	161	GH_13_6	-2.07527	0.07	-3.25692	0.09	971.00
	162	GH_13_6	-2.32691	0.07	-3.67028	0.09	964.67
	163	GH_13_6	-2.30637	0.07	-2.84795	0.09	958.33

Table D-1. Micromill $\delta^{18}O$ and $\delta^{13}C$ data (continued)

	164	GH_13_6	-2.35723	0.07	-3.27429	0.09	952.00
	165	GH_13_6	-2.80876	0.07	-3.53924	0.09	945.67
	166	GH_13_6	-1.19552	0.07	-2.79688	0.09	939.33
403	167	GH_13_6	-0.74162	0.07	-2.49639	0.09	933.00
	168	GH_13_6	-1.35284	0.07	-2.5875	0.09	926.75
	169	GH_13_6	-1.36154	0.07	-2.63693	0.09	920.50
	170	GH_13_6	-2.87691	0.07	-2.92374	0.09	914.25
402	171	GH_13_6	-3.16568	0.07	-2.98605	0.09	908.00
	172	GH_13_6	-2.96253	0.07	-2.65276	0.09	901.75
	173	GH_13_6	-2.80837	0.07	-2.63622	0.09	895.50
	174	GH_13_6	-2.50271	0.07	-2.41049	0.09	889.25
401	175	GH_13_6	-2.5587	0.07	-2.6784	0.09	883.00
	176	GH_13_6	-2.67109	0.07	-2.87083	0.09	879.43
	177	GH_13_6	-2.56651	0.07	-3.62493	0.09	875.86
	178	GH_13_6	-2.25462	0.07	-3.17787	0.09	872.29
	179	GH_13_6	-2.3519	0.07	-2.83039	0.09	868.71
	180	GH_13_6	-2.65381	0.07	-2.93804	0.09	865.14
	181	GH_13_6	-2.94792	0.07	-3.02415	0.09	861.57
400	182	GH_13_6	-2.7743	0.07	-2.39404	0.09	858.00
	183	GH_13_6	-2.88303	0.07	-2.68678	0.09	851.50
	184	GH_13_6	-2.9017	0.07	-2.8024	0.09	845.00
	185	GH_13_6	-2.64647	0.02	-2.16357	0.09	838.50
399	186	GH_13_6	-2.92099	0.02	-2.08038	0.09	832.00
	187	GH_13_6	-2.92217	0.02	-2.24437	0.09	827.00
	188	GH_13_6	-3.20967	0.02	-2.83703	0.09	822.00
	189	GH_13_6	-3.15885	0.02	-2.38643	0.09	817.00
	190	GH_13_6	-3.26245	0.02	-2.86323	0.09	812.00
398	191	GH_13_6	-3.31346	0.02	-2.96574	0.09	807.00
	192	GH_13_6	-3.35868	0.02	-2.60792	0.09	801.44
	193	GH_13_6	-3.37136	0.02	-2.57212	0.09	795.89
	194	GH_13_6	-3.47397	0.02	-2.42139	0.09	790.33
	195	GH_13_6	-3.6852	0.02	-2.83223	0.09	784.78
	196	GH_13_6	-3.61492	0.02	-2.44394	0.09	779.22
	197	GH_13_6	-3.38689	0.02	-2.46241	0.09	773.67
	198	GH_13_6	-3.14509	0.02	-2.18247	0.09	768.11
	199	GH_13_6	-2.71222	0.02	-2.58527	0.09	762.56
396	200	GH_13_6	-2.65482	0.02	-2.62233	0.09	757.00
	201	GH_13_6	-2.62868	0.02	-2.5837	0.09	752.45
	202	GH_13_6	-2.55693	0.02	-2.81637	0.09	747.91
395?	203	GH_13_6	-2.91804	0.02	-2.87336	0.09	743.36
	204	GH_13_6	-2.84423	0.02	-2.63318	0.09	738.82
	205	GH_13_6	-2.92551	0.02	-2.43705	0.09	734.27
	206	GH_13_6	-3.20682	0.02	-2.822	0.09	729.73
	207	GH_13_6	-3.44095	0.02	-2.53193	0.09	725.18
	208	GH_13_6	-3.45225	0.02	-2.57181	0.09	720.64
	209	GH_13_6	-3.076	0.02	-2.07955	0.09	716.09
	210	GH_13_6	-2.41726	0.02	-2.31545	0.09	711.55
394	211	GH_13_6	-1.7652	0.02	-1.97172	0.09	707.00
	212	GH_13_6	-2.40232	0.02	-2.25856	0.09	700.63
	213	GH_13_6	-2.14765	0.02	-2.03007	0.09	694.25
	214	GH_13_6	-2.32427	0.02	-2.01744	0.09	687.88
393	215	GH_13_6	-2.74515	0.02	-2.08341	0.09	681.50
	216	GH_13_6	-3.2656	0.02	-2.34937	0.09	675.13
	217	GH_13_6	-3.3634	0.02	-2.41283	0.09	668.75
	218	GH_13_6	-3.35976	0.02	-2.25251	0.09	662.38
392	219	GH_13_6	-4.41245	0.02	-2.624	0.09	656.00
	220	GH_13_6	-3.92109	0.02	-2.38382	0.09	651.00

Table D-1. Micromill $\delta^{18}O$ and $\delta^{13}C$ data (continued)

	221	GH_13_6	-5.2483	0.02	-2.69518	0.09	646.00
	222	GH_13_6	-4.8172	0.02	-2.47609	0.09	641.00
	223	GH_13_6	-4.18007	0.09	-2.33643	0.15	636.00
391	224	GH_13_6	-4.18586	0.09	-2.44574	0.15	631.00
	225	GH_13_6	-3.92665	0.09	-2.82335	0.15	626.00
	226	GH_13_6	-3.77524	0.09	-2.59243	0.15	621.00
	227	GH_13_6	-2.72224	0.09	-2.38911	0.15	616.00
	228	GH_13_6	-3.08954	0.09	-2.49988	0.15	611.00
390	229	GH_13_6	-3.44606	0.09	-2.39338	0.15	606.00
390	230	GH_13_6	-3.38518	0.09	-2.49343	0.15	601.00
	231	GH_13_6	-3.17218	0.09	-2.50009	0.15	596.00
	232	GH_13_6	-2.60476	0.09	-2.19276	0.15	591.00
	233	GH_13_6	-2.22159	0.09	-1.80318	0.15	586.00
389	234	GH_13_6	-1.85799	0.09	-1.81921	0.15	581.00
389	235	GH_13_6	-1.39916	0.09	-1.63441	0.15	576.00
	236	GH_13_6	-1.04793	0.09	-1.46523	0.15	571.00
	237	GH_13_6	-1.26452	0.09	-1.80359	0.15	566.00
	238	GH_13_6	-1.54868	0.09	-1.61318	0.15	561.00
388	239	GH_13_6	-1.54628	0.09	-1.81702	0.15	556.00
	240	GH_13_6	-1.88723	0.09	-1.67929	0.15	550.90
	241	GH_13_6	-2.06609	0.09	-1.30126	0.15	545.80
	242	GH_13_6	-1.81547	0.09	-1.8265	0.15	540.70
	243	GH_13_6	-1.99722	0.09	-1.90218	0.15	535.60
387	244	GH_13_6	-2.12358	0.09	-1.50063	0.15	530.50
387	245	GH_13_6	-1.74021	0.09	-1.79964	0.15	525.40
	246	GH_13_6	-0.5353	0.09	-1.13604	0.15	520.30
	247	GH_13_6	-1.2747	0.09	-1.48356	0.15	515.20
	248	GH_13_6	-1.65298	0.09	-1.9709	0.15	510.10
386	249	GH_13_6	-2.22179	0.09	-2.06231	0.15	505.00
	250	GH_13_6	-2.64818	0.09	-1.96236	0.15	498.75
	251	GH_13_6	-2.61544	0.09	-2.26511	0.15	492.50
	252	GH_13_6	-2.22179	0.09	-1.67064	0.15	486.25
385	253	GH_13_6	-2.78542	0.09	-2.16964	0.15	480.00
	254	GH_13_6	-2.19844	0.09	-2.30988	0.15	475.00
	255	GH_13_6	-1.61565	0.09	-2.36204	0.15	470.00
	256	GH_13_6	-1.34866	0.09	-1.85055	0.15	465.00
	257	GH_13_6	-1.24745	0.09	-2.07438	0.15	460.00
384	258	GH_13_6	-1.70987	0.09	-2.23773	0.15	455.00
	259	GH_13_6	-2.69649	0.09	-2.2749	0.15	450.45
	260	GH_13_6	-3.23197	0.09	-2.8196	0.15	445.91
	261	GH_13_6	-3.32766	0.09	-2.46796	0.09	441.36
	262	GH_13_6	-3.76412	0.09	-2.59727	0.09	436.82
383	263	GH_13_6	-3.82097	0.09	-2.66272	0.09	432.27
383	264	GH_13_6	-4.10816	0.09	-2.97264	0.09	427.73
	265	GH_13_6	-4.26105	0.09	-2.59476	0.09	423.18
	266	GH_13_6	-3.97296	0.09	-2.40388	0.09	418.64
	267	GH_13_6	-4.35095	0.09	-2.64479	0.09	414.09
	268	GH_13_6	-4.43241	0.09	-2.48663	0.09	409.55
382	269	GH_13_6	-4.764	0.09	-3.03913	0.09	405.00
	270	GH_13_6	-3.01456	0.09	-2.10423	0.09	400.67
	271	GH_13_6	-2.1738	0.09	-2.35899	0.09	396.33
	272	GH_13_6	-1.70731	0.09	-1.93726	0.09	392.00
	273	GH_13_6	-1.3269	0.09	-1.70003	0.09	387.67
	274	GH_13_6	-1.73282	0.09	-1.90748	0.09	383.33
381	275	GH_13_6	-1.29857	0.09	-1.72488	0.09	379.00
	276	GH_13_6	-1.55101	0.09	-1.88199	0.09	374.00
	277	GH_13_6	-1.60153	0.09	-1.95384	0.09	369.00

Table D-1. Micromill $\delta^{18}O$ and $\delta^{13}C$ data (continued)

	278	GH_13_6	-2.02443	0.09	-2.2324	0.09	364.00
	279	GH_13_6	-2.2196	0.09	-2.11032	0.09	359.00
380	280	GH_13_6	-2.36375	0.09	-2.45726	0.09	354.00
	281	GH_13_6	-2.46801	0.09	-2.40262	0.09	347.75
	282	GH_13_6	-2.80673	0.09	-2.74516	0.09	341.50
	283	GH_13_6	-2.2408	0.09	-2.4044	0.09	335.25
379	284	GH_13_6	-2.1978	0.09	-2.99781	0.09	329.00
	285	GH_13_6	-2.26872	0.09	-2.25872	0.09	322.75
	286	GH_13_6	-2.41759	0.09	-2.68579	0.09	316.50
	287	GH_13_6	-2.60352	0.09	-2.68758	0.09	310.25
378	288	GH_13_6	-2.90718	0.09	-2.86084	0.09	304.00
	289	GH_13_6	-2.88709	0.09	-2.73802	0.09	298.33
	290	GH_13_6	-3.01406	0.09	-2.95292	0.09	292.67
	291	GH_13_6	-3.02928	0.09	-2.09952	0.11	287.00
	292	GH_13_6	-3.59182	0.09	-2.10418	0.11	281.33
377	293	GH_13_6	-2.93283	0.09	-1.90533	0.11	275.67
	294	GH_13_6	-2.87938	0.09	-2.19275	0.11	270.00
	295	GH_13_6	-2.70537	0.09	-2.04623	0.11	264.33
	296	GH_13_6	-2.94378	0.09	-2.15048	0.11	258.67
376	297	GH_13_6	-3.25152	0.09	-2.42359	0.11	253.00
	298	GH_13_6	-3.3317	0.09	-2.19815	0.11	248.00
	299	GH_13_6	-3.33853	0.09	-2.73601	0.11	243.00
	300	GH_13_6	-3.4385	0.09	-3.16612	0.11	238.00
	301	GH_13_6	-3.16512	0.09	-2.99895	0.11	233.00
375	302	GH_13_6	-2.63956	0.09	-2.66789	0.11	228.00
	Re_run	GH_13_6	-2.53981	0.09	-2.83834	0.15	223.00
	304	GH_13_6	-2.08647	0.09	-2.85084	0.11	218.00
	305	GH_13_6	-2.55286	0.09	-2.82288	0.11	213.00
	306	GH_13_6	-2.38859	0.09	-2.84608	0.11	208.00
374	307	GH_13_6	-2.35288	0.09	-1.297	0.09	203.00
	308	GH_13_6	-2.28559	0.09	-1.46151	0.09	198.00
	309	GH_13_6	-2.35129	0.09	-1.17021	0.09	193.00
	310	GH_13_6	-2.75465	0.09	-0.41682	0.09	188.00
	311	GH_13_6	-2.78596	0.09	-1.46681	0.09	183.00
373	312	GH_13_6	-3.22263	0.09	-1.5135	0.09	178.00
	313	GH_13_6	-2.51311	0.09	-1.85626	0.09	173.00
	314	GH_13_6	-2.45854	0.09	-1.31775	0.09	168.00
	315	GH_13_6	-1.48243	0.09	-1.43017	0.09	163.00
	316	GH_13_6	-1.36802	0.09	-1.62397	0.09	158.00
372	317	GH_13_6	-1.61811	0.09	-1.63845	0.09	153.00
	318	GH_13_6	-1.77924	0.09	-1.80567	0.09	147.57
	319	GH_13_6	-2.09861	0.09	-1.8876	0.09	142.14
	320	GH_13_6	-2.40874	0.09	-1.9811	0.09	136.71
	321	GH_13_6	-2.31819	0.09	-2.15221	0.09	131.29
371	322	GH_13_6	-2.64442	0.09	-2.35877	0.09	125.86
	323	GH_13_6	-2.9957	0.09	-2.06217	0.09	120.43
	324	GH_13_6	-3.02055	0.09	-1.75779	0.09	115.00
	325	GH_13_6	-2.91349	0.09	-1.34337	0.09	109.57
	326	GH_13_6	-2.8301	0.09	-1.58225	0.09	104.14
370	327	GH_13_6	-2.88735	0.09	-1.51285	0.09	98.71
370	328	GH_13_6	-2.8293	0.09	-1.06742	0.09	93.29
	329	GH_13_6	-2.66599	0.09	-1.26825	0.09	87.86
	330	GH_13_6	-2.72921	0.09	-1.49113	0.09	82.43
369	331	GH_13_6	-1.98639	0.09	-1.95321	0.09	77.00
	332	GH_13_6	-2.0348	0.09	-1.93257	0.09	72.83
	333	GH_13_6	-1.71235	0.09	-1.73098	0.09	68.67
	334	GH_13_6	-1.54317	0.09	-1.4026	0.09	64.50

Table D-1. Micromill $\delta^{18}O$ and $\delta^{13}C$ data (continued)

	335	GH_13_6	-1.63879	0.09	-1.63856	0.09	60.33
	336	GH_13_6	-1.68183	0.09	-1.93732	0.09	56.17
368	337	GH_13_6	-1.76016	0.09	-1.80816	0.09	52.00
	338	GH_13_6	-1.86453	0.09	-1.98423	0.09	47.00
	339	GH_13_6	-2.07148	0.09	-1.1166	0.09	42.00
	340	GH_13_6	-2.17485	0.09	-1.23236	0.09	37.00
367	341	GH_13_6	-2.20467	0.09	-0.7318	0.09	32.00
	342	GH_13_6	-2.05547	0.09	-2.03525	0.09	27.00
	343	GH_13_6	-2.19931	0.09	-1.87279	0.09	22.00
	344	GH_13_6	-2.37047	0.09	-1.86512	0.09	17.00
	345	GH_13_6	-2.3676	0.08	-2.29488	0.13	12.00
	346	GH_13_6	-2.4273	0.08	-2.30262	0.13	7.00
366	347	GH_13_6	-2.80905	0.08	-2.66069	0.13	2.00
	348	GH_13_6	-3.21765	0.08	-1.70224	0.13	-3.20
	349	GH_13_6	-3.47068	0.08	-2.05723	0.13	-8.40
	350	GH_13_6	-3.20082	0.08	-2.05469	0.13	-13.60
	351	GH_13_6	-3.16015	0.08	-1.47137	0.13	-18.80
365	352	GH_13_6	-3.58347	0.08	-1.80442	0.13	-24.00
	353	GH_13_6	-3.59128	0.08	-1.93766	0.13	-29.00
	354	GH_13_6	-3.69776	0.08	-2.22895	0.13	-34.00
	355	GH_13_6	-3.53008	0.08	-2.91731	0.13	-39.00
	356	GH_13_6	-3.66931	0.08	-3.02533	0.13	-44.00
364	357	GH_13_6	-3.74724	0.08	-2.78206	0.13	-49.00
	358	GH_13_6	-3.82668	0.08	-2.9859	0.13	-54.00
	359	GH_13_6	-3.63916	0.08	-2.84492	0.13	-59.00
	360	GH_13_6	-3.7226	0.08	-2.81916	0.13	-64.00
	361	GH_13_6	-3.77038	0.08	-2.64913	0.13	-69.00
363	362	GH_13_6	-3.66921	0.08	-2.78015	0.13	-74.00
	363	GH_13_6	-3.70567	0.08	-1.96967	0.13	-79.00
	364	GH_13_6	-3.99406	0.08	-2.00635	0.13	-84.00
	365	GH_13_6	-3.83229	0.08	-2.04186	0.13	-89.00
	366	GH_13_6	-3.66851	0.08	-2.09942	0.13	-94.00
362	367	GH_13_6	-3.9542	0.08	-1.99575	0.13	-99.00
	368	GH_13_6	-3.88057	0.08	-1.97487	0.13	-104.00
	369	GH_13_6	-3.8397	0.08	-1.98271	0.13	-109.00
	370	GH_13_6	-2.1299	0.08	-1.10641	0.13	-114.00
8361	390	GH_13_6	-0.57076	0.12	-1.69235	0.11	-119.00
	391	GH_13_6	-0.89741	0.12	-1.82609	0.11	-124.00
	392	GH_13_6	-0.98175	0.12	-2.31761	0.11	-128.64
	393	GH_13_6	-0.57357	0.12	-1.76667	0.11	-133.27
	394	GH_13_6	-0.77014	0.12	-1.45108	0.11	-137.91
	395	GH_13_6	-1.08816	0.12	-2.02015	0.11	-142.55
8360	396	GH_13_6	-1.31572	0.12	-2.01584	0.11	-147.18
8360	397	GH_13_6	-1.23007	0.12	-1.26654	0.11	-151.82
	398	GH_13_6	-1.75639	0.12	-1.20802	0.11	-156.45
	399	GH_13_6	-2.3456	0.12	-1.22005	0.11	-161.09
	400	GH_13_6	-2.49874	0.12	-1.53833	0.11	-165.73
8359	401	GH_13_6	-2.75448	0.12	-1.07141	0.11	-170.36
	402	GH_13_6	-2.07261	0.12	-0.96406	0.11	-175.00
	403	GH_13_6	-1.4826	0.12	-1.18396	0.11	-180.00
	404	GH_13_6	-1.28844	0.12	-1.98766	0.11	-185.00
	405	GH_13_6	-0.15627	0.12	-0.85688	0.11	-190.00
8358	406	GH_13_6	-0.12528	0.12	-0.92331	0.11	-195.00
	407	GH_13_6	-0.1328	0.12	-0.67557	0.11	-200.00
	408	GH_13_6	-0.69111	0.12	-1.39292	0.11	-205.00
	409	GH_13_6	-0.69573	0.12	-1.52271	0.11	-210.00
	410	GH_13_6	-0.90363	0.12	-1.26977	0.11	-215.00

Table D-1. Micromill $\delta^{18}O$ and $\delta^{13}C$ data (continued)

8357	411	GH_13_6	-1.09237	0.09	-1.32835	0.15	-220.00
	412	GH_13_6	-1.43467	0.09	-1.64882	0.15	-225.00
	413	GH_13_6	-1.75457	0.09	-1.70742	0.15	-229.64
	414	GH_13_6	-1.90141	0.09	-1.70742	0.15	-234.27
	415	GH_13_6	-2.21221	0.09	-1.32485	0.15	-238.91
8356	416	GH_13_6	-2.10518	0.09	-0.70122	0.15	-243.55
8356	417	GH_13_6	-2.06666	0.09	-0.88911	0.15	-248.18
	418	GH_13_6	-2.13218	0.09	-0.7113	0.15	-252.82
	419	GH_13_6	-1.91467	0.09	-1.52651	0.12	-257.45
	420	GH_13_6	-1.84864	0.09	-1.525	0.12	-262.09
	421	GH_13_6	-1.78482	0.09	-1.35271	0.12	-266.73
8355	422	GH_13_6	-1.97718	0.09	-1.39826	0.12	-271.36
	423	GH_13_6	-2.15718	0.09	-1.80357	0.12	-276.00
	424	GH_13_6	-2.23044	0.09	-1.48214	0.12	-281.56
	425	GH_13_6	-2.13999	0.09	-1.76997	0.12	-287.11
	426	GH_13_6	-2.48933	0.09	-1.83512	0.12	-292.67
8354	427	GH_13_6	-2.61314	0.09	-0.66636	0.12	-298.22
	428	GH_13_6	-2.58058	0.09	-1.61082	0.12	-303.78
	429	GH_13_6	-2.54862	0.09	-0.49719	0.12	-309.33
	430	GH_13_6	-2.73244	0.09	-1.19733	0.12	-314.89
8353	431	GH_13_6	-2.78972	0.09	-0.88797	0.12	-320.44
	432	GH_13_6	-2.73214	0.09	-1.14037	0.12	-326.00
	433	GH_13_6	-2.90952	0.09	-0.7454	0.12	-331.00
	434	GH_13_6	-2.86098	0.09	-0.47351	0.12	-336.00
	435	GH_13_6	-2.61123	0.09	-1.98318	0.12	-341.00
8352	436	GH_13_6	-2.48531	0.09	-1.86085	0.12	-346.00
	437	GH_13_6	-2.73234	0.09	-2.03863	0.12	-351.00
	438	GH_13_6	-2.7648	0.09	-1.96229	0.12	-356.00
	439	GH_13_6	-2.92841	0.09	-2.02593	0.12	-361.00
	440	GH_13_6	-3.17886	0.09	-1.8559	0.12	-366.00
8351	441	GH_13_6	-3.11253	0.09	-1.71452	0.12	-371.00
	442	GH_13_6	-3.11333	0.09	-1.66068	0.12	-376.00
	443	GH_13_6	-3.00107	0.09	-0.78545	0.12	-381.00
	444	GH_13_6	-2.93625	0.09	-0.54694	0.12	-386.00
	445	GH_13_6	-2.9866	0.09	-0.71406	0.12	-391.00
8350	446	GH_13_6	-2.85223	0.09	-0.73689	0.12	-396.00
	447	GH_13_6	-2.84098	0.09	-0.85685	0.12	-401.00
	448	GH_13_6	-2.6445	0.09	-0.72838	0.12	-406.20
	449	GH_13_6	-2.44873	0.09	-0.52605	0.12	-411.40
	450	GH_13_6	-2.39044	0.09	-0.45531	0.12	-416.60
8349	451	GH_13_6	-2.13486	0.09	-1.78537	0.12	-421.80
	452	GH_13_6	-2.02582	0.09	-1.6329	0.12	-427.00
	453	GH_13_6	-2.08492	0.09	-1.77633	0.12	-432.00
	454	GH_13_6	-2.43174	0.09	-1.03107	0.12	-437.00
	455	GH_13_6	-2.54886	0.06	-2.33793	0.14	-442.00
8348	456	GH_13_6	-2.47664	0.06	-2.06701	0.14	-447.00
	457	GH_13_6	-2.31511	0.06	-2.13209	0.14	-452.00
	458	GH_13_6	-2.40013	0.06	-2.13155	0.14	-457.00
	459	GH_13_6	-2.49905	0.06	-2.11975	0.14	-462.00
	460	GH_13_6	-2.70509	0.06	-2.26722	0.14	-467.00
8347	461	GH_13_6	-2.71029	0.06	-2.0642	0.14	-472.00
	462	GH_13_6	-2.65198	0.06	-2.12451	0.14	-477.00
	463	GH_13_6	-2.88972	0.06	-1.41376	0.14	-482.00
	464	GH_13_6	-2.80431	0.06	-1.08502	0.14	-487.00
	465	GH_13_6	-3.05566	0.06	-1.27776	0.14	-492.00
8346	466	GH_13_6	-3.54516	0.06	-1.15616	0.14	-497.00
	467	GH_13_6	-3.43053	0.06	-1.10755	0.14	-502.00

Table D-1. Micromill $\delta^{18}O$ and $\delta^{13}C$ data (continued)

	468	GH_13_6	-3.7709	0.06	-1.13018	0.14	-507.00
	469	GH_13_6	-3.86882	0.06	-1.36287	0.14	-512.00
	470	GH_13_6	-3.87522	0.06	-1.70146	0.14	-517.00
8345	471	GH_13_6	-3.81671	0.06	-2.46852	0.14	-522.00
	472	GH_13_6	-3.61017	0.06	-2.47382	0.14	-527.00
	473	GH_13_6	-3.60737	0.06	-2.40333	0.14	-532.20
	474	GH_13_6	-3.72559	0.06	-2.95415	0.14	-537.40
	475	GH_13_6	-3.61177	0.06	-2.55038	0.14	-542.60
8344	476	GH_13_6	-3.47084	0.06	-3.07478	0.14	-547.80
	477	GH_13_6	-3.67568	0.06	-2.73586	0.14	-553.00
	478	GH_13_6	-3.62087	0.06	-2.80624	0.14	-558.00
	479	GH_13_6	-3.84532	0.06	-0.9043	0.14	-563.00
	480	GH_13_6	-3.87772	0.06	-1.44505	0.14	-568.00
8343	481	GH_13_6	-4.13307	0.06	-1.43336	0.14	-573.00
	482	GH_13_6	-4.15188	0.06	-1.68013	0.14	-578.00
	483	GH_13_6	-4.32491	0.06	-1.44246	0.14	-584.25
	484	GH_13_6	-4.37372	0.06	-1.42546	0.14	-590.50
	485	GH_13_6	-4.54816	0.06	-1.24679	0.14	-596.75
8342	486	GH_13_6	-4.59487	0.06	-0.99515	0.14	-603.00
	487	GH_13_6	-4.14488	0.06	-2.50327	0.14	-608.00
	488	GH_13_6	-3.84341	0.06	-2.70208	0.14	-613.00
	489	GH_13_6	-3.81741	0.06	-2.84511	0.14	-618.00
	490	GH_13_6	-3.7529	0.06	-0.8611	0.14	-623.00
8341	491	GH_13_6	-3.77168	0.09	-1.5484	0.15	-628.00
	492	GH_13_6	-4.00394	0.09	-1.94933	0.15	-633.00
	493	GH_13_6	-4.48119	0.09	-1.93405	0.15	-638.00
	494	GH_13_6	-4.534	0.09	-3.03036	0.15	-643.00
	495	GH_13_6	-4.91382	0.09	-3.17865	0.15	-648.00
8340	496	GH_13_6	-4.8405	0.09	-3.12823	0.15	-653.00

APPENDIX E: COMPARISON OF $\delta^{13}C$ BURACA GLORIOSO DATA WITH NORTHERN HEMISPHERE TEMPERATURE RECONSTRUCTIONS

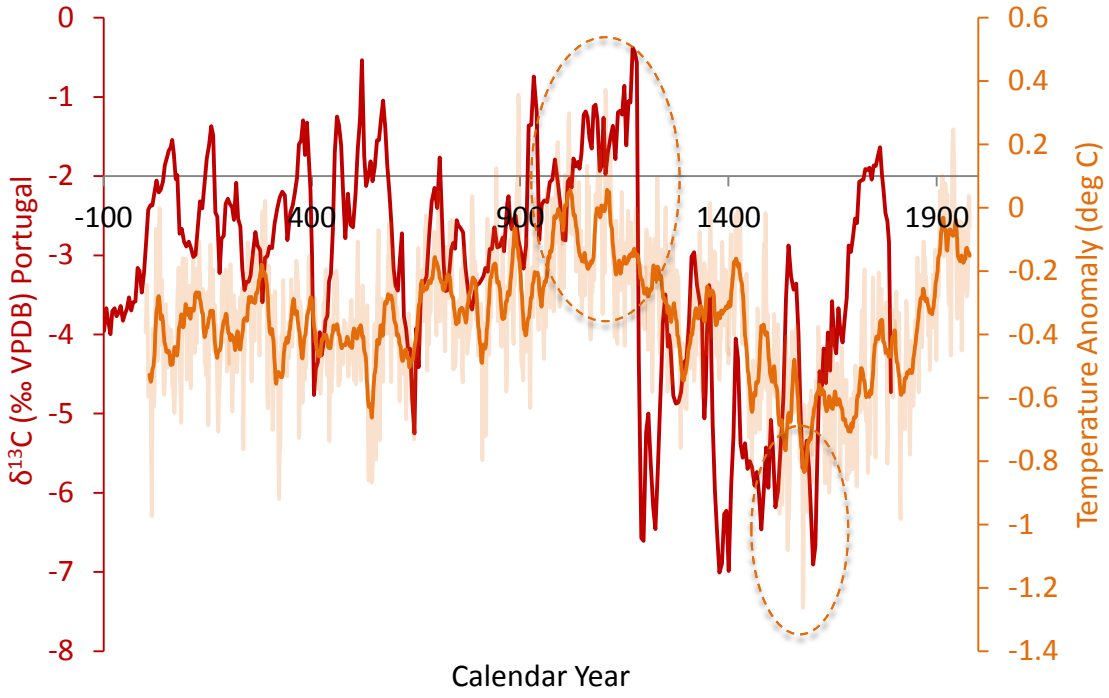

Figure E-1. Moberg et al. (2005) NH Temperature reconstruction (orange) compared to $\delta^{13}C$ data from Buraca Glorioso (red). Highest and lowest values of Moberg et al. (2005) reconstruction are circled.

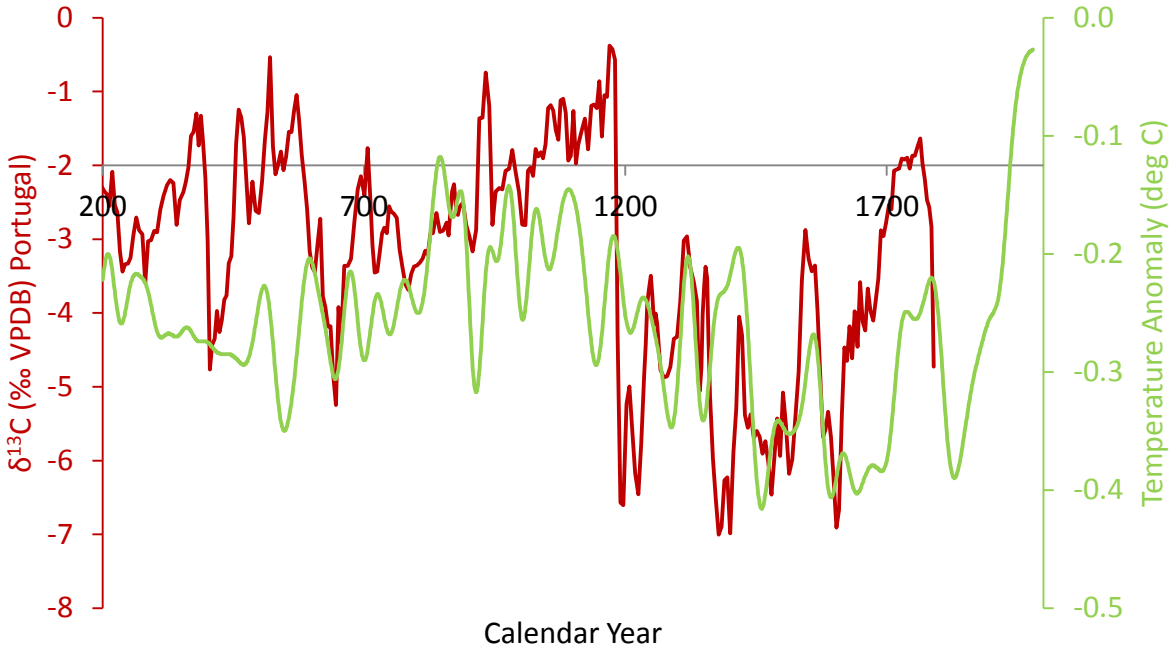

Figure E-2. Mann and Jones (2004) NH Temperature reconstruction (green) compared to $\delta^{13}C$ data from Buraca Glorioso (red).

APPENDIX F: BURACA GLORIOSO ROCK, SOIL, AND VEGETATION CARBON VALUES

ROCKS

Two separate rocks from Buraca Glorioso with five samples milled from each rock.

Table F-1. Buraca Glorioso rock carbon and oxygen values.

Sample	Identifier	$\delta^{13}C$	error	$\delta^{18}O$	error
1	GH_ROCK A	3.3521	0.09	-1.7311	0.15
2	GH_ROCK A	2.9480	0.09	-2.6655	0.15
3	GH_ROCK A	3.3779	0.09	-2.8836	0.15
4	GH_ROCK A	3.1514	0.09	-2.4889	0.15
5	GH_ROCK A	0.3924	0.09	-8.2899	0.15
1	GH_ROCK B	3.3030	0.09	-4.0715	0.15
2	GH_ROCK B	2.6499	0.09	-7.1632	0.15
3	GH_ROCK B	3.7352	0.09	-4.3763	0.15
4	GH_ROCK B	4.2849	0.09	-3.8368	0.15
5	GH_ROCK B	3.5667	0.09	-4.7587	0.15

SOIL AND VEGETATION

Soil and vegetation samples from above the cave at Buraca Glorioso. Three samples of each were measured for $\delta^{13}C$ and $\delta^{15}N$.

Table F-2. Buraca Glorioso soil and vegetation carbon and nitrogen values.

Identifier	$\delta^{13}C$ (VPDB)	error	$\delta^{15}N$ (Air)	error
GH_soil 1	-28.7275	0.09	-4.6112	0.21
GH_soil 2	-29.2526	0.09	-5.3030	0.21
GH_soil 3	-28.6665	0.09	-4.3465	0.21
GH_veg 1	-26.7528	0.09	1.7254	0.21
GH_veg 2	-27.0183	0.09	1.9242	0.21
GH_veg 3	-26.6604	0.09	1.7618	0.21